Investigating methods of pulsar detection in radio continuum surveys using the Australian Square Kilometer Array Pathfinder.

by

Andrew D. Cameron

Advanced Science Physics (Honours)
Faculty of Science

Supervised by Dr. Maria Cunningham (UNSW)
& Dr. George Hobbs (CSIRO)

University of New South Wales

November 14, 2010

Abstract

The vast majority of pulsars so far discovered have been found using concentional single-antenna searching techniques. These techniques are often not sensitive to specific types of pulsar, such as millisecond pulsars or pulsars in fast binaries. An alternative approach is to try detecting pulsars in radio continuum surveys, but with the exception of a few notable cases, the majority of previous attempts using this method have been unsuccesful. However, the few pulsars succesfully detected via this method have been of high scientific interest, and with the rapid approach of the new and powerful instruments such as the Australian Square Kilometer Array Pathfinder (ASKAP), which will be conducting new, highly sensitive radio continuum surveys with wide sky coverage, there is reason to pursue methods of pulsar detection in radio continuum. In this thesis, we present an investigation into these methods, presented in two parts. The first of these details the investigation of a selection of infrared-faint radio sources (IFRS), detected in radio continuum as part of the Australia Telescope Large Area Survey (ATLAS) as to their possible identity as pulsars, and concludes with a non-detection of any pulsars. The second section investigates in further detail the suitability of the values of spectral index, fractional linear polarisation and fractional circular polarisation as means by which pulsar candidates can be selected from two of the the radio continuum surveys to be performed on ASKAP, EMU and POSSUM. It is concluded that of these candidate criteria, only circular polarisation presents any real prospect for future application in detecting pulsars in radio continuum.

Acknowledgments

I would first like to thank my primary supervisor, Dr. George Hobbs, for providing an enormous amount of support and understanding through the course of this project. Conducting this research project between two institutions has not been easy, and he has always been willing to work around our mutually complex schedules as much as possible to find the time to help me when I needed it. His guidance and assistance have over the past few months have been invaluable, and I am very grateful to him for taking me on as an honours student. I would also like to thnk my secondary supervisor, Dr. Maria Cunningham, for her continual support and counsel through year, and supervision over the past few months of this project despite the fact that it was outside of her field of expertise.

Others who deserve thanks include my co-authors on the IFRS paper, Dr. Michael Keith, Dr. Ray Norris, Minnie Mao and Dr. Enno Middelberg (and Dr. George Hobbs) for sticking with me throughout the process of publishing my first academic paper. Their patience and encouragement wil not be soon forgotten. Finally, I would like to thank my family, for their understanding and support throughout this research project.

Contents

Chapter 1

Introduction

This thesis details a thorough investigation into the possibility of techniques that may be used to detect pulsars in radio continuum surveys. The sections below contain a considerable amount of the background material required in order to understand the project. Section 1.1 borrows heavily from Carr, 2007 [64], with supplemental references included as required.

1.1 Radio Astronomy

The primary method of investigation used in the field of astronomy is the measurement of electromagnetic radiation that arrives at the Earth from some other point of origin in the Universe. As per its name, radio astronomy focuses on the use of radio wavelength electromagnetic radiation (radiation with a wavelength approximately greater than $\sim 10^{-3} - 10^{-4}$m). Although imperceptible to the human eye (which responds only to the visual spectrum between $\sim 400 - 700$ nm), radio waves are able to induce electrical currents in a receiving conductor. However, because of the fact that radio waves arriving from space are generally very weak, they must first be amplified before they can be measured. This is typically achieved through the use of a large parabolic reflector, which directs the incoming radiation onto a central focus. A receiver placed at this point can then be used to convert the radio signal into a weak electrical current, which is then electronically amplified to a level suitable for practical use. Also, as well as measuring the overall intensity of an incoming electromagnetic signal, such receivers can also divide the signal into numerous frequency components, allowing for a full spectral analysis of that signal and the extraction of a much larger amount of information, particularly regarding motions in the emitting source.

The SI unit of measurement for the strength of observed radio signals, taken as the *flux density*, is Watts per square meter per Hertz (or mathematically, $W \cdot m^{-2} \cdot Hz^{-1}$). However, in radio astronomy it is more common (and convenient) to use the *Jansky* as the unit of measurement. The Jansky is defined as 1 Jy $= 10^{-26} \times W \cdot m^{-2} \cdot Hz^{-1}$. Most astronomical sources in the radio spectrum have flux densities between 1 and 100 Jy [33], and the total flux density of a source is derived by integrating the observed flux density over the total solid angle Ω subtended by the source.

1.1.1 Antenna Theory

The full technical workings of radio antennas are long and complex, but there are some key fundamental parameters worth making note of. The first of the these is the *aperture efficiency*, defined as

$$\eta = \frac{A}{A_g} \tag{1.1}$$

where A is the maximum absorption area, and A_g the geometrical area of the antenna aperture. The antenna efficiency essentially quantifies the efficiency with which the antenna can convert a real intensity arriving at the detector into an observed intensity, and so may be re-written as

$$\eta = \frac{T_{obs}}{T_{true}} \tag{1.2}$$

where T_{obs} is the observed intensity and T_{true} is the real intensity arriving at the antenna. In simple terms, η gives the antenna's sensitivity. The quantity can also be expressed as the product of a string of inter-related efficiency factors, such as those relating to illumination, spillover, surface scattering, radiation loss and focus errors [34].

Another important quantity is the *angular resolution*, which defines the smallest angular separation that two sources can have on the sky and still be detected as two individual sources. Mathematically, it is given by

$$\delta \sim \frac{\lambda}{D_\lambda} \tag{1.3}$$

where λ is the wavelength being observed and D_λ is the diameter of the telescope, known as the *aperture*. It should be noted that this expression is valid for single antenna telescopes only. A similar expression exists for multi-antenna interferometric telescopes, but as the observations in this project have been taken with only a single antenna, this extension of the theory will not be discussed.

Resolution can also be thought of in terms of the telescope's *beam size*. A parabolic single dish antenna does not have a uniform sensitivity over the entire sky, instead, its sensitivity obeys a power pattern as depicted in Figure 1.1. This patterns includes a main, primary beam as well as several minor side lobes. Resolution may be thought of as the *Half Power Beam Width* (HPBW), the angular distance between the edges of the beam where the power in the main lobe has fallen to half of the peak value.

1.1.2 Interferometry

Radio interferometry is a technique by which many single dish telescopes separated by a large distance can be synthesised into one much larger telescope so as to dramatically improve the angular resolution of the telescope above that which is conventionally possible using a single dish. This is achieved through the use of the basic principles of electromagnetic interference. The neccessity for such technology arises simply because of the scale of typical radio wavelengths ($\sim$ 1 mm $-$ 10 km). Single-dish telescopes are hindered by diffraction effects and relatively poor resolution [64]. In addition, while in optical wavelengths ideal resolutions can be achieved with a telescope of only a few meters in diameter, by equation (1.3) observations at radio wavelengths may require telescope diameters on the order of kilometers in order to achieve a similar resolution. Since current technology and engineering methods deem the building of such a single-dish telescope impossible, radio interferometry has been developed and utilised to overcome this limitation.

A basic radio interferometer as depicted in Figure 1.2 consists of just two antennas pointed at the same radio source, the angular dimensions of which are very small. Two antennas are used for simplicity in this example, but the same principles can be scaled up to much larger antenna configurations. Let both of the antennas be fitted with a suitable receiving system so that both only admit the same narrow band of frequencies. The observed source is approximated as being far enough away from the observing antennas with respect to their separation that the light being received by both antennas can be considered as essentially parallel. The output of the two antennas is then proportional to the spatial coherence function of the radiation from the source. This output is produced by cross-correlating the responses from each telescope. The spatial coherence function describes the correlation of the electric field from each antenna, and is defined as the time average of the signal from one antenna multiplied by the complex conjugate of the other. The resultant quantity is known as the *complex visibility,* and

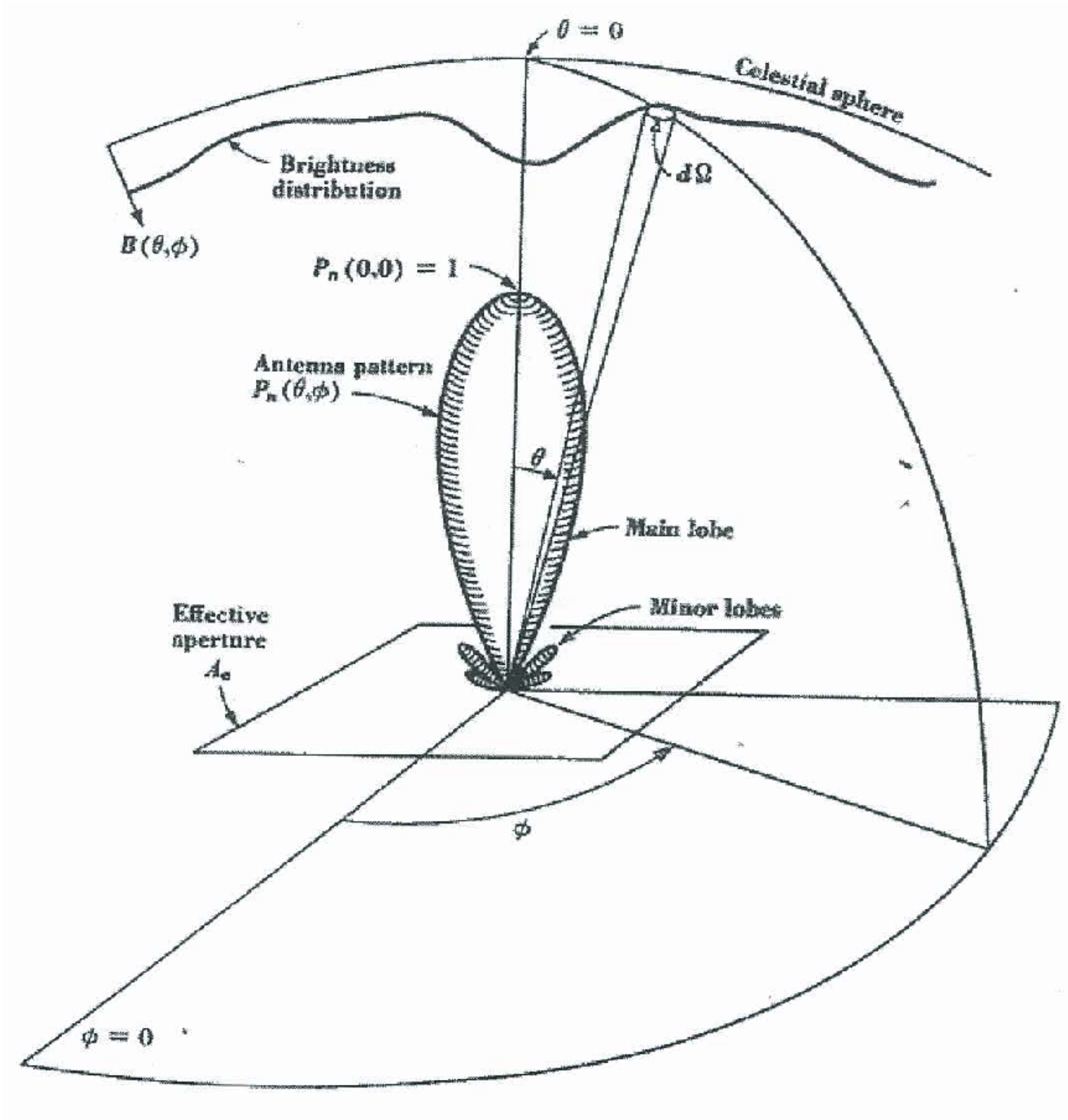

Figure 1.1: Single dish telescope response pattern. Diagram from Hunt, 2001 [32].

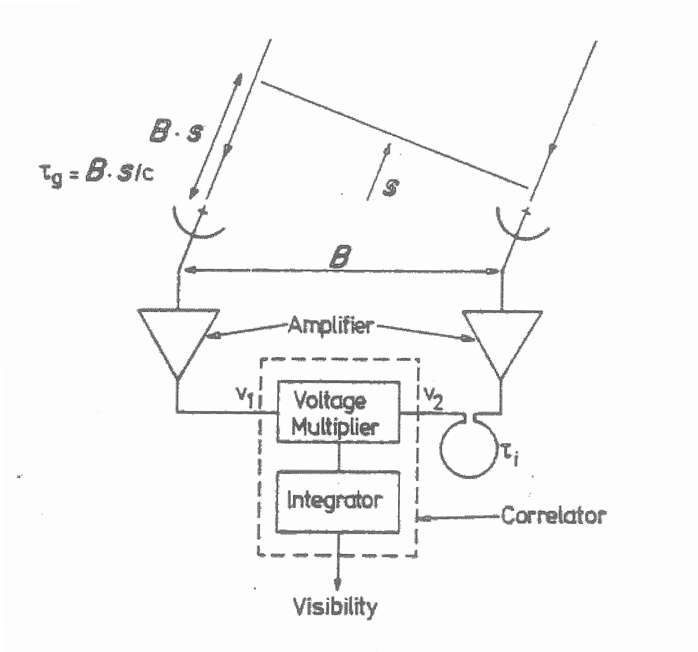

Figure 1.2: A diagram of a basic two-antenna interferometer, showing the baseline length B, geometric time delay τ_g, and correlation system. Diagram from Hunt, 2001 [32].

is a function of the baseline separation (distance between the antennas), storing amplitude and phase information.

Because of their physical separation, the coherent parts of an incoming wave are received by the two antennas at different times. This time difference is called the geometric time delay, and is given by

$$\tau_g = \left(\frac{D}{c}\right) \sin\theta \tag{1.4}$$

where D is the distance between antennas and θ is the angle of deflection of the antennas from the vertical. A full derivation of the interferometric theory produces a simplified output of

$$F = \cos\left(2\pi\nu\tau_g\right) = \cos\left(\frac{2\pi D}{\lambda}\right) \sin\theta \tag{1.5}$$

where F is the complex visibility. This function generates lobes in the interferometer response pattern similar to the power pattern for a single dish telescope, as depicted in Figure 1.1.

1.1.3 The Australia Telescope Compact Array (ATCA)

Some of the key observations undertaken as part of this project were carried out using the Australia Telescope Compact Array (ATCA), an interferometer consisting of six 22-m telescopes located approximately 25 km outside the town of Narrabri in northern New South Wales. It is operated by the Australia Telescope National Facility (ATNF), a subdivision of CSIRO Astronomy and Space Science (CASS). Five of the six antennas are mobile and can be moved to any of 44 fixed stations along a 3 km section of track running east-west, with an additional 214 m north-south spur line. The sixth antenna is fixed in position at a distance of 3 km west of the western end of the east-west track. The array has a maximum baseline of 6 km, with a minimum baseline of 30.612 m [59]. The telescope operates as an earth-rotation aperture synthesis radio interferometer, and ideally requires a full 12-hour observation to fully resolve an observed source. The ATCA is capable of observing at 20, 13, 6, and 3 cm as well as 12, 7 and 3 mm. As of April 2009 it has been upgraded with the Compact Array Broadband Backend (CABB), which improves the telescope's total observing bandwidth from 128 MHz to 2048 MHz, with 2048 1 MHz channels. The full implementation of CABB will include a "zoom mode" capability, allowing for much finer resolution (on the order of 1 kHz) over a much smaller bandwidth [60].

1.1.4 The Parkes Radio Telescope

Key observations in this project were also undertaken using the the Parkes Radio Telescope. The telescope consists of a single 64-m parabolic dish, and is located approximately 25 km north of the town of Parkes in western New South Wales. As with the ATCA, it is operated by the ATNF. The telescope can be equipped with any one of a large number of receivers, and is capable of observing over a frequency range of $0.44 - 26$ GHz [77]. The observations conducted as part of this project used the Parkes 20-cm 13-multibeam receiver. As its name suggests, this receives consists of 13 indidivual feed horns, each with a beam FWHM of 14.4 arcminutes. The receiver is capable of recording polarisation information, and can observe between 1230 and 1530 MHz. The telescope can also be configured with a number of backend data processing systems, including the Berkeley-Parkes-Swinburne Recorder (BPSR), the high-reolution digital filterbank [78] used in the observations required for this thesis.

1.1.5 The Australian Square Kilometer Array Pathfinder (ASKAP)

The Australian Square Kilometer Array Pathfinder (ASKAP) is a next generation radio telescope, currently being constructed in the mid-west of Western Australia at the Murchison Radio-astronomy Observatory (MRO), approximately 315 km north-east of Geraldton. The purpose of ASKAP is two fold, as not only will it provide a powerful new observing instrument for astronomers worldwide, but will also help to pave the way for the future construction of the Square Kilometer Array (SKA), to be built between 2016 and 2023 [69]. This telescope is so named as it will have a total collecting surface area of 1 square kilometer. ASKAP will serve as a testbed for developing the technologies required for operation of the SKA (many of which do not yet exist), as well as acting as an additional incentive in Australia's bid to host the SKA. Should this bid be successful, ASKAP will be upgraded to become part of the SKA.

ASKAP will operate as an interferometer, and will consist of thirty six 12-m telescopes, the first six of which have already been constructed and installed at the MRO [68]. These first six telescopes, known as the Boolardy Engineering Test Array (BETA), are expected to be operational by 2011, with the construction and testing of the remaining thirty antennas to be completed by 2013. The telescope will be capable of observing at frequencies between 700 and 1800 MHz, with a bandwidth of 300 MHz and a maximum of 16384 channels. With a maximum baseline of 6 km, the telescope will have a field of view of some 30 square degrees.

1.2 Pulsars

Pulsars (or more specifically, radio pulsars) are a special class of neutron star, possessing high degrees of magnetisation and a rapid rate of rotation. Their name derives from their primary observational feature, in that they appear to emit regularly timed broadband radio pulses. The first pulsar was discovered in 1967, and was reported by Hewish et al, 1968 [25]. This pulsar, PSR B1919+21 was observed to pulse with a period of aproximately 1.34s. So unusual was the discovery of a regularly pulsing object that it was briefly speculated that the signal might have originated with an extraterrestrial society [30], although the discovery of other pulsars (along with several other indicators) quickly dispelled this hypothesis. The ATNF Pulsar Catalog (PSRCAT) [46] lists a total of 1880 discovered pulsars as of November, 2010.

The majority of pulsars are found in close proximity to the Galactic plane, although some of been discovered at higher Galactic latitudes. Three current populations or classes of pulsars are currently proposed to exist [12]. These are:

'Normal' pulsars: The first discovered class of pulsars, with rotation periods between 50 ms and several seconds (the longest observed period for a pulsar being 8.5 s for the pulsar J2144-3933 [25])

Millisecond pulsars: Pulsars with periods less than about 10 ms. These are regarded as being re-cycled pulsars, having been 'spun-up' by accreting matter in a binary system

Young pulsars: Physically young pulsars, strong emitters in gamma radiation, notable examples including the Crab and Vela pulsars.

The physical properties of these pulsar classes appear on the whole to be remarkably similar, although they each have their own distinct identifying characteristics. The overview of pulsars contained in this Section will largely borrow from the *Handbook of Pulsar Astronomy*, (Lorimer & Kramer, [25]), with other references supplemented where required.

1.2.1 Structure

The physical structure of pulsars is still not well understood despite over four decades of research. Although a great deal of progress has been made, many key questions remain to be answered. An approximate 'toy' model of pulsar structure is displayed in Figure 1.3. In this model, the observed radio emission originates from one of two radio beams emerging from opposite sides of the neutron star along its *magnetic axis*. The neutron star rotates around a second axis with a regular period, causing the radio beams to sweep out a cone trajectory through space. If the path of this beam happens to cross the Earth, it can be detected as a regularly pulsing radio signal. This sweeping radiation pulse is often termed the *lighthouse effect*, as it is similar in some respects to the sweeping beam of light emitted by a lighthouse.

Some aspects of the pulsar model are described in more detail below:

Neutron Star: At the heart of every pulsar is believe to lie a neutron star, a mass of highly compressed degenerate material left behind after the previous supernova event of a massive star. Observations of glitches (a rotational instability which can cause a rapid change in pulse period, followed by a relaxation into the original behaviour, described in Section 1.2.2) in young pulsars indicates that the neutron star has a solid crust. Common models of neutron stars include a solid crystalline crust of iron nuclei and degenerate electrons with a density of $\rho \simeq 10^6$ g.cm^{-3}, followed deeper down by a neutron-rich inner crust, and finally a superfluid sea of free neutrons in the core regions, with a density of $\rho \simeq 2 \times 10^{14}$ g.cm^{-3}. It has been speculated that in extreme cases the core may contain free exotic matter, such as quarks [35].

The mass of the typical neutron star is believed to be approximately 1.4 solar masses (1.4 $M_\odot$), although this appears to be higher for re-cycled milliseceond pulsars as they draw mass from their binary companion. Estimates of a neutron star's radius are complicated by the thin plasma atmosphere believed to surround the star. The absolute limit of a neutron star's radius is that

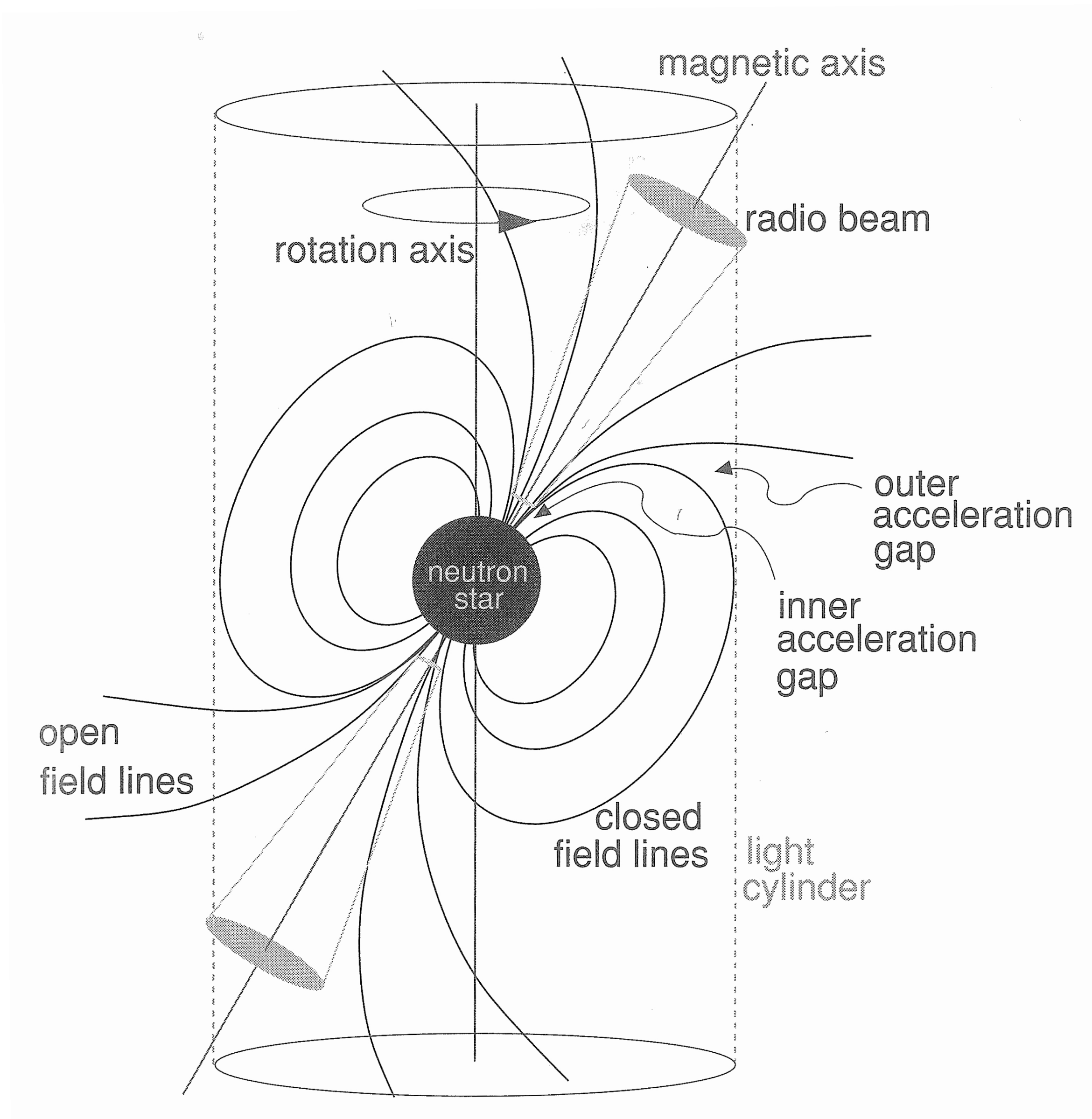

Figure 1.3: "Toy" model of a pulsar and its surrounding magnetosphere, showing features including the radio beam, open and closed magnetic field line regions, light cylinder, as well as the magnetic and rotation axes. Diagram from *Handbook of Pulsar Astronomy*, Lorimer & Kramer, p55 [25].

it must be greater than the Schwarzschild radius, the point at which an object collapses to form a black hole. This radius is given by

$$R_S = \frac{2GM}{c^2} \simeq 4.2 \text{ km} \left(\frac{M}{1.4 \text{ M}_\odot}\right). \tag{1.6}$$

Using arguments that the speed of sound inside the neutron star should be less than the speed of light, one can derive a better lower radius limit for the pulsar of

$$R_{min} \simeq 1.5 R_S = \frac{3GM}{c^2} = 6.2 \text{ km} \left(\frac{M}{1.4 \text{ M}_\odot}\right). \tag{1.7}$$

Similarly, by arguing that the radius must be small enough to prevent break-up against centrifugal force, one can obtain an upper radius limit of

$$R_{max} \simeq \left(\frac{GMP^2}{4\pi^2}\right)^{1/3} = 16.8 \text{ km} \left(\frac{M}{1.4 \text{ M}_\odot}\right)^{1/3} \left(\frac{P}{\text{ms}}\right)^{2/3}. \tag{1.8}$$

For a pulsar such as PSR B1937+21 (the first millisecond pulsar discovered, and covered in greater detail in Section 2.1.1), with a period of 1.56 ms and an assumed mass of 1.4 $\text{M}_\odot$, this gives a constrained radius of 6.2 km $\leq R \leq$ 22.6 km.

Magnetosphere: A neutron star may be viewed as a highly magnetised, rotating superconducting sphere although its magnetic axis almost never lies along the same axis as its rotation. A situation such as this gives rise to enormous electric and magnetic fields surrounding the pulsar. The high field strength also leads to the extraction of a plasma from the pulsar's surface, forming what is called the pulsar *magnetosphere*. The structure and behaviour of this magnetosphere and the magnetic field incorporated with it is highly complex, and after multiple attempts to derive suitable mathematical solutions to proposed models, no clear answers have presented themselves. However, this full analysis is beyond the scope of this thesis.

The plasma above the surface of the neutron star co-rotates with the star as it is influenced by the combined Lorentz forces of the electric and magnetic fields, and further away this plasma is from the pulsar, the faster it travel to match the pulsar's rotation. However, the velocity of this plasma is still limited by the speed of light, and so its domain is limited by an imaginary surface known as the *light cylinder*, aligned along the rotation axis of the pulsar and possessing a radius of

$$R_{LC} = \frac{c}{\Omega} = \frac{cP}{2\pi} \simeq 4.77 \times 10^4 \text{ km} \times \left(\frac{P}{\text{s}}\right) \tag{1.9}$$

where Ω is the angular frequency of the pulsar. Such a radius divides the pulsar's magnetic field lines into two regions, one where the lines are able to close within the confines of the light cylinder (closed field lines), and another where the lines do not close, terminating at R_{LC} (open field lines). The region on the surface of the pulsar defined by the open field line region is known as the *polar cap*, and is the source of the pulsar's radio beam. These feature is highlighted in Figure 1.3.

Radio beam: As noted, a pulsar's radio beam originates from the polar cap region, and is aligned with the pulsar's magnetic axis. It is generally accepted that this beam is cone shaped, and originates with plasma flows extending out from the surface of the pulsar along the open field lines. This plasma emits photons at a given given emission height, which continue away from the pulsar along a path tangential to the field lines, creating the shape of the radio cone. Emission at lower altitudes results in a narrower cone shape. As the pulsar rotates and the radio beam cuts the line-of-sight from an observer on Earth, a curved path is traced through the beam. The

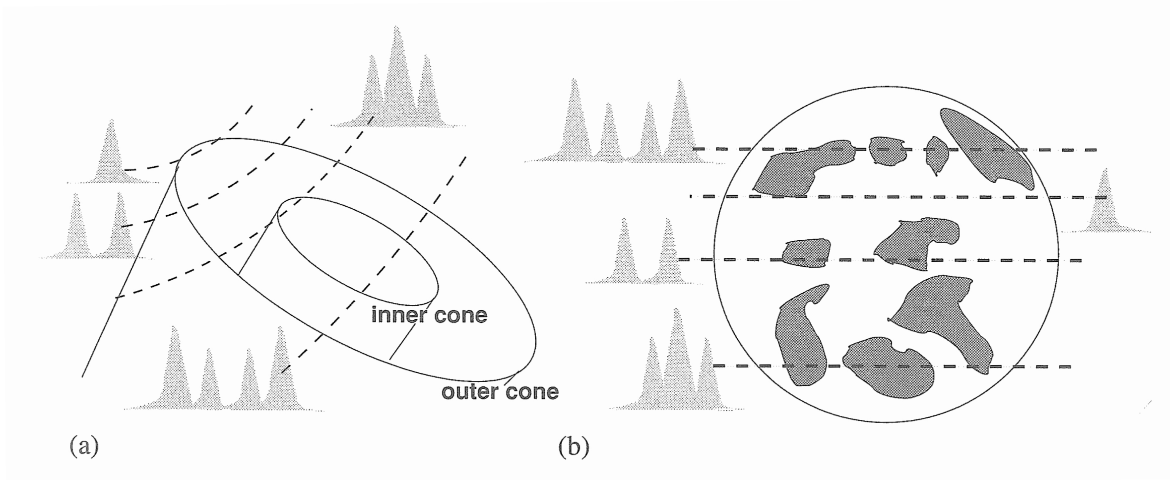

Figure 1.4: Diagram presenting two of the complex cone models described in Section 1.2.1. (a) shows the nested cone model, with several concentric cones of emission nested within each other. (b) shows the "patchy" cone model, where only certain irregular regions within the cone produce emission. The dotted lines show the pulse profiles that would be observed for different lines-of-sight cutting through the cone. Diagram from *Handbook of Pulsar Astronomy*, Lorimer & Kramer, p73 [25].

changing intensity of emission across this curved path generates the observed pulse profile.

The precise geometry and properties of the cone, as with the magnetosphere, is a subject of continuing study. It has been proposed that the central region of the emission cone, along the magnetic axis, is actully weaker than the surrounding radio beam. This model is used to explain the "double-peaked" or two-component models observed in some pulse profiles, which would be generated by the line-of-sight cutting through the middle of the radio beam. For single component profiles, according to this model the line-of-sight would only graze the outside regions of the cone. However, many pulsars have been observed with more than one or two simple components. For these pulsars, more complex models of the radio beam structure have been put forward. These include nested cone structures, where multiple radio cones are located concentrically inside one another, and a "patchy" cone model, where the interior of the radio beam is randomly filled with discrete regions of emission. These two models are shown in Figure 1.4.

1.2.2 Observational Properties

As noted, the primary observational feature of pulsars is their regular radio pulsations. However, pulsars also display several other key emmission characteristics that are useful in both identifying them and understanding their mechanics and underlying structure. Several of the most significant features are described below.

Integrated pulses: Despite the high degree of variability between individual pulses for a single pulsar in terms of both overall intensity and pulse shape, *integrated pulse profiles* at a given frequency remain relatively stable. These profiles are produced by integrating or *folding* several hundred to thousand individual pulses. These pulse shapes fall into a range of morphologies, from classical single Gaussian pulses to double-peaked pulses as well as more complicated, multiple component profiles. These pulse shapes can be used to infer information about the shape of the emission beam. Pulse shapes from normal and millisecond pulsars are not believed to vary significantly. A quantity known as the *duty cycle* can be defined which describes the amount of time that the pulsar is observed to be 'pulsing', i.e., the pulse width in the time domain divided by the pulsar's period,

$$DC = \frac{\text{pulse width}}{\text{pulsar period}}.$$

A typical pulsar has a duty cycle of $\sim 0.05 - 0.1$ [39], although this does vary, and pulsars have been observed to have duty cycles as high as ~ 1, indicating that the pulsar's rotational and magnetic axes are closely enough aligned (and pointing closely enough at Earth) so as to keep the Earth within the emission beam throughout the pulsar's period. Other integrated pulse shape features of note include their evolution over frequency, such as an increase in pulse width and component separation at lower frequencies, and the presence of *interpulses*, which are offset the main pulse by 180°, representing either the detection of the pulsar's opposite polar emission beam or the re-detection of an especially wide primary beam.

Individual pulses: Individual pulses are generally highly variable, and have an overall low flux, but for data sets with sufficient signal to noise many important features become visible. These include the presence of *microstructure*, short duration (on the order of μs) broadband quasi-periodic profile structure more dominant in normal pulsars, *giant pulses*, where pulses several orders of magnitude larger are detected in several key pulsars such as the pulsar associated with the Crab supernova remnant, *pulse nulling*, where a pulsar appears to 'switch off' for several pulse periods before continuing to pulse as normal, *sub-pulse drifting*, in which components of the pulse profile appear to drift across the profile at a fixed rate, and *mode changing*, in which the shape of the pulse profile can abruptly switch into a secondary 'abnormal' mode for short periods of time before returning to its 'normal' emmission mode.

Period fluctuations: The pulse period of any given pulsar appears to be constant over short time periods, and pulsar spin-down rates are well understood over much longer time scales. However, short-term irregularities can occur. One such irregularity is a phenomenon known as *glitching*. A glitch is a rotational instability which can cause a rapid change in pulse period, followed by a relaxation into the original behaviour. It is observed as the sudden early arrival of pulses from an otherwise stable pulsar, followed by an exponential decay into the pre-glitch pulsation rate. These glitches are thought to be caused by seismic events within the neutron star itself, with one model postulating the idea of 'starquakes' created by changes in the solid crust of the neutron star, much like their terrestrial equivalent. Another model explains these glitches as the result of eddys and vortices in the interior neutron superfluid.

Flux density spectra: Pulsar flux densities can be defined in two ways, the *peak flux density* (the maximum intensity of a pulse profile) and the *mean flux density* (the integrated intensity averaged over a single pulse period). At 1400 MHz, mean flux densities vary between 20 μJy and 5 Jy, with a mean of 0.8 mJy. It should be noted that the lower value of the flux is not due to any intrinsic physical characteristic of pulsars, but is instead due to the physical limitations in the sensitivity of our current instrumentation. The mean flux density also depends highly upon the frequency at which the pulsar is being observed. For most pulsars, this dependence can be approximated as a power law defined by a *spectral index* α such that

$$S_{mean}(\nu) \simeq S_0 \nu^{\alpha}. \tag{1.10}$$

Values for α can range between $-4 \lesssim \alpha \lesssim 0$, with a mean of approximately $\alpha = -1.8 \pm 0.2$ [38], which is considered unusually steep for astronomical sources [11]. Similarly, Manchester et al. 2005 ([46]) reports a range of $-3.5 \lesssim \alpha \lesssim +0.9$ with a median of -1.7. Only approximately 5-10% of pulsars require modelling using a two-component power law, the rest being able to be modelled with a single spectral index, and both normal pulsars and millisecond pulsars appear to fit into a similar range of spectral indices.

Dispersion: Pulse dispersion is an effect caused by the interstellar medium (ISM), and describes the way in which radio pulses observed at higher frequencies arrive earlier than their lower frequency counterparts. This delay is caused by the ionised component of the ISM, which results in the group velocity of a packet of radio waves over a range of frequencies becoming distributed in velocity, effectively 'smearing' the pulse as it propagates through the medium. The signal delay is inversely proportional to the frequency of the electromagnetic radiation. The amount of dispersion that occurs can be characterised through the constant of proportionality in this expression known as the *dispersion measure* (DM), which represents the integrated column density of free electrons along the line-of-sight to the pulsar. Hence,

$$\Delta t_\nu = \frac{\mathrm{DM}}{\nu}. \tag{1.11}$$

By the nature of its calculation, the dispersion measure is related to the distance between the observer (Earth) and the pulsar. One can write an expression for the dispersion measure as

$$\mathrm{DM} = \int_0^d n_e\left(x\right) dx \tag{1.12}$$

where d is the distance to the pulsar, and $n_e\left(x\right)$ is the free electron density as a function of position. If it is assumed that $n_e\left(x\right)$ is constant (only a very crude approximation), then it can be shown from Equation (1.12) that the distance is related to the disperion measure by

$$d \sim \frac{DM}{n_e}. \tag{1.13}$$

Scintillation: Scintillation is another phenomena caused by the transmission of the pulsar radiation through the ISM. The ISM is highly turbulent as well as being inhomogenous, and these irregularities can result in phase modulations which result in an apparent oscillation of the radiation seen by an observer. These oscilaltions can occur over several different timescales and bandwidths. Scintilation in the ISM is analogous to the 'twinkling' of stars as seen in optical wavelengths, caused by the non-uniformity of the Earth's own atmosphere.

Polarisation: A prominent feature of pulsar radio emmission is the relatively high fractional amounts of both linearly and circularly polarised radiation across a large number of pulsars. Pulsars are among the most polarised sources in our Galaxy, with the mean linear polarisation fraction lying at approximately 20% and the mean circular polarisation fraction lying at approximately 10% [4]. The amount of polarised flux does vary from pulsar, with some pulsars showing up to 100% linearly polarised flux in an individual pulse profile [5]. For example, the Vela pulsar, PSR B0833-45, displays almost total linear polarisation in its pulse profile.[30]. However, the polarisation across a single pulse can vary across a given pulse or from pulse to pulse. A common phenomenon is that of a changing polarisation angle (PA) over the space of a single pulse. Discontinuous jumps of 90° in the angle of linear polarisation are observed in many pulsars [79]. This in part has led to the development of the *rotating vector model*, which supports the concept of a cone shaped emission structure, and predicts a sharp S-shaped swing in PA as the observer's line-of-sight traces its trajectory through the emission cone, changing its orientation with respect to the magnetic axis and hence the observed linear

A similar phenomenon related to circular polarisation is that of *sense-change*. Circular polarisation, which describes light whose polarisation vector is continually and regularly oscillating, tracing out a circular trajectory in time as viewed along the direction of propagation, can be either left or right-handed, depending on the direction of motion of polarisation angle [19]. Pulsars classed as *symmetric* experiene the same hand of polarisation across the entire pulse profile, whereas pulsars classed as *anti-symmetric* experience a sense change near the center of the pulse

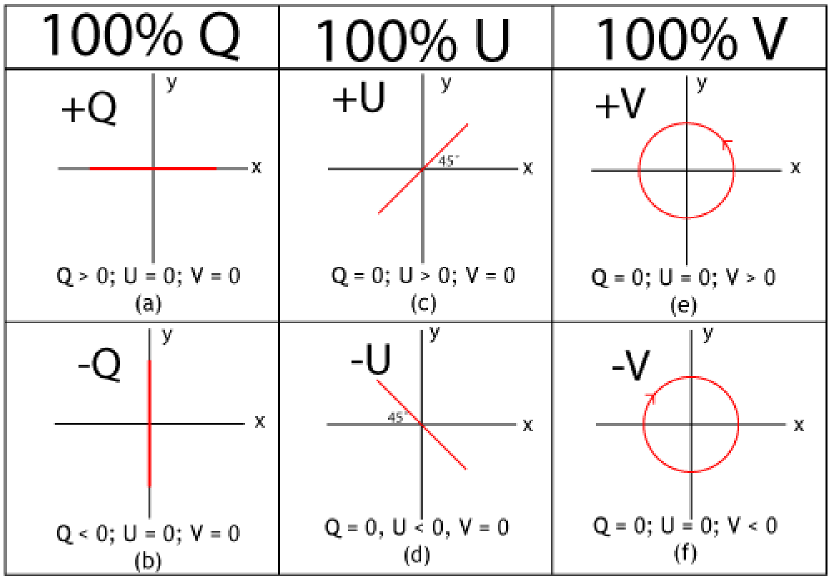

Figure 1.5: Schematic diagram of the Stokes Parameters related to polarisation. Image from Wikipedia [62].

profile [6]. Such changes in circular and linear polarisation, as well as ever-present noise and random oscillations in polarised flux, can lead to an overall reduction in the visibly polarised flux as seen in integrated, stable pulse profiles, and can present an even larger problem in the detection of these polarised fluxes in radio continuum surveys, where such oscillations are averaged over a period of several hours.

1.2.2.1 The Stokes Parameters

The Stokes Parameters are a system of four parameters used to describe the polarisation characteristics of electromagnetic radiation. If we have an electromagnetic wave seprated into two orthogonal components E_x and E_y, described mathematically by

$$E_x = e_x\left(t\right)\cos\left[\omega t + \delta_x\right]$$

$$E_y = e_y\left(t\right)\cos\left[\omega t + \delta_y\right]$$

then the four parameters, I, Q, U and V are defined as

$$I = \left\langle e_x^2\left(t\right)\right\rangle + \left\langle e_y^2\left(t\right)\right\rangle \tag{1.14}$$

$$Q = \left\langle e_x^2\left(t\right)\right\rangle - \left\langle e_y^2\left(t\right)\right\rangle \tag{1.15}$$

$$U = 2\left\langle e_x\left(t\right)e_y\left(t\right)\cos\left[\delta_x - \delta_y\right]\right\rangle \tag{1.16}$$

$$V = 2\left\langle e_x\left(t\right)e_y\left(t\right)\sin\left[\delta_x - \delta_y\right]\right\rangle \tag{1.17}$$

where the angled brackets indicate an average in time [61]. Qualitatively speaking, I represents the total flux, Q and U represent two different components of the linearly polarised flux, offset from each other by 45°, and V represents the total circualrly polarised flux. These quantities are represented schematically in Figure 1.5.

1.2.2.2 Rotation Measure

A further effect caused by propagation of electromagnetic radiation through the ISM is that of Faraday rotation, which is similar to dispersion in that it is a frequency dependent phenomenon (although it is often characterised using wavelength). Faraday rotation is caused by the difference in refractive index experienced by the two modes of circular polarisation, left and right, resulting in different propagation speeds for each mode [63]. This difference in speeds has an effect on the polarisation angle seen in linearly polarised flux, rotating it by an angle β. This angle is related to the wavelength of the radiation by

$$\beta = \mathrm{RM} \times \lambda^2$$

where RM is the *rotation measure*, given by

$$\mathrm{RM} = \frac{e^3}{2\pi m^2 c^4} \int_0^d n_e B_{||} dl$$

where n_e is the free electron density and $B_{||}$ is the magnetic field parallel to the direction of propagation of the electromagnetic wave. Theoretically, while the polarisation angle of linearly polarised flux will be affected by Faraday rotation, circularly polarised flux should remain unaffected.

1.2.3 Search Techniques

One of the key challenges with pulsar detection is being able to uncover a signal of unknown period, as well as an unknown dispersion measure, from a time series of radio data taken from a pointing (typically lasting $\sim 30 - 60$ minutes) with a single-dish telescope. This pointing effectively only looks at one 'pixel' on the surface of the sky (13 pixels in the case of the Parkes Radio Telescope, see Section 1.1.4). Knowledge of the pulse period allows for the folding and summation of a signal to form a reasonably coherent pulse profile, but for a pulsar this pulse must be visible over a wide frequency range, otherwise the signal may well be due to radio frequency interference (RFI). Knowledge of the dispersion measure allows for the signal dispersion over a range of frequencies to be effectively removed, allowing for the full pulse profile to be revealed if indeed one is present. Unless these two parameters can be accurately determined, a pulsar that exists in a given region of sky is likely to remain invisible. Hence, increasingly sophisticated techniques for pulsar searching have been developed. The techniques and methods of data reduction can vary greatly between observations, but a description of the typical steps involved is briefly presented below:

De-dispersion: This step involves producing modified time series of the recorded data, each one having been recalibrated using a wide range of trial dispersion measure values, so as to attempt to remove the effects of dispersion from the observed data. These time series can then be indepently searched for the presence of periodic radio pulsations. Various algorithms exist for performing de-dispersion including simple de-dispersion algorithms, which are based on the foundational principles of de-dispersion but require a computational power of the order of n_{chans}^2 for every n_{chans} time samples, and the tree de-dispersion algorithm, which improves the computational effieicncy to an order of $n_{chans} \log_2 n_{chans}$. The effectiveness of both these algorithms depends highly on the choise of step size in trial DM values, and the proximity of tested DM values to the true DM value of the pulsar.

Barycentric correction: In order to accurately time a pulsar, corrections must be made to take into account the motion of the Earth, or more precisely, the relative motion between the target object and the observer. This is not normally a problem for typical pulsar observations, which last ~ 30 minutes, for but extneded observations this correction is vital. Corrections are usually made with respect to the solar system barycenter, and involve appropriately modifying the arrival times of the received measurements.

Fourier analysis: Once the data has been appropriately calibrated, a Fourier transform is then applied to search for periodic signals. Given a discrete de-dispersed time series of τ_j with N data points, the basic discrete Fourier transform is given by

$$F_k = \sum_{j=0}^{N-1} \tau_j \exp\left(-\frac{2\pi ijk}{N}\right) \tag{1.18}$$

where for each k component, the corresponding frequency $\nu_k = \frac{k}{T}$, where T is the total time of the observation. Should a pulse be present at a particular frequency, application of the Fourier transform should produce a strong Fourier signal at the corresponding k component to that frequency. An example of a detected pulse using a Fourier transform can be seen in Figure 1.6. Once a candidate period has been determined, the Fourier transformation can be used in order to reproduce the original profile of the candidate pulsar signal.

Candidate selection: Following this process, a number of candidates will have been identified, each with varying dispersion measures, pulse periods and signal-to-noise ratios. A real pulsar will ideally appear multiple times in this candidate list with similar parameters in each case, the one with the highest signal-to-noise ratio being the closest representation of the true pulsar. Further stages of analysis are then required to verify the accuracy of the detected pulsar signal.

In addition to the question of how to detect pulsars, there remains the problem of determining which regions of the sky to survey. Theoretically, pulsars can be detected in any part of the sky, but the vast majority of normal and yonuger pulsars are found in or around the Galactic plane. This is primarily due to the fact that pulsars originate from dying stars, hence they will be detected in regions with the highest concentrations of stellar activity. For this reason, previous pulsars surveys have often focused on regions of low Galactic latitude. This brings with it however the problem of seeing through the background effects imposed on observations by electromagnetic radiation recieved from other Galactic sources. Attempts to avoid this contamination have pushed standard Galactic pulsar searches into the region of 1400 MHz. Likewise, millisecond pulsars, given their age, are often found at greater distances from the Galactic plane, as they have existed for a sufficient time that their relative velocities have allowed them to travel large distances from their points of origin.

Generally, these pulsar searches are untargeted, however, there are specific examples of ways in which pulsars searches can be intelligently focused on certain regions. Given that pulsars are born from supernova, many searches have chosen to search for pulsars in the interiors of supernova remnants. Also, globular clusters are known as breeding grounds for millisecond and binary pulsars, so another strategy in pulsar detection is to specifically survey globular clusters.

1.3 Continuum Imaging Surveys

Radio continuum surveys are means by which deep observations of wide areas of sky can be produced in a relatively short amount of time. As opposed to pulsar observations, which are performed through the use of a single-dish, continuum surveys employ the use of interferometric telescopes to obtain wide fields of view of the sky with the much higher resolution provided by the extended baseline. Such surveys are normally carried out over an extended period of time, and key examples of recent radio continuum surveys can be seen in Section 2.2.

Several key differences exist between the single-dish time series observations common to pulsar surveys and radio continuum surveys. The primary and most apparent of these is the fact that in continuum surveys observational data is averaged in time, rendering the information critical to pulsar detection (the ability to extract pulse profiles from time series) unusuable. This integration in time is performed

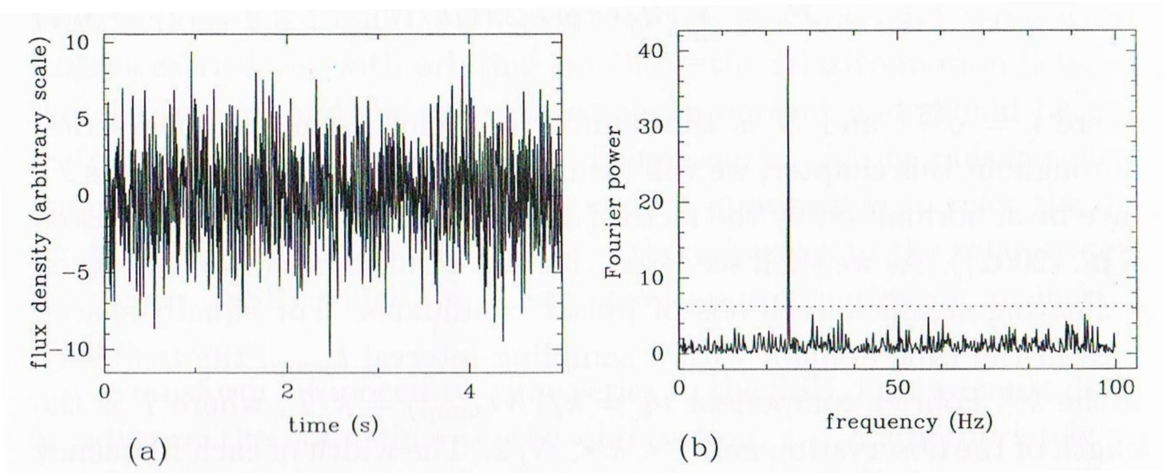

Figure 1.6: Diagram presenting the initial results of a Fourier analysis. Plot (a) shows a noisy time series containing a 25 Hz signall, while plot (b) shows the same data after a Fourier transform has been applied. Note the strong spike at 25 Hz, indicating the detection of the periodic signal. Diagram from *Handbook of Pulsar Astronomy*, Lorimer & Kramer, p134 [25].

due to the fact that these surveys are carried out through the use of interferometers. Inherent in the design of most interferometers is the need for extended observations in order to be able to properly simulate a full telescope of matching diameter and obtain optimal resolution. Also, continuum surveys by their very design aim to uncover large amounts of radio sources [65], which often requires integrating extended observations of the same area of sky in order to uncover sources with lower levels of radio flux. It is due to this primary point of difference that radio continuum surveys are not typically suited for use in pulsar detection. However, there are exceptions to this rule, which will be further explored in Chapter (2).

1.4 Thesis Aims

The primary aim of this thesis is to investigate, analyse, evaluate and recommend new methods and techniques by which pulsars may be more effectively discovered through the use of radio continuum surveys. To achieve this goal, two different sub-projects are to be conducted, both with similar and complementary aims.

The first sub-project aims to analyse Parkes Radio Telescope data taken of 17 infrared-faint radio sources (IFRS) detected as part of the Australia Telescope Large Area Survey (ATLAS), the forerunner continuum survey to the future EMU and POSSUM surveys to be conducted using ASKAP. These sources were selected for analysis based upon criteria intended to be further investigated in the second sub-project, hence any detection or non detection of pulsars will be useful in shaping the direction of this second stage of investigation.

The second sub-project aims to study the population statistics of pulsars in continuum surveys against those of background radio sources in order to determine new source selection criteria that can be employed to select and refine pulsar candidate sourcs from continuum surveys, with particular application to the EMU and POSSUM surveys. These two surveys are expected to produce on the order of millions of sources, and so discovering new methods of cutting down the number of sources that warrant investigation as pulsars will be critical if future continuum surveys are to be harnessed as a means of detecting new and unusual pulsars.

Chapter 2

Literature Review

2.1 Pulsar Searching using Continuum Surveys

As described in Section 1.2.3, pulsars are normally discovered through the use of single-dish telescopes in untargeted searches for pulsations [21], with a dispersion measure and Fourier analysis used in order to determine if a candidate target is indeed a pulsar [25]. However, this is not the only technique that has been used to find discover new and interesting pulsars. A very small handful of pulsars have been found through the analysis of targets discovered from radio continuum imaging surveys and related work, despite the apparent difficulties presented in Section 1.3.

It is already known that many previously discovered pulsars are visible in existing continuum surveys. The source catalogs of both the NRAO VLA Sky Survey (NVSS, see Section 2.2.1) and the Westerbork North Sky Survey (WENSS, see Section 2.2.2) have been cross referenced with known pulsar positions, with numerous positive detections having been made. Kaplan et al, 1998 ([3]) were able to cross reference 73 NVSS sources with known pulsars, while Han & Tian, 1999 ([1]) were able to increase this number by another 24. Likewise, Kouwenhoven, 2000 ([8]) was able to match 39 WENSS sources to known pulsar positions, 19 of these pulsars also belonging to the collection confirmed by Han & Tian. However, none of these efforts discovered any new pulsars through use of the continuum surveys they studied.

Continuum surveys remove the key marker of a pulsar (its periodic pulsations) by their very nature, hence rendering this feature useless [22]. Therefore, we need other useful indicators of pulsars that will still remain detectable in a continuum survey. Previous attempts to detect pulsars using radio continuum imaging have focused on several common pulsar features including flux intensities, compactness, spectral indices as well as linear and circular polarisation. Many of these characteristics have been described more fully in Sections 1.2.1 and 1.2.2

As described by Navarro et al, 1995 ([21]) searching for pulsars using continuum techniques also presents several distinct advantages over single-dish search techniques, despite the indisputable productivity of the latter method. For single-dish pulse surveys, three main selection effects exist that may prevent pulsar detection:

- The pulsar period must be at least twice that of the spectral channel sampling rate so as to avoid aliasing (and in practice, the period must usually be $4 - 8$ times greater than the sampling rate)
- Pulse smearing across channels sets an upper limit on the value of DM/P, where DM is the pulsar's dispersion measure and P is the pulsar's period. This upper limit effectively rules out an entire region of possible pulsars.

- Pulsars in tight binary systems can undergo rapid changes during a period of a single-dish observation, compromising its apparent periodicity and making such pulsars much harder to detect via conventional methods.

However, continuum techniques are not enough to confirm the presence of a pulsar. They can only guide further and more rigorous single-dish pulse searches by selecting targets for detailed observation and analysis.

Four key examples of pulsars initially discovered using continuum techniques include B1937+21, the first ever millisecond pulsar discovered [20], B1821-24, found during a VLA imaging search of globular clusters [22], B1951+32, initially identified as a steep-spectrum polarised point source central to the supernova remnant CTB 80 [23], and J0218+4232, originally uncovered by the Westerbork Synthesis Radio Telescope (WSRT) [21]. Note that in some of these cases, particularly B1937+21, pulse searches of their respective regions had already been carried out, and these pulsars had been missed.

2.1.1 Case study: B1937+21 - the First Millisecond Pulsar

The discovery of the first millisecond pulsar, B1937+21, originated with a search for the explanation of the unusual radio features of the source 4C21.53 [20]. The source was known to display interplanetary scintillations (IPS) at 81 MHz, indicating structure on a scale below 1 arcsecond, and also possessed an unusually steep spectrum, with a spectral index of $\alpha = -2$, both of which pointed to the existence of an undiscovered pulsar. Such a pulsar may not have been discovered earlier due to pulse broadening due to interstellar scattering. An upper limit placed on this scattering by the IPS constrained the period of any pulsar present to be $P \leq 10$ ms. In an effort to reduce pulse broadening, observations were carried out in 1979 at centimeter wavelengths using the Arecibo Observatory and Owens Valley Radio Observatory, but without success.

Further continuum images of the region were taken through the period of 1980-82, most notably using the VLA and WSRT. Both of these surveys identified the compact component of the object, 4C21.53W as a steep-spectrum source, including at decametric wavelengths, which combined with an anlysis of WSRT polarisation maps in September 1982 showing strong linear polarisation at the position of the object rekindled the pulsar search in the region. A series of measurements taken using the Arecibo telescope finally confirmed the presence of the pulsar in November 1982, with a flux density of approximately 0.017 Jy at 1415 MHz and a period of ~ 1.558 ms.

There are several key lessons to take away from this example:

- B1937+21 was originally missed by conventional pulsar searching techniques due to the pulsar's low average flux, small period, pulse broadening and short-term variability (in the first positive Arecibo detection, the detected signal was only visible for 3 minutes out of a 7 minute observation period, and was not detected during a second observation shortly thereafter), as well as other technical limitations
- The key observational factors used to isolate the candidate pulsar were its unusually steep spectrum (although quite common among pulsars), high linear polarisation and its compact size.
- Although it was up to the Arecibo telescope to perform the final detections and confirmation of the pulsar, continuum images (particularly those taken with the WSRT) were critical in identifying 4C21.53W as a candidate for a new pulsar.

2.1.2 Failed attempts

The majority of past attempts to specifically apply the technique of continuum detection of pulsars have unfortunately been unsuccessful. In 1985, spurred on by the discovery of B1937+21, Hamilton et al ([22]) conducted a search for pulsars in globular clusters after speculation that low-mass X-ray binaries (LMXB's), a class of object dominantly found in the core regions of globular clusters, were likely progenitors of millisecond pulsars. Searches were conducted using the VLA at 1465 MHz across 12 globular clusters above $\delta = -40$, with a distance no greater than 10 kpc, and achieved an rms noise level of ~ 0.2 mJy with a detection threshold of $\lesssim 1$ mJy. 21 radio sources were detected with 10 core radii of the center of the clusters, with one source detected in the globular cluster M28 lying within 1 core radius. These populations showed no significant statistical features to highlight the presence of new pulsars. Further examination using linear polarisation data was also inconclusive. Data taken at 6cm was used to calculate the spectral indices of four targets. Three showed indices of $\sim 0.1 - 0.6$, normal for extragalactic sources [36]. The fourth target (the M28 core detection), was not visible at 6cm, leading to a lower limit of $\alpha > 1.09$. This, combined with the an upper linear polarisation limit of 30% led to the target being isolated for further study, and it was eventually found to be a pulsar, B1821-24, however many more were expected to be detected.

A number of attempts have also been made using the NVSS data (see Section 2.2.1). In a three paper series, Kaplan et al, 2000 (Paper I - [11]) used NVSS data in conjuction with observations taken from the Texas 365 MHz survey. The Texas survey limited the search region to $-35°30' \leq \delta \leq 71°30'$, with 30,000 objects common to both surveys lying within this region. Targets were chosen on the basis of a steep spectral index ($\alpha \geq 1.5$), compactness ($\theta \leq 25$") and integrated fluxes ≥ 2.5 mJy for the NVSS and ≥ 200 mJy for the Texas survey. The positional offset was also required to be less than 3 times the quadratic sum of the individual positional uncertainties. These criteria selected 74 targets for further study, 6 of which coincided with known pulsars and one with a high-redshift galaxy. Of the remaining 67 targets, the majority were found to be high-redshift extragalactic sources (probably radio galaxies) after further morphology studies were conducted using follow-up data from the VLA (Kaplan et al, 2000, Paper II - [37]). Up to 16 of the sources remained unresolved and, although unlikely, their potential as candidates for undiscovered pulsars has not yet been ruled out. Further analysis of these sources was to be provided in Paper III of the series, but this was never published.

Another NVSS data anlysis was made later in the same year by Crawford et al, 2000 ([9]), this time in conjunction with data taken as part of the FIRST (Faint Images of the Radio Sky at Twenty centimeters) survey. This survey focused on the north and south Galactic caps, was conducted using the VLA at 1400 MHz and spanned a region between and $7^h < \alpha < 18^h$ and $28° < \delta < 42°$. Pulsar targets were selected from both surveys as objects with a flux of ≥ 1.5 mJy, with a linearly polarised flux component $\geq 5\%$. The angular resolution of FIRST is greater than that of the NVSS, hence extended sources will show a smaller flux in the FIRST survey. Therefore, for sources occuring in both catalogs, only those sources with stronger NVSS fluxes, or whose NVSS flux agreed to within a few percent of their FIRST flux were included. This helped to eliminate extended sources, however, it does rule out scintillating pulsars whose flux happened to be weaker during the FIRST observations. For those NVSS sources without matching FIRST data, follow-up observations equivalent to FIRST were taken with the VLA. Overall, 92 candidates were selected as possible pulsars, and were then observed using the Lovell Telescope at the Jodrell Bank Observatory at a frequency of 610 MHz. However, no significant pulsations were detected.

This second NVSS study is particularly useful in that it discusses potential reasons as to why the study failed to make any pulsar detections, despite the identification of 92 reasonable candidates, and whether these reasons actually contributed to the non-detection result. These reasons include:

- A lack of flux at 610 MHz. With a typical pulsar spectral index of $\alpha = 1.6$, a minimal flux of approximately 58 mJy would be expected at 600 MHz given the minimum flux requirement of 1.5 mJy at 1400 MHz. This limit is well above the detection limit for the Lovell Telescope.

- Dispersion smearing and scattering effects distorting any periodic signal. However, given the high galactic latitude of most sources, this is not thought to be a significant factor.

- A wide pulsar beam reducing the ability to modulate any periodic signal. However, this would likely only occur for an aligned rotator (i.e., one whose spin and magnetic axes are aligned and pointing towards the observer), but such systems would not likely not display signifcant integrated linear polarisation and hence would not have been selected as targets to begin with.
- Scintillations in pulsar flux, expected to only be a factor in a small number of candidates.

However, most of these issues are related primarily to the follow-up work performed using the Lovell Telescope, as well as other standard single-dish pulsar searches. Furthermore, most of these potential problems were identified as being of minimal significance to the non-detection result, reinforcing the paper's conclusion that the population of 92 sources is not one of pulsars. This raises the question of why the initial target selection criteria did not produce any viable pulsars candidates.

2.2 Survey Details

Below are described the fundamental parameters of the continuum radio surveys most important to this project. This is followed by the a tabular summary of each survey's critical parameters in Table (2.1).

2.2.1 NRAO VLA Sky Survey (NVSS)

The NVSS was conducted using the Very Large Array (VLA) radio telescope in New Mexico, a tri-axis interferometer consisting of 27 antennas, between September 1993 and October 1996. Observations were taken at 1.4 GHz (20 cm), and the survey covered the entire region of sky with J2000.0 $\delta \geq -40°$. Data was taken using the compact VLA antenna configurations D and DnC, and recorded both total continuum intensity (Stokes I) and orthogonal axes of linear polarisation (Stokes Q and U). The survey produced some 2326 $4° \times 4°$ image cubes, the third axis storing linear polarisation data. The resolution of the survey (beamsize) was 45 arcminutes, with an achieved noise level (rms) of $\sigma \approx 0.45$ mJy beam^{-1} at ≈ 0.14 K for Stokes I and $\sigma \approx 0.29$ mJy beam^{-1} at ≈ 0.09 K for Stokes Q and U.

In addition to this image data, a source catalog was produced containing nearly 2×10^6 objects with fluxes over 2.5 mJy (approximately $5\sigma_{rms}$). The positional uncertainty for a strong source is on the order on 1 arcsecond. More details of the NVSS and the NVSS Source Catalog may be found in Condon et al. 1998 ([2]) and the Catalog Description ([28]).

2.2.2 Westerbork North Sky Survey (WENSS)

The WENSS was conducted using the WSRT, a single-axis 14 antenna interferometer located near the village of Westerbork in the northeastern Netherlands. Observations were taken at both 325 and 609 MHz across the region of sky with J2000.0 $\delta > 30°$(limited to a galactic latitude of $|b| > 20°$ for 609 MHz). 80 different evenly spaced fields were observed over the course of several 12 hour synthesis observations using different array configurations to produce images mosaics. All four Stokes parameters, I, Q, U and V were recorded. Final image maps were released in $6° \times 6°$ frames, with a resolution of 54 arcseconds at 325 MHz and 28 arcseconds at 610 MHz. The limiting flux density for source detection was 18 mJy for 609 MHz and 15 for 325 MHz. More details on the WENSS may be found in Rengelink et al, 1997 ([15]).

2.2.3 Australia Telescope Large Area Survey (ATLAS)

ATLAS is a deep-field survey conducted using the Australia Telescope Compact Array (ATCA) (see Section 1.1.3). The survey encompasses the Chandra Deep Field South (CDFS), which covers the region of the sky between right ascensions 3h : 26m $< \alpha_{J2000} <$ 3h : 36m and declinations $-29°00' < \delta_{J2000} < -27°12'$, and the European Large Area ISO Survey - South 1 (ELAIS-S1), which covers the region of the sky approximately between right ascensions 0h : 29m $< \alpha_{J2000} <$ 0h : 40m and declinations $-44°40' < \delta_{J2000} < -42°45'$. The CDFS also includes the Great Observations Origins Deep Survey (GOODS) field. Surveyed areas were chosen to coincide with the Spitzer Wide-Area Infrared Extragalactic Survey (SWIRE). These fields have corresponding deep optical, near-infrared, far-infrared and in some cases deep X-ray coverage, providing a large multi-wavelength suite of data for the entire region. Data was recorded using two 128 MHz bands centered at 1344 and 1472 MHz, with 33 channels per band and a FWHM of 35". All four Stokes parameters were recorded [57][42].

2.2.4 Evolutionary Map of the Universe (EMU)

The EMU survey is one of the primary science projects approved for the upcoming Australian Square Kilometer Array Pathfinder (ASKAP) telescope (see Section 1.1.5). Two different stages of EMU are planned, EMU-wide and EMU-deep [65] A full technical description of the survey may be found in Section 4.1, although the basic parameters are outlined in Table 2.1. The primary scientific goals of EMU include tracing the evolutionary stages of star-forming galaxies, understanding the role that black holes play in star formation, studying the distribution of radio sources and large scale structure of the Universe, and discovering new classes of object [65].

2.2.5 Polarisation Sky Survey of the Universe's Magnetism (POSSUM)

As with EMU, the POSSUM survey is another of the primary science projects approved for ASKAP, although it has not been guaranteed the same level of support as EMU [74]. The survey is intended to work in close partnership with EMU, and will provide full polarisation data to complement the total flux meausrements provided by EMU (Hobbs, 2010, pers. comm. 11 November). Three stages of the POSSUM survey are currently planned. POSSUM-wide and POSSUM-deep are to match the planned EMU-wide and EMU-deep surveys, and an additional POSSUM-diffuse survey has also been proposed. A full technical description of the survey may be found in Section 4.1, although the basic parameters are outlined in Table 2.1. The primary scientific goals of POSSUM include determining the 3D geometry of the Galaxy's magnetic field and mapping the Faraday rotation (and hence rotation measure) of 3 million extragalactic radio sources[74].

	NVSS	WENSS		ATLAS	EMU	POSSUM
Frequency (MHz)	1400	609	325	~ 1400	1400	1400
Sky Coverage	$\delta > -40°$	$\delta > 30°$ $\lvert b \rvert > 20°$		see Section 2.2.3	$\delta < 30°$	$\delta < 30°$
Lim. Flux density ($5\sigma_{rms}$, mJy)	2.5	18	15	0.15	0.01	0.01
Resolution	45"	28"	54"	35"	10"	10"
Positional Uncertainty	1"	1.5"		Unkown	Unknown	Unknown
Polarisation	I, Q, U	I, Q, U, V		I, Q, U, V	I	I, Q, U, V

Table 2.1: Table comparing the major surveys described in this paper. The details provided for EMU and POSSUM are still under review and may be subject to change. Structure modelled on Rengelink et al, 1997 ([15]), Table 1

Chapter 3

Analysis of the Infrared-Faint Radio Sources (IFRS)

This work for this chapter was conducted in collaboration with M. Keith, G. Hobbs, R.P. Norris, M.Y. Mao and E. Middelberg, and is the subject of a paper submitted to the *Monthly Notices of the Royal Astronimcal Society* (MNRAS). The submitted version of this work may be viewed in Appendix (B)

3.1 Discovery of the IFRS

Infrared-Faint Radio Sources (IFRS) are radio sources which have typicl flux densities of several mJy at 1.4 GHz but have no corresponding infrared counterparts at 3.6 μm in observational data with μJy sensitivities taken with the Spitzer Space Telescope (see Section 3.1.1)[42]. They were an unexpected discovery in ATLAS (see Section 2.2.3 for details of ATLAS). There are currently approximately 50 IFRS in ATLAS, and they account for 2.5% of the current ATLAS source catalog. All of the IFRS are unresolved at 1.4 GHz and have flux densities of up to tens of mJy.

The primary goals of ATLAS are to trace the cosmic evolution of active galactic nuclei (AGN) and star-forming galaxies. The sources expected to be found during the course of the survey have relatively well known spectral energy distributions (SEDs) that, for any strong radio source, predict infrared emission detectable by Spitzer. This expectation of infrared detection is reinforced by the existence of a strongly observed radio-FIR (faint infrared) correlation function, as detailed in Yun et al. 2001 ([43]). However, even after stacking multiple 3.6 μm images taken by Spitzer, the IFRS could not be detected in the infrared region of the spectrum [42].

Since the discovery of IFRS in 2006, several publications have attempted to understand their nature and emission mechanisms. Very long baseline interferometry (VLBI) observations of a total of six IFRS by Norris et al. 2007 ([44]) and Middelberg et al. 2008 ([27]) have resulted in the detection of high-brightness temperature cores in two IFRS. A recent study of four IFRS (not included in this study) by Huynh et al. 2010 ([26]) concluded that their target objects were likely to be non-galactic sources. Ultra-deep Spitzer imaging had become available for these sources, and the study attempted to fit template SEDs corresponding to known classes of galaxies and quasars to the IFRS. Norris et al. 2010 ([53]) have extended this work using deep imaging data from the Spitzer Extragalactic Representative Volume Legacy Survey project [52], and have shown that most IFRS sources can be fitted by SEDs typical of high-redshift radio-loud galaxies or quasars. They also determined a median 3.6 μm flux density of the IFRS as 0.2 μJy. Middelberg et al. 2010 ([51]) have found that the spectra of many of the IFRS are remarkably steep, with a median spectral index of $\alpha = -1.4$ and a prominent lack of spectral indices greater than -0.7, leading to speculation about their possible identification as pulsars.

However, the nature of the IFRS remains unclear, largely because they simply cannot be detected by even the most sensitive optical/infrared observations. While at least some are likely to be high-redshift radio galaxies or quasars, it is likely that the class may encompass several different types of object. A brief summary of the proposed candidate objects for the IFRS include very high redshift AGNs, heavily obscured radio AGN, stray radio lobes, radio relics and radio pulsars [42][44][27][45]. Norris et al. 2007 ([44]) propose that the IFRS may even represent a stage of AGN evolution.

3.1.1 The Spitzer Space Telescope

Launched in 2003, the Spitzer Space Telescope is the fourth and last of NASA's Great Observatories, along with the Hubble Space Telescope, the Chanda X-Ray Observatory and the Compton Gamma Ray Observatory (now de-orbited) [48]. The telescope is designed to observe at infrared wavelengths, and is equipped with three on-board instruments, IRAC, IRS and MIPS [47][49]. Both the IRAC and MIPS instruments were used in the discovery and analysis of the IFRS, and are described below:

IRAC The Infrared Array Camera is capable of observing simultaneously at 3.6, 4.5, 5.8 and 8 μm. The instrument has a 5.2 arcminute square field of view with a pixel count of 256×256, and observes two fields simultaneously, with their centers separated by approximately 6.5 arcminutes.

MIPS The Multiband Imaging Photometer for Spitzer has three detector arrays that observe in the far-infrared, centered at 24, 70 and 160 μm. All three arrays observe simultaneously, with fields of view of 5 square arcminutes, 2.5×5 square arcminutes and 0.5×5 square arcminutes respectively.

3.2 Motivation

The reason we have chosen to observe and analyse the IFRS as part of this thesis is because there is a considerable possibility that some of them may be pulsars, despite the increasing evidence that many of them will be extragalactic in nature. Given that ATLAS is a radio continuum survey as well as the predecessor to the EMU survey, investigating a sample of the IFRS chosen using the selection criteria described in Section 2.1 should provide a useful test of how well these criteria, when applied to a deep radio survey, actually perform in the selection and identification of viable pulsar candidates. The results of the analysis, should they result in a detection or non-detection, will then be able to help shape the next stages of our investigation into appropriate pulsar selection criteria for the EMU and POSSUM surveys.

A rough application of these criteria allow for the selection of 19 of the IFRS, whose measured flux densities and spectral indices are consistent with those measured for pulsars in our own galaxy. As the ATLAS surveys are well away from the Galactic plane, it is unlikely that all 19 of these sources actually are pulsars, but it is possible that some are. If so, it is important to identify them so that (a) they can be removed from the extragalactic source statistics, and (b) so that they can be accounted for in models of pulsar populations. If a significant fraction of putative extragalactic radio sources are pulsars, then it is important to identify them so that they do not contaminate radio source count statistics, which are used as a tool to understand the cosmic evolution of star-forming galaxies and AGN.

However, it is difficult to estimate how many pulsars would be expected to be found in any given region of the sky, particularly at any considerable distance away from the Galactic plane. The most recent pulsar surveys have covered regions close to the Galactic plane (eg, Manchester et al. 2001 ([40])), but while these surveys discovered a large number of new pulsars, they discovered only a relatively small number of new millisecond pulsars. The Galaxy is likely to contain similar numbers of both regular and millisecond pulsars [54], but the millisecond pulsars are likely to have travelled significant distances from the Galactic plane and are difficult to find due to their relatively low luminosities, fast spin rates and because they are commonly in binary systems, which disrupts the periodicity of their emitted pulses and affects their ability to be detected in conventional pulsar searches, as descibed in Chapters (1) and (2). The only deep, 20cm pulsar survey that covers a large area that is a considerable distance from the Galactic plane is the Parkes High Latitude Survey, which covers the Galactic longitudes $220° < l < 260°$ and latititudes $|b| < 60°$ [56], with 6456 pointings of 265 seconds each. The survey detected 42 pulsars with a flux sensitivity of ~ 0.5 mJy. Even though this survey made relatively few new pulsar discoveries, the pulsars it detected away from the Galactic plane were of great astrophysical interest, including the first double pulsar system PSR J0737-3039 [55] as well as three other millisecond pulsars. Burgay et al. 2006 ([56]) discussed the Galactic latitude distribution of their detections in detail, and suggested a roughly uniform distribution. However, their survey was relatively insensitive to millisecond pulsars, because of the restricted sampling time and number of frequency channels, and so the total number of millisecond pulsars detected was small. Hence, it is currently impossible to make a reasonable estimate of the number of pulsars likely to be detected per square degree at high Galactic latitude. Any detections of the IFRS as pulsars will help to increse the understanding of this distrubution, and so this adds a further motivation to this study.

3.3 Observations

19 of the IFRS were selected for observation, based upon their flux densities and spectral indices falling into the ranges typical of pulsars. The full details of each of the IFRS as recorded by the ATLAS survey may be found in Table 3.1, and their positions are shown in Figure 3.1. The sources range from bright to weak (0.5 mJy to 26.1 mJy) and from very steep to almost flat spectral indices ($\alpha = -2.4$ to -0.2). As described in Section 1.2.2, these values sit well within the observed properties of pulsars at 1400 MHz. However, the density of IFRS in the two ATLAS fields is much larger than would be expected at this Galactic latitude if they were all pulsars.

Observations of the chosen IFRS were taken in May of 2009 using the Parkes 64-meter radio telescope equipped with the 20-cm 13-Multibeam Receiver and the Berkeley-Parkes-Swinburne Recorder (BPSR) (see Section 1.1.4). The observing setup is almost identical to the High-Time resolution survey by Keith at al. 2010 ([41]). Data was recorded for all 13 beams of the Parkes Multibeam Receiver for each of the IFRS, although only the data for the central primary beam was required. The full parameters of our observing setup are recorded in Table 3.2. Data was recorded to magnetic tape for later offline processing, and was later transferred to a series of external hard drives. It was processed using the HITRUN pipeline, as detailed in Section 3.4.1, in order to search for periodic signals in dedispersed time series using trial dispersion measures between 0 and 1000 cm^{-3}pc.

3.3.1 Theoretical Sensitivity

We can determine the theoretical sensitivity of the observations taken using the *radiometer equation*, which gives the fundamental limiting flux of the central beam of a radio telescope, and is defined as

$$S_{min} = \frac{\sigma\,(T_{sys} + T_{sky})}{G\sqrt{2B\tau_{obs}}} \times \sqrt{\frac{W}{1-W}}. \tag{3.1}$$

In equation (3.1), σ is the minimum acceptable ratio of signal to noise (S/N) for a positive signal detection, T_{sys} is the system noise temperature of the telescope system, T_{sky} is the sky noise temperature

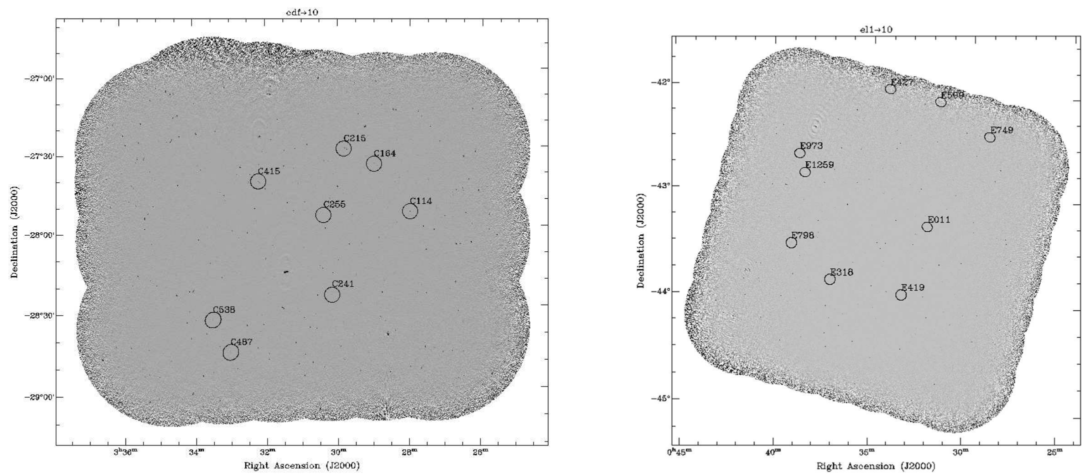

Figure 3.1: Plots showing the positions of our chosen IFRS within the two ATLAS fields, CDFS (left panel) and ELAIS-S1 (right panel). The circles show both the positions of the IFRS and the size of the beams that were surveyed for pulsars. Note that while Table 3.1 contains 19 IFRS, the two fields only contain the 17 sources that were used in the final analysis. For further details, see Section 3.4.1.1.

Source	Right ascension (hms)	Declination (dms)	Flux Density (mJy)	Spectral Index
ES011	00:32:07.44	-44:39:57.8	9.5	-1.44
ES318	00:37:05.54	-44:07:33.7	2.0	-0.78
ES419	00:33:22.80	-43:59:15.4	4.4	-1.35
ES427	00:34:11.59	-43:58:17.0	22.3	-1.08
ES509	00:31:38.63	-43:52:20.8	22.7	-1.02
ES749	00:29:05.23	-43:34:03.9	10.3	-1.08
ES798	00:39:07.93	-43:32:05.8	11.7	-0.81
ES973	00:38:44.14	-43:19:20.4	11.6	-1.15
ES1259	00:38:27.17	-42:51:33.8	4.5	
CS114	03:27:59.89	-27:55:54.7	7.7	-1.34
CS164	03:29:00.20	-27:37:54.8	1.6	-0.92
CS194	03:29:28.59	-28:36:18.8	7.0	-1.12
CS215	03:29:50.02	-27:31:52.6	1.6	-0.76
CS241	03:30:10.22	-28:26:53.0	1.6	-1.96
CS255	03:30:24.08	-27:56:58.7	0.5	
CS415	03:32:13.97	-27:43:51.1	2.6	-2.38
CS487	03:33:01.20	-28:47:20.8	1.5	-0.21
CS538	03:33:30.20	-28:35:11.2	2.0	-0.88
CS703	03:35:31.03	-27:27:02.2	26.9	-0.99

Table 3.1: ATLAS parameters for each of the IFRS observed for analysis as potential pulsars. Sources whose name begins with an 'E' are those found within the ELAIS-1 field, and those whose names begin with a 'C' are those found within the CDFS field. All flux and spectral index data is obtained from Middelberg et al. 2010 ([51]), with the exception of ES1259 and CS255 \citep{naa+06}

Parameter	Value
Central frequency	1352 MHz
Bandwidth	340 MHz
Frequency channels	870
Sample size	2 bit
Sampling rate	64 μs
Integration time	35 minutes

Table 3.2: Observational parameters of the Parkes IFRS data.

(dependant upon the galactic latitude of the region of sky being observed), G is the system gain, B is the observing bandwidth, τ_{obs} is the integration time of the observations and W is the fractional pulse width, that is, the width of the pulse in time as a fraction of the entire pulse period. In other words, W is the duty cycle as specified in Section 1.2.2. The higher the value of W, the poorer the flux sensitivity, and as mentioned, the typical value of W is ~ 0.1. It can be as high as $W \sim 1$, although this value is rare, and we instead take $W = 0.5$ as our worst case of sensitivity. Also, at the high galactic latitude of the IFRS, the value of T_{sky} is negligable, so this quantity is set to zero. Finally, the values for B and τ_{obs} are defined in Table 3.2, and we borrow the remaining parameters from Keith et al. 2010 ([41]), setting $G = 0.735$, $\sigma = 8$ and $T_{sys} = 23$ K.

Using these values, we calculate a minimum sensitivity of $S_{min} = 0.07$ mJy assuming a duty cycle of $W = 0.1$, and $S_{min} = 0.21$ mJy assuming a duty cycle of $W = 0.5$. As all of the chosen IFRS candidates possess fluxes above the higher of these two flux limits, if any of them are indeed pulsars they should be easily detectable by the observations at the 8σ confidence level using the higher of the two limits, $S_{min} = 0.21$ mJy.

3.4 Analysis

3.4.1 Hitrun processing

Hitrun is a pulsar processing pipeline developed by Keith et al. 2010 ([41]) as part of the High Time Resolution Universe Pulsar Survey. The pipeline is designed to produce a list of candidate pulsar signals from a given dataset produced by the BPSR by applying a more sophisticated version of the approach described in Section 1.2.3. It does this in several stages, a summary of which is presented below:

RFI removal Frequency channels of known poor quality are removed from the data, then all remaining channels are subjected to a Fourier analysis. All channels with a signal-to-noise ratio of greater than 15 are removed. The data is then recursively summed in frequency at zero dispersion measure to produce a time series. Any bursts of emission are removed and replaced by a statistically random data sample indistinguishable from the remaining data.

Dedispersion The most computationally intensive step in the algorithm is to analyse the data using a large number of trial dispersion measure values. Hitrun does not use the standard "tree" algorithm often used in other pulsar searches, which assumes a linear dependance of signal delay on frequency ν. Instead, a ν^{-2} algorithm is used which, along with multi-core parallel processing and specialised data compression method, provides a very efficient dedispersion procedure.

Time series anaylsis Analysis is performed in both the time domain and frequency domains. In the frequency domain, a power spectrum of the data is taken using a Fast Fourier transform. Noise is then subtracted and the spectrum is normalised. A search is then conducted for candidate pulse signals with a signal-to-noise ratio of greater than 6, with additional harmonic summing so as not to lose narrow pulse candidates. In the time domain, bright single pulses are searched for by collating all points 6σ above the mean, and detections for a single pointing are then compared to beams across the sky so as to isolate localised events, indicative of a confined pulsing object.

Candidate sorting, folding and optimisation Candidate detections of the same pulse frequency are grouped together, and harmonically related candidates are also grouped so as to produce a more manageable number for inspection. The data is then folded to produce an average pulse profile for each candidate detection, and is then subjected to a final optimisation analysis by the PSRCHIVE software package [50]. The remaining 100 candidate signals with the highest optimised signal-to-noise ratio are then output for inspection by the user.

3.4.1.1 Unusable data

During the course of the data analysis, a number of problems were encountered. Due to the extended period of time between the observations being recorded and the actual data anlysis being performed (a period of approximately 1 year, 3 months), the quality of the external hard drives on which the data had been stored was found to be severely compromised. Of the three hard drives, one remained operational, one could not be powered up, and the third intermittently lost power for several days before eventually becoming unusable. An effort was made to recover this third hard drive, during the course of which a short circuit caused the unit to ignite, resulting in the loss of all data stored on the drive. This data spanned nine of the IFRS, however it was later found that some of this data, including the central primary beam files for all IFRS affected by the fire had been backed up to central CSIRO servers, and this data was successfully recovered.

Also affecting the data analysis was the apparent corruption of two IFRS primary beam files, those for sources CS194 and CS703. Despite several attempts to process these files through the HITRUN pipeline, they continually caused the system to crash unexpectedly, resulting in the sources being discarded.

3.4.2 Candidate review

The folded pulse profiles (intensity as a function of pulse phase) of every candidate produced were viewed by eye using the JREAPER software package (Keith et al. 2009, [80]). This sample included a total of 1800 individual candidates as produced by the HITRUN pipeline The well known pulsar PSR J0437-4715 was used as a reference case, and can be seen in Figure 3.2. This set of plots demonstrates several key features that pulsar candidates should ideally exhibit, including:

- A well constrained dispersion measure (DM), depicted in the *Period-DM Plane* plot as a small, isolated region of maximum intensity and the *DM Curve* plot as a single, well defined maximum peak.
- A well-defined pulse profile that can be observed across the entire bandwidth, shown in the *Sub-Bands* and *Sub-Integrations* as a dark stripe, with the profile shape given in the *Profile* plot window.

Only candidates with a signal-to-noise ratio above 8σ as determined by HITRUN (an example is presented in Figure (3.3)) were given serious consideration, however, all 1800 candidates were checked irrespective of their signal-to-noise ratio. This was to ensure that no substantial detections were missed, even if they lay just below the 8σ cutoff. None of these candidates were determined to be significant enough to warrant further investigation. An example of a 7σ candidate that was initially considered promising can be seen in Figure 3.4. Also, many candidates with a very high signal-to-noise

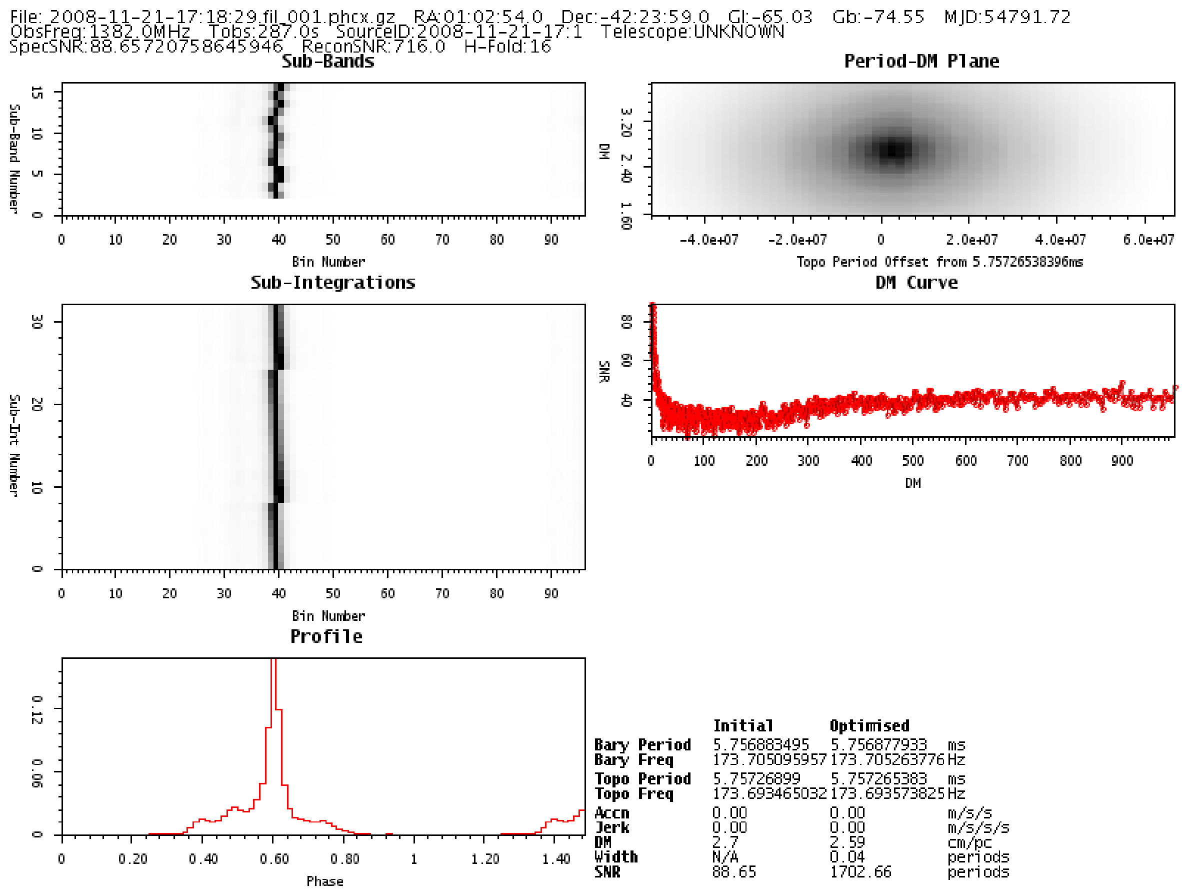

Figure 3.2: JReaper plots showing the known pulsar, PSR J0437-4715. This pulsar was used as a demonstration and point of reference to identify viable candidates in the IFRS analysis. Note the clearly defined pulse profile and well constrained DM.

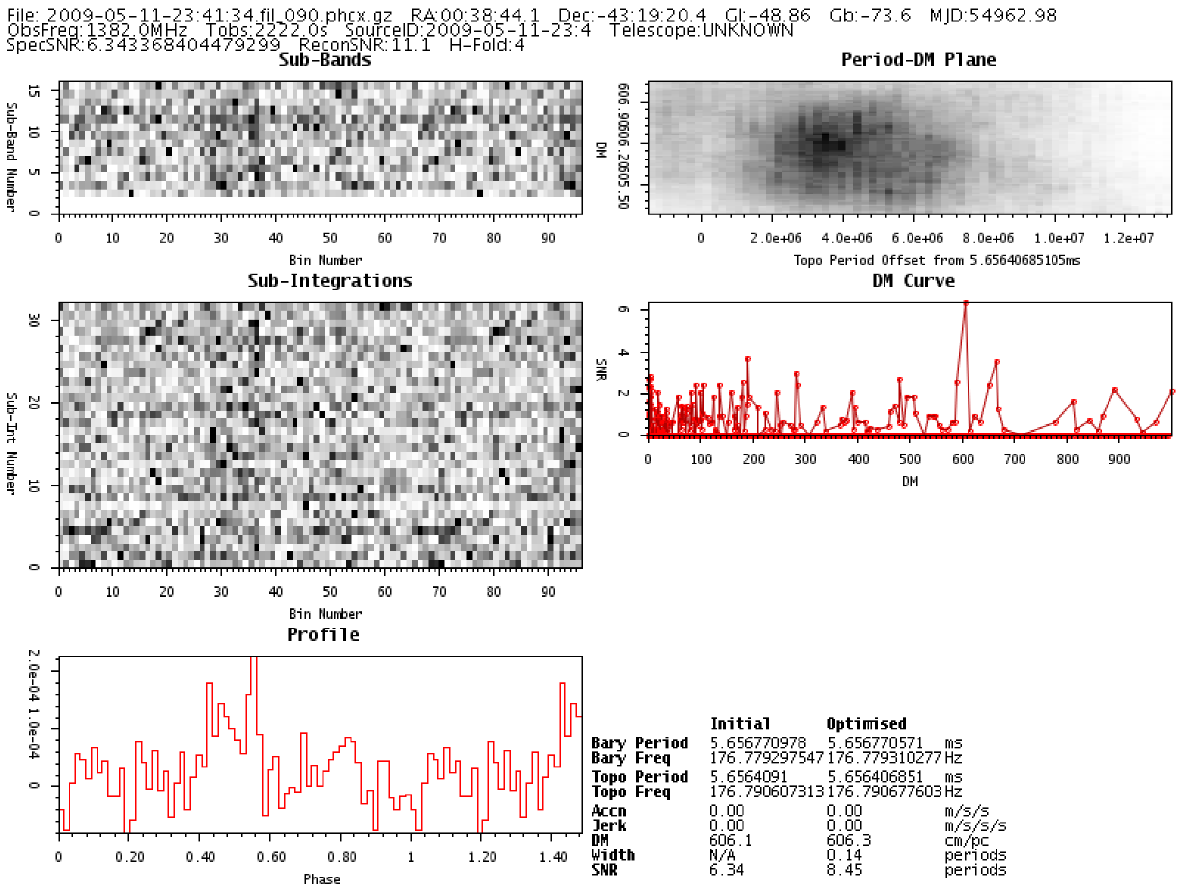

Figure 3.3: An example of an 8σ candidate for source ES973 as plotted by JReaper, with the appearance of a semi-defined pulse profile and semi-constrained DM. This candidate was dismissed due to the presence of extremely similar candidates for the same IFRS at very different frequencies / DM's.

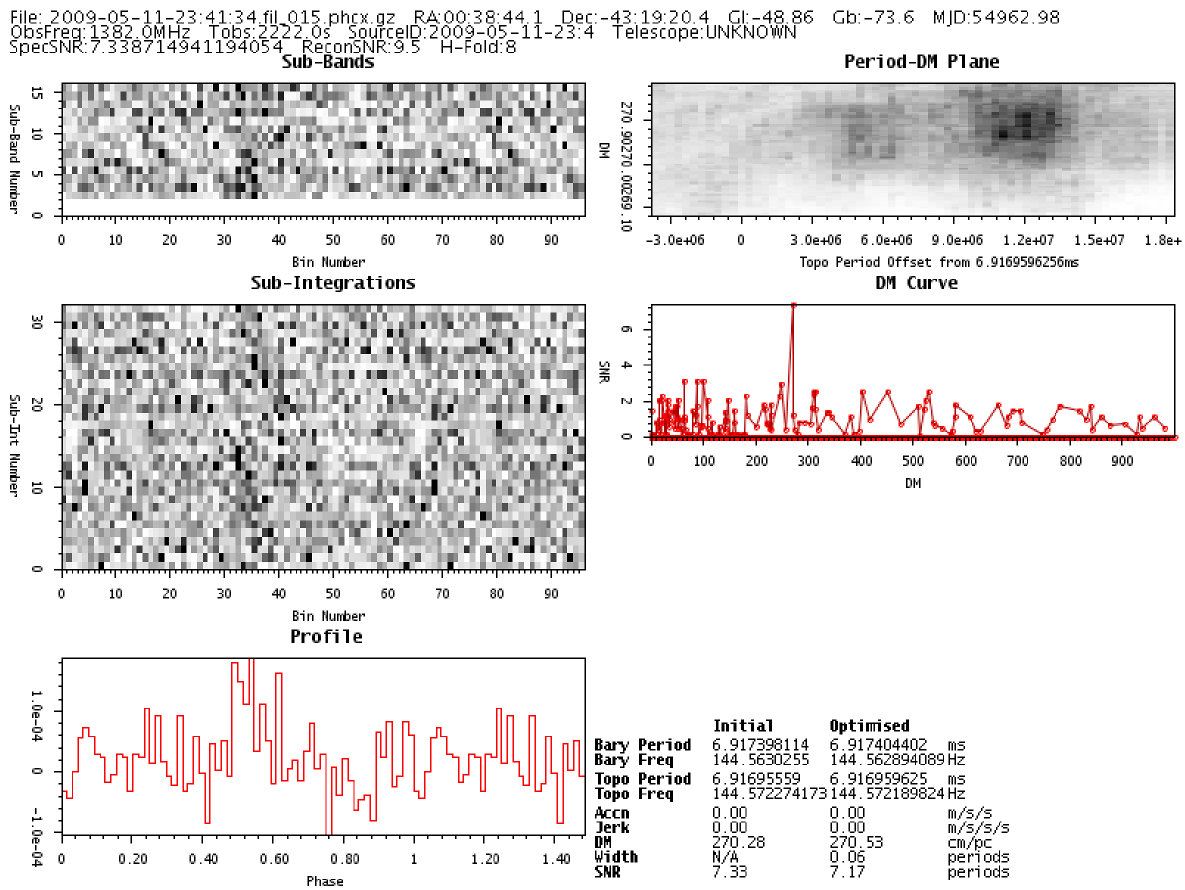

Figure 3.4: A JReaper plot showing a 7σ candidate for the source ES973.

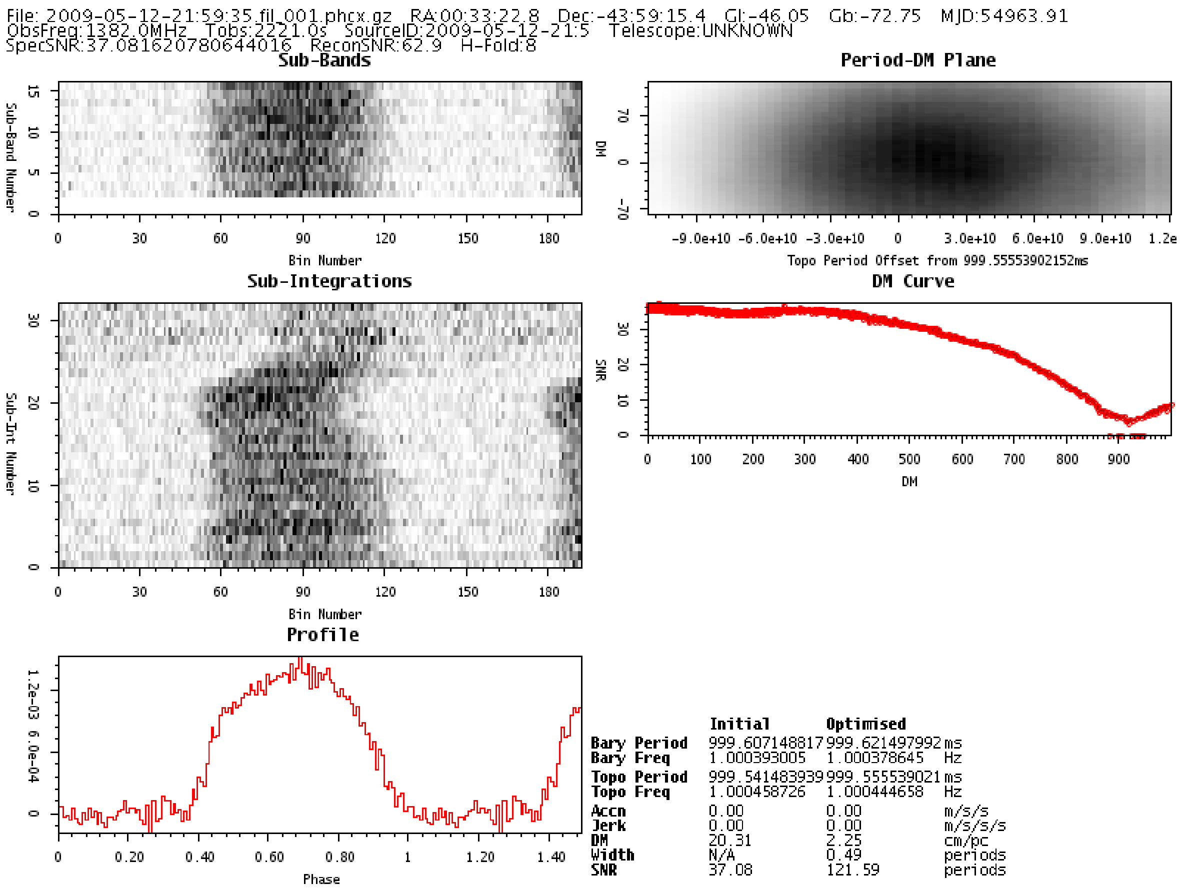

Figure 3.5: A JREAPER plot showing a clear example of RFI in the primary candidate for IFRS ES419. Note the frequency of almost exactly 1 Hz.

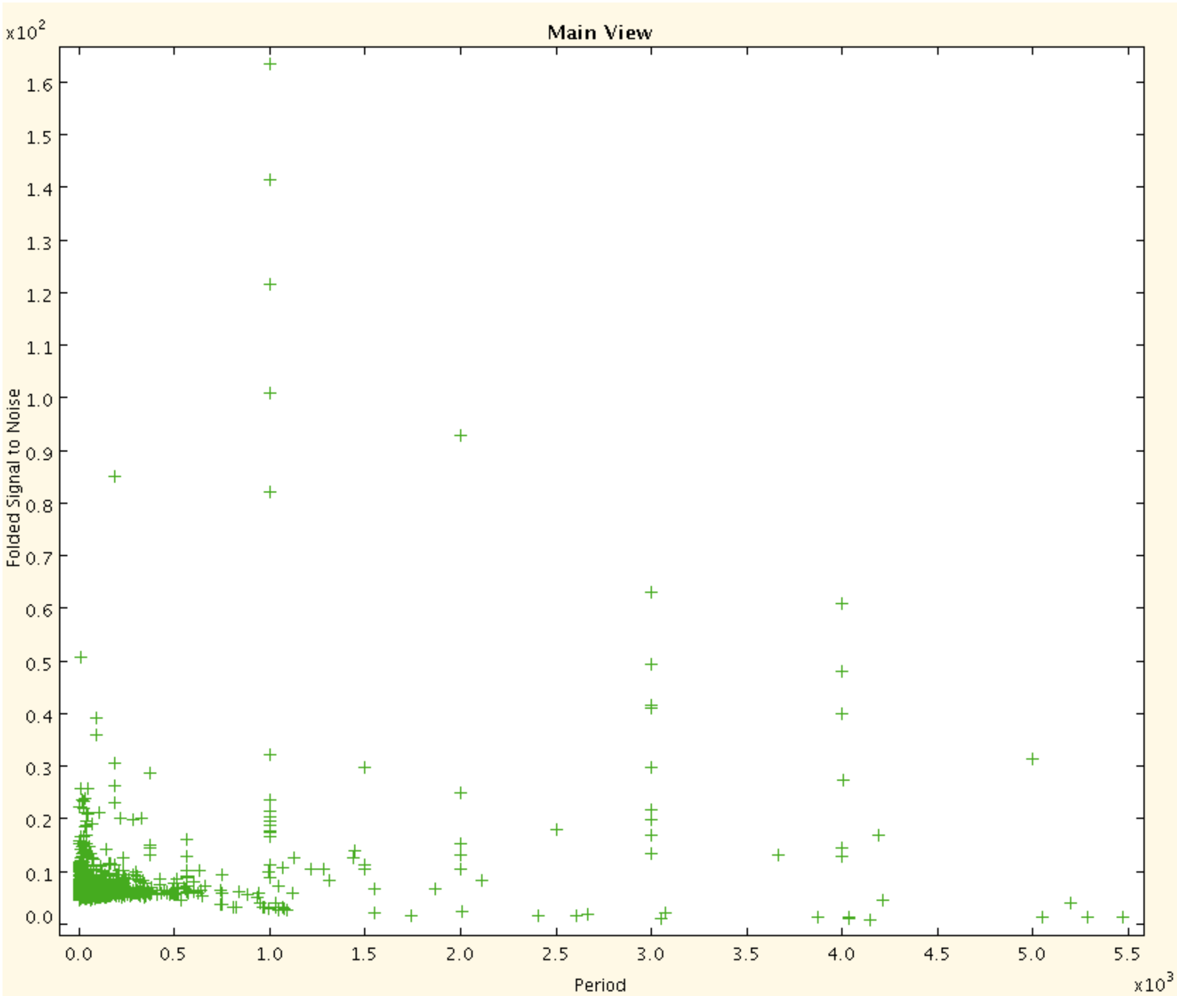

Figure 3.6: JReaper plot of all 1800 candidates across the 17 remaining IFRS. The vertical linear artefacts are indications of false candidates caused by radio-frequency interference.

ratio were clearly due to radio frequency interference, and an example of this can be seen in Figure 3.5. Tell-tale signs of RFI include distortions limited only to a limited number of sub-bands, as well as candidates possessing a period of almost exactly an integer number of seconds. These later cases of interference are independent of their source object, and so stand out as clear linear groupings when all IFRS candidates are plotted together. This can be seen in Figure 3.6.

Of the candidates with a signal-to-noise ratio above 8σ, only eight were initially deemed to be worthy of future investigation, showing semi-defined pulse profiles and marginally constrained DM's. However, these candidates did not vary significantly from the features of the population less than the 8σ signal-to-noise cutoff value, and after further review it was decided that none of them presented any significant detections requiring further observation.

3.5 Results & Discussion

The observed folded pulse profiles (intensity as a function of pulse phase), including all those above the 8σ signal-to-noise cutoff, were clearly caused by radio frequency interference or processing artefacts. It should be noted that the the mean flux density of the IFRS is approximately 6.9 mJy, with a median flux of 4.4 mJy. If the fluxes of the IFRS were indeed due to pulsars, then these fluxes would have been detectable in these observations at a level of 263σ and 168σ respectively. It can therefore be concluded that none of the 17 IFRS observed and analysed in this project were found to be a pulsar with a pulse strength of at least 0.21 mJy. The possiblity that the remaining 2 IFRS which could not be processed are still pulsars cannot at this stage be ruled out, but it is considered extremely unlikely.

The absence of pulsar detections in our analysis of the ATLAS IFRS emphasises the difficulty of identifying pulsar candidates through the use of radio continuum surveys. Despite the positive detections outlined in Section 2.1, the fact remains that the vast majority of radio continuum survey pulsar searching techniques have found no positive results, some of the most prominent examples having been mentioned in Section 2.1.2. This analysis attempted to take advantage of the typically steep values of pulsar spectral indices in order to select appropriate IFRS targets, however, this selection criteria was not well defined at the outset of the project, which began before this thesis project was commenced. Also, the primary means of searching for pulsar candidates in continuum surveys has been to identify sources with significant linear and/or circular polarisation, as opposed to the spectral index values used in this study. Clearly, all of these criteria need to be studied in greater detail so that future continuum searches are able to better select pulsar candidates without also bringing with them a large selection of non-pulsar 'background' objects.

Refining these selection criteria is of critical importance when considered in the context of the EMU and POSSUM surveys to be conducted using ASKAP. These surveys are expected to produce approximately 70 milion radio sources to a sensitivity limit of ~ 10 μJy, with over million of these sources expected to be classified as IFRS. Clearly, conducting observations similar to those recorded for the 17 IFRS in this chapter, as well as their subsequent analysis, will be impractical for such a large number of sources. Therefore, useful selection criteria must be developed to lower this source count to a more reasonable and practical number for pulsar observations. This will be the main subject of discussion in Chapter 4.

Chapter 4

Future observations with ASKAP

4.1 Pulsar detection using EMU & POSSUM

The Polarisation Sky Survey of the Universe's Magnetism (POSSUM) and the Evolutionary Map of the Universe (EMU) survey, as briefly described in Section 2.2.4 and 2.2.5, are two of ten science projects chosen for the initial operational stages of ASKAP. EMU, along with the Wide-field ASKAP L-band Legacy All-sky Blind Survey (WALLABY) is one of the two highest priority projects and will be provided with full observing support. The POSSUM project is on the second priority tier along with five other projects, and will be provided with 'all reasonable support'. Two more projects lie on the third and final priority tier, making up a total of ten different ASKAP Survey Science Projects (SSP's). These ten projects will be allocated a minimum of 75% of ASKAP observing time over the first 5 years of its operation [66].

Given that ASKAP is not expected to commence full operations until 2013, the SSP's, EMU and POSSUM included, are still in their planning and design stages. Therefore, while many details of the EMU and POSSUM surveys have been laid down, some specifications are stillunknown at the time writing, and those that are known are subject to change over the next few months as the design process continues.

Two surveys are currently planned as part of EMU. The first of these is the EMU-wide survey, which will survey the portion of the sky for which $\delta_{J2000} \leq +30°$ (aproximately 75% of the sky) to a sensitivity of 10 μJy. This is a sensitivity of at least 45 times greater than the NVSS [65]. A corresponding POSSUM survey (POSSUM-wide) is also planned, which will provide full polarisation information to complement the Stokes I data recorded by EMU. It is likely that these two surveys will be carried out concurrently (Hobbs, 2010, pers. comm. 11 November). The sky coverage of these two surveys is almost equal to the amount surveyed by the NVSS, which covered the region of the sky for which $\delta_{J2000} \geq -40°$. The survey is projected to have an angular resolution of 10 arcseconds, five times higher than the NVSS, and will require a total of 2000 hours of integration time to complete. This integration is expected to be completed over a real-time period of approximately 1.5 years [67].

The second survey planned as part of the EMU project is the EMU-deep survey. As with EMU-wide, a matching POSSUM survey, POSSUM-deep, is also planned. Neither of these surveys are presently a supported project for ASKAP, and they will be submitted for consideration after the commencement of EMU and POSSUM-wide. EMU-deep intends to image one 30 square degree region of the sky to a sensitivity of approximately ~ 1 μJy. The project will require an integration time of approximately 100 hours, using multiple wavelength data to distinguish between confusing sources. It is intended that the chosen field will be one already well studied [70], particularly at multiple wavelengths, so as to make available the maximum amount of supporting information in studying and identifying the sources detected during the course of the survey. A comparison of both the EMU-wide and EMU-deep surveys in terms of their survey area and sensitivity can be seen in Figure 4.1.

EMU-wide and POSSUM-wide are currently antiticpated to survey a 30 square degree region of the sky every 12 hours, with the resultant catalogue for each field containing approximately $\sim 60,000$ sources at a sensitivity of ~ 10 μJy. Over the course of the survey, it is expected that on the order of tens of millions of sources will be detected[67], with one estimate placing the expected source count at 70 million[65]. Current plans for EMU include the implementation of real time source extraction followed by the application of cross-identifcation algorithms, so that sources correlating with known objects from other surveys are automatically identified with this sources, matched up and catalogued. This cross-identification requires substantial time and processing power, with current proposals suggesting a distributed approach similar to the SETI@Home initiative [65].

Given the unprecedented size of the source count expected to be produced by EMU and POSSUM, in order to successfully use the surveys as tools by which we might find suitable candidate sources for pulsars, a means of reducing the number of sources to be checked must be identified. Some sources will be removed as their identities are determined by the cross-identification pipeline, but this processing will take time to carry out, while in the meantime more sources continue to be identified. The ideal approach is to select candidate sources as they are produced by the survey on a day-by-day basis. In this chapter, an investigation is conducted into the criteria by which sources may be automatically selected as pulsar candidates, based upon some of the radio continuum features commonly associated with pulsars.

4.2 Source Selection Criteria

The key in choosing any selection criteria, not only in attempting to isolate pulsars but for any object class, is that the criteria must allow the majority of the type of object in question into the group of candidate sources while at the same time excluding the majority of 'background' sources. The criteria should maximise the number of desired objects detected while at the same time minimsing the number of false sources. In other words, the criteria must be as unique as possible to the object being studie so as to ensure that only the desired object class is allowed into the selection of candidate sources.

As described in Sections 1.2.2 and 2.1, there are several observational properties that are widely established as being common across and in some cases unique to radio pulsars, including spectral indices, compactness, and both fractional linear and circular polarisation. Here, the most promising of these criteria are analysed in an effort to derive their suitability for future continuum searches using EMU, POSSUM and other similar surveys. To do this, the population statistics of both pulsars and background radio sources are used to evaluate the overall trends of each parameter and hence derive their application suitability.

4.2.1 Spectral Index

Steep values of spectral index were the defining characteristic used in order to select the IFRS investigated in Chapter 3. The fact that none of the IFRS chosen by this rough selection criteria could be positively identified as pulsars immediately brings into question the suitability of this characteristic as a means of identifying pulsars. However, in order to investigate the true appropriateness of the spectral index parameter, a full evaluation must be carried out.

To uncover trends in the spectral indices of pulsars, data from the ATNF Pulsar Catalogue, PSRCAT[1] was used [46]. PSRCAT stores two spectral index fields,

[1] http://www.atnf.csiro.au/research/pulsar/psrcat/

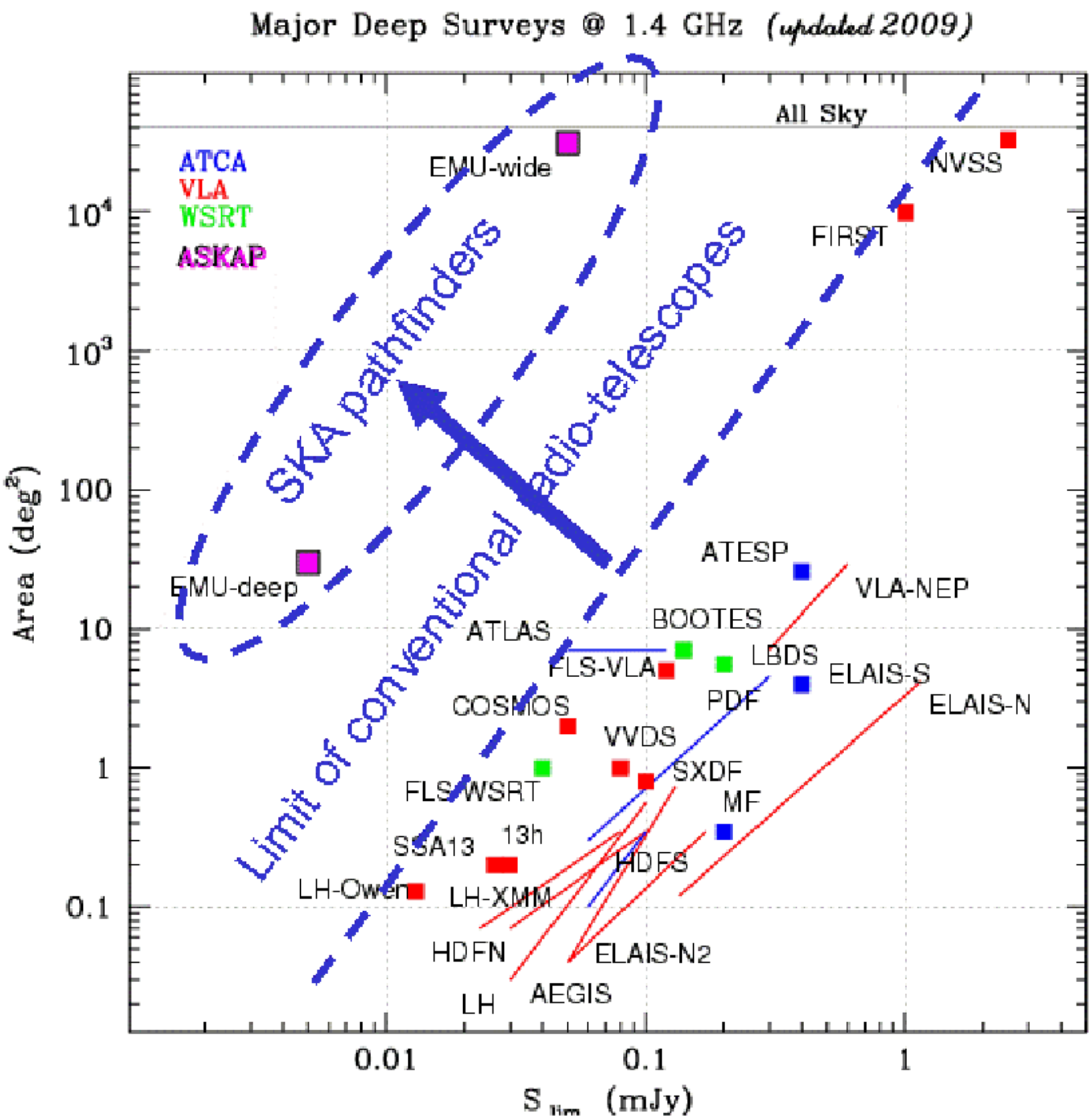

Figure 4.1: Plot of Survey Area vs. Survey Sensitivity for the major 1400 MHz radio surveys conducted to date. Note the positions of ATLAS, NVSS and FIRST. The positions of EMU-wide and EMU-deep are indicated in purple, and are in an area of the plot currently unattainable and unexplored by current radio telescopes. Figure taken from Norris, 2009, Figure 1, p2 [65].

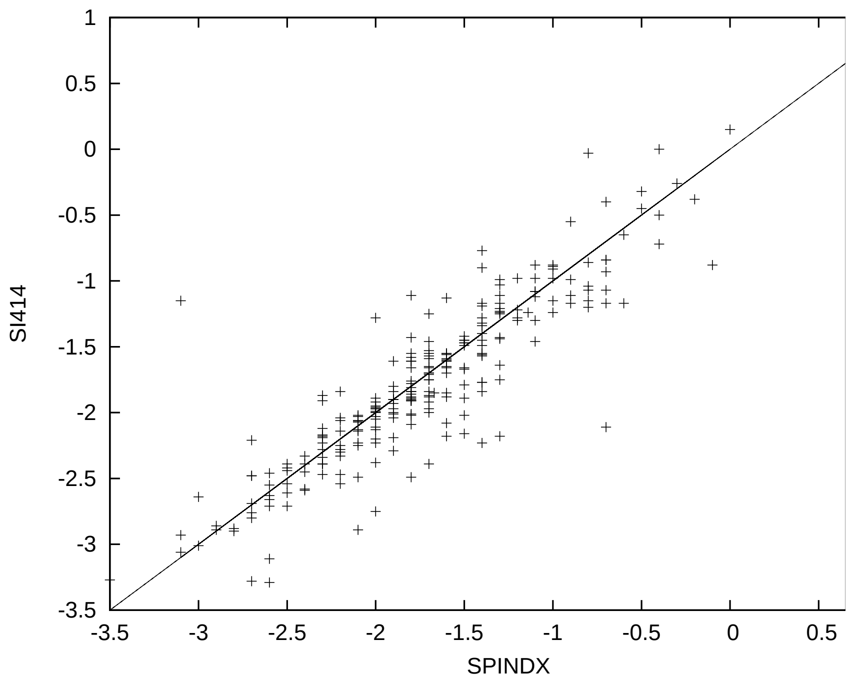

Figure 4.2: Plot showing the correlation between the two measures of spectral index, SPINDX and SI414 stored by PSRCAT. The central line is the ideal 1:1 correlation, which the data roughly approximates.

- SPINDX, which records the spectral index of a pulsar calculated as part of its initial discovery.
- SI414, which stores the spectral index calculated using the recorded catalogue values of the S400 (flux at 400 MHz) and S1400 (flux at 1400 MHz) fields.

Figure 4.2 shows how these two measures of spectral index compare against each other for those pulsars in PSRCAT which have both values recorded. It is clear from observation that the two fields strongly correlate, and this correlation follows a linear 1:1 trend. Figures 4.3 and 4.4 show the distribution of the SPINDX and SI414 values across all the pulsars in PSRCAT for which either value was recorded. Both of these distributions appear extremely similar, with a peak just below $\alpha = -2$ and an approximate range of $-3.5 < \alpha < 0$. This is in good agreement with Manchester et al. 2005 ([46]), who reported a range of $-3.5 < \alpha < +0.9$ with a median of $\alpha = -1.7$. The similarity in both of these parameters inidcates that the spectral index is a well-defined parameter, and allows either of the two measures to be used in this analysis.

To analyse the spectral index distributions of other 'background' radio sources, a unified catalogue of radio objects compiled by Kimball & Ivezic 2008 ([58])[2] was employed. This catalogue combines the NVSS, FIRST, WENSS, SDSS (Sloan Digital Sky Survey) and GB6 (Green Bank 6cm survey) projects and stores a comprehensive list of radio sources with stored flux values across multiple surveys. This catalogue of sources was produced through a thorough process of cross-correlation. The catalogue does not store explicit values of spectral index, but as it stores flux values at multiple frequencies, values of the spectral index for each source could be easily calculated. For the purposes of this study, only those sources with both WENSS data and either FIRST or NVSS data were used (described as Sample D in Table 8 of [58]). Approximately 71,400 sources matched these specifications. The reason

[2]http://www.astro.washington.edu/users/akimball/radiocat/

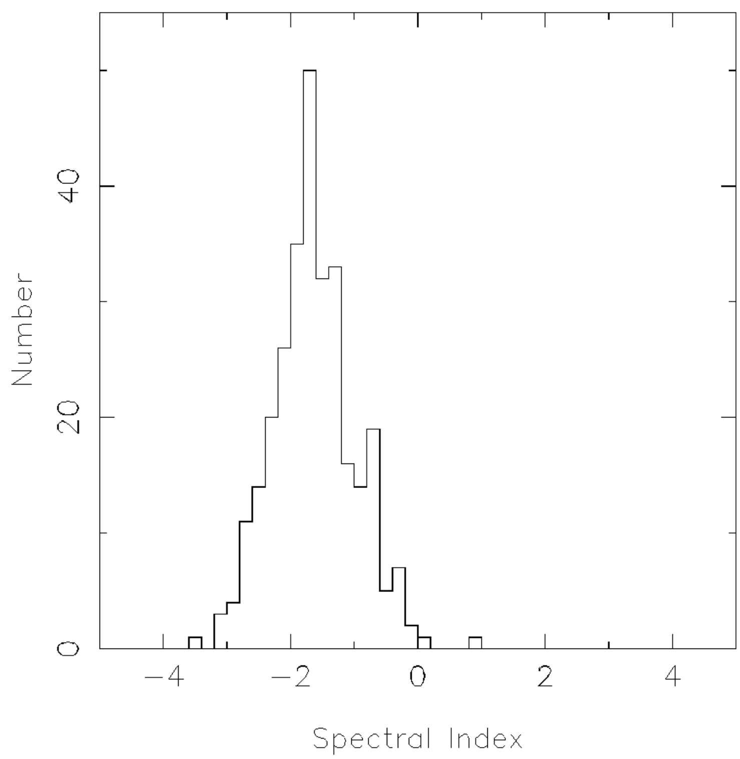

Figure 4.3: Histogram displaying the distribution of the SPINDX spectral index measure for pulsars in PSRCAT.

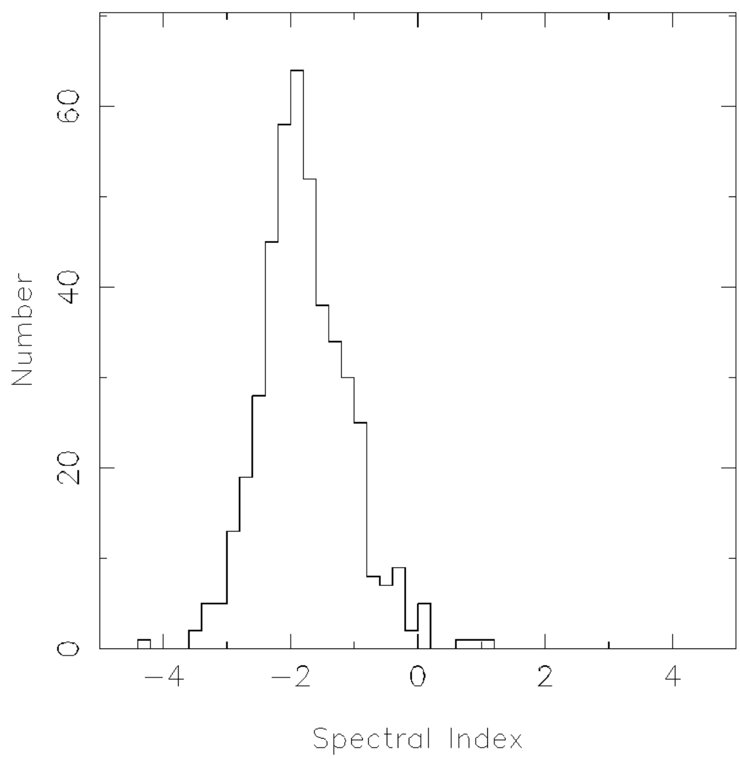

Figure 4.4: Histogram showing the distribution of the SI414 spectral index measure for pulsars in PSRCAT.

for this selection is that both the observations for both FIRST and NVSS projects were conducted at a frequency of approximately 1400 MHz, and the observations for WENSS were conducted at a frequency of approximately 325 MHz. These two observing frequencies are almost identical to the 1400 MHz and 400 MHz frequencies used to calculate the SI414 spectral index measure stored in PSRCAT, hence using the NVSS, FIRST and WENSS data allows for the best comparison to the pulsar population data. Using the same system of naming as for the SI414 measure of spectral index, this new spectral index measure for the spectral index of background sources is known as SI314, in reference to the frequencies used to calculate it.

Figure 4.5 shows the distribution of SI314 across the 71,400 radio background sources. The distribution is notably different than those produced for both SPINDX and S1414, possessing a narrower peak with shallow tails extending away in either direction. The majority of sources appear to possess SI314 values of $-1.5 < \alpha < 0$, with the full range extending to $-4 < \alpha < +1.5$, and a median sitting just below $\alpha = -1$. It should be noted that radio pulsars have not been removed from this catalogue of background sources. However, as PSRCAT only records a total of 1880 pulsar that have been discovered to date, these pulsars can only make up a maximum of approximately 2.6 % of the background sources obtained from the unified catalogue, Furthermore, earlier research conducted as part of a summer studentship revealed that of the 1324 pulsrs stored in PSRCAT that lie within the NVSS region, only approximately 260 could be detected in NVSS continuum images. Using these numbers, the fraction of pulsars in the unified catalogue sources is likely to be closer to 0.4 %. Hence, the presence of pulsars is the background source count should have a negligable impact on the distribution of the SI314 spectral index measure.

Given the different distributions between the pulsar spectral index measures SPINDX and SI414 and the background source spectral index measure SI314, it seems possible that spectral index may be a useful criterion for selecting pulsar candidates. A final point of analysis is presented in Figure 4.6. This Figure presents the fraction of pulsars that will be missed and the fraction of background sources that will be included for a given upper cutoff value of spectral index. This data plot was produced through the use of the script `cutoff.sh`, which is visible in Appendix A.1. An upper cutoff value is used due to the fact that the median pulsar spectral index is lower than that of the background sources, hence an upper cutoff chosen between these two median values will include most pulsars (the population of pulsars lying predominently below the cutoff) while excluding most background sources (the population of background sources lying predominently above the cutoff). For example, if an upper cutoff value of $\alpha = -3$ is taken, and only those sources with $\alpha < -3$ are accepted as candidates, almost 100% of pulsars will be missed, while at the same time, only a very small fraction of background sources will be collected. Conversely, at an upper cutoff value of $\alpha = 0$, almost no pulsars will be missed (i.e. all pulsars will be included) in those sources allowed through, but at the same time nearly 100% of the background sources will also be accepted, severely polluting the sample.

Ideally, the two curves (pulsars and background sources) in Figure 4.6 should not overlap, and the fact that they do means that a compromise will need to be reached if the spectral index parameter is to be used as one of the criteria for candidate selection in future continuum surveys. For an upper spectral index cutoff value of $\alpha = -1.5$, for example, only around 30% of pulsars will not be accepted as candidates, while 7% of the background sources will. It is likely that an optimal value of spectral index cutoff which maximises the total percentage of pulsars in the allowed sources exists, and this will be further explored in Section 4.3.

4.2.2 Linear Polarisation

Pulsars are also typically known for their high fractional amount of linearly and circularly polarised flux. In order to analyse the linear polarisation characteristics of the pulsar population, a sample of pulse profiles containing high resolution time series of all four Stokes parameters was used to derive

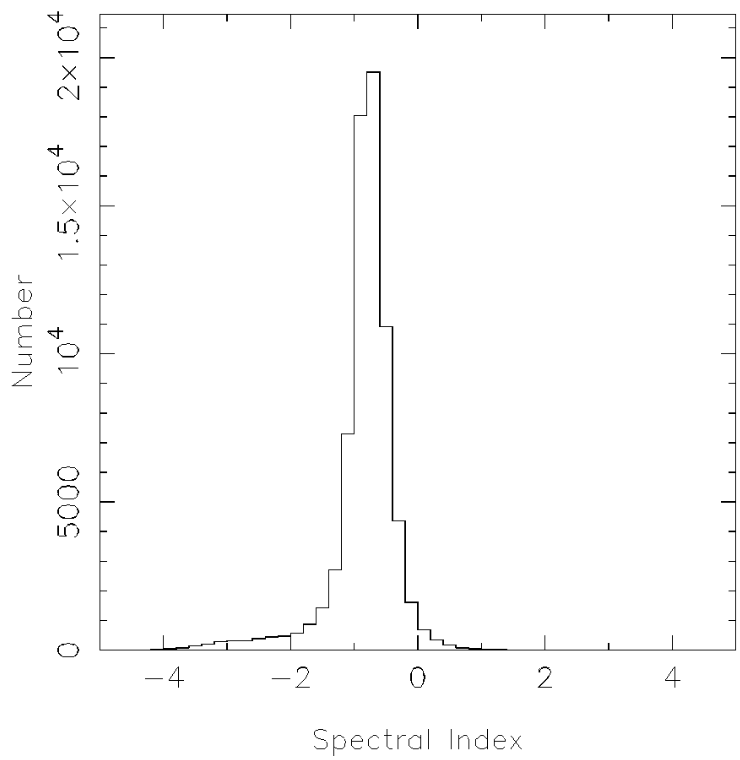

Figure 4.5: Histogram showing the distribution of the SI314 spectral index measure derived for background radio sources in the unified radio source catalog [58].

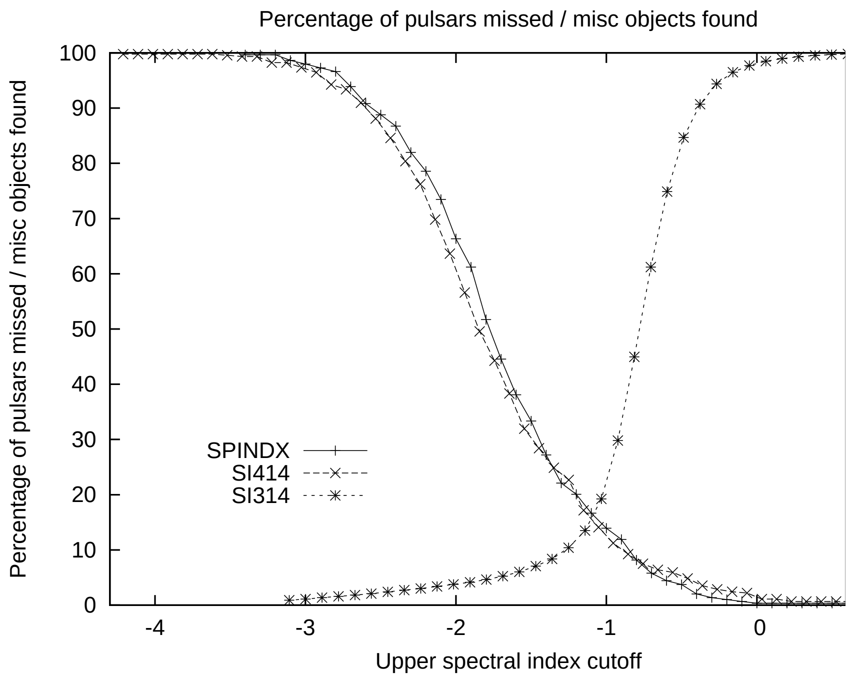

Figure 4.6: A plot showing the fraction of pulsars/background sources that will be missed/included respectively in the sample of sources selected using an upper limit of spectral index as indicated on the horizontal axis.

polarisation statistics (see Section 1.2.2.1 for information about the Stokes parameters). Subtle differences between the typical methods of pulsar observation and those of radio continuum surveys mean that in the case of linear polarisation, this normally defining feature may be reduced in visibility in a continuum survey to the point where it no longer becomes useful as a selection criteria for candidate pulsars in continuum sources.

The two Stokes parameters relating to the total linear polarisation, Q and U, can be combined to give an the total linear polarisation L using the following expression:

$$L = \sqrt{Q^2 + U^2}. \tag{4.1}$$

In a standard pulsar observation, L is calculated for each individual phase bin, and then summed together to give the average linear polarisation,$\langle L_{pulsar} \rangle = \left\langle \sqrt{Q^2 + U^2} \right\rangle$. However, in a continuum survey, the two Stokes parameters Q and U are individually summed across separare phase bins, and then averaged before L is calculated. This changes the expression to $\langle L_{continuum} \rangle = \sqrt{\langle Q \rangle^2 + \langle U \rangle^2}$. It is likely that this difference in the order of operations will affect the amount of linearly polarised flux visible in a continuum survey. To analyse the way in which this change affects the total visible linearly polarised flux, a handwritten mathematics package produced by G. Hobbs was used to perform operations on the time series profiles of a large selection of pulsars. Three quantities relating to linear polarisation were calculated for each pulsar:

- L_{pulsar}, determined by calculating L for each phase bin in the pulse profile and then summing over the entire profile to give a final value
- $L_{continuum}$, determined by summing the phase bin entries for Q and U and then calculating L

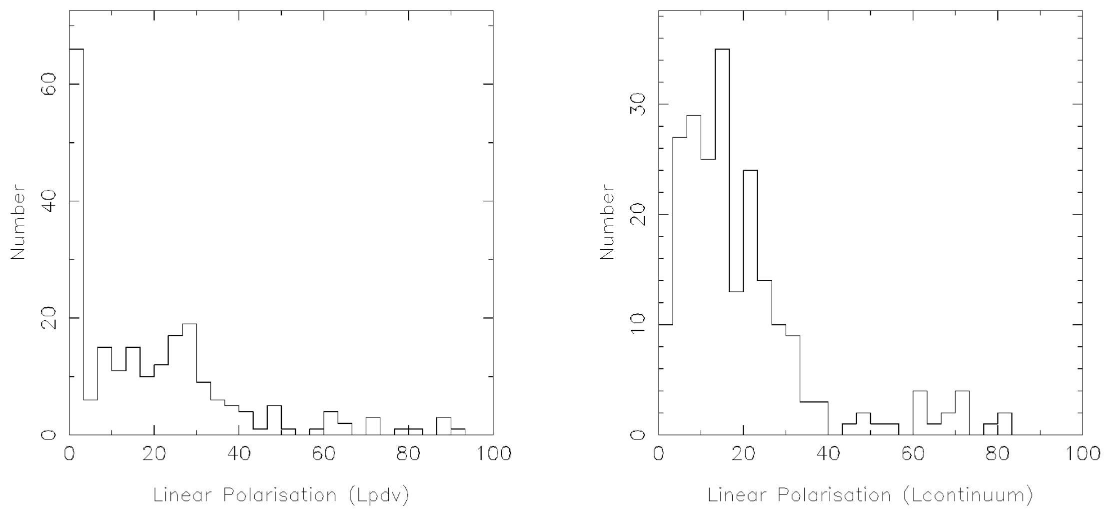

Figure 4.7: Distributions of the fractional pulsar linear polarisation. The left plot (L_{pdv}) shows the distribution as observed in standard pulsar observations, while right plot ($L_{continuum}$) shows the distribution as would be observed in a radio continuum survey.

- L_{pdv}, a measure of linear polarisation similar to L_{pulsar} in that it represents the polarisation that would be observed through standard pulsar observations, but determined through the use of PSRCHIVE application PDV [50].

All values of L were normalised using the total intensity I so that they represented the fractional component of linear polarisation. The calculations were overseen through the use of two shell scripts, `getStats` and `overscript.sh`. Several different versions of each of these scripts were created to be run on different sets of files where certain parameters were altered to examine their effects on the visible linear polarisation, although the core functionality of each script remained the same. Examples of each of the scripts can be viewed in Appendices A.2 and A.3. Due to an irregularity in the data processing (the source of which has yet to be determined at the time of writing) the figures produced for L_{pulsar} were unrealistic, in some cases producing fractional polarisations of 500% or more. As a result, all values of L_{pulsar} were discarded. However, the values of L_{pdv} and $L_{continuum}$ and their distributions were consistent with previous studies of linear polarisation distribution such as Gould & Lyne, 1998 ([4]). Histograms depicting the distribution of these parameters can be viewed in Figure 4.7. It can be seen in this Figure that continuum observations reduce both the overall range of the distribution of fractional polarisations and, ignoring the artifical spike at $L_{pdv} = 0$, shifts the central distribution peak from $\sim 25-30\%$ to $\sim 10\%$. Hence, it is reasonable to conclude that the fractional linear polarisation of a pulsar will be noticeably reduced in a continuum survey simply from the difference in the treatments of polarisation data.

Another problem facing the use of linear polarisation is the fact that the rotation measure for a particular source may not be known at or shortly after the time of observation. As described in Section 1.2.2.2, Faraday rotation has an effect on the visiblity of linearly polarised flux, and in order to fully evaluate the amount of linearly polarised flux that a pulsar possesses, the rotation measure of that pulsar must be known. Without knowledge of the rotation measure, the amount of visible linear polarisation in a given pulse profile may be significantly reduced, even to the point where it is no longer discernible. An example of this is provided in Figure 4.8, which shows a comparison between two pulse

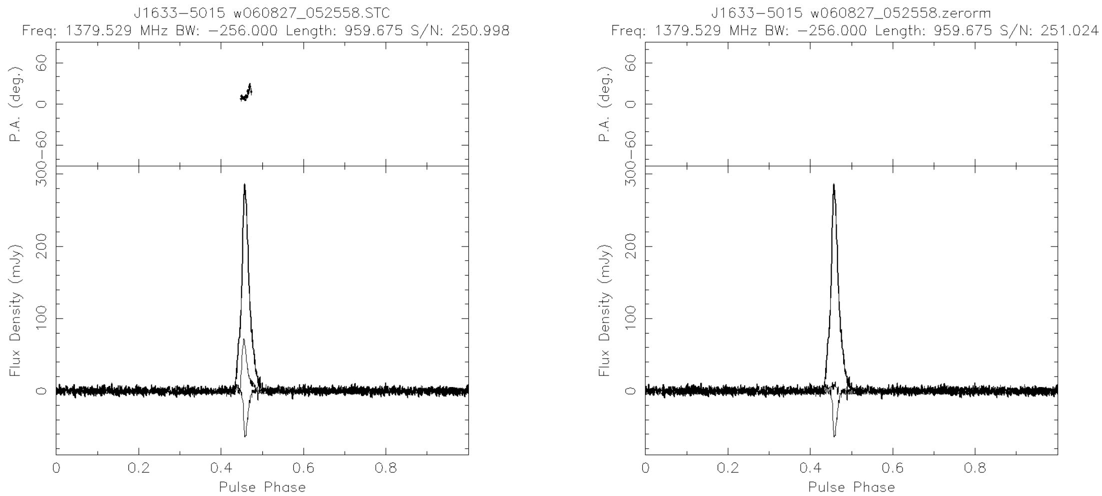

Figure 4.8: An example of the effect that the removal of rotation measure has on linear polarisation. Both profiles are for the pulsar PSR J1633-5015. The left profile is the pulsar's normal profile, in which the total flux I is the strong positive curve, the total linearly polarised flux L is the smaller positive curve, and the total circularly polarised flux V is the negative curve. The right profile is the same pulsar with the rotation measure set to 0. Note that the linear polarisation L vanishes almost completely, while the circular polarisation V remains unaffected.

profiles for the same pulsar. One of these profiles is calibrated with the correct rotation measure, while the other is uncalibrated, with RM = 0. It can be clearly seen that by setting RM = 0, the linearly polarised component of this pulsar's flux is almost completely removed. It should be noted that the circularly polarised flux component remains unaffected (this will be further discussed in Section 4.2.3).

One final factor that needs to be considered in the use of linear polarisation as a criterion for selecting candidate pulsar sources is the dispersion measure. This is similar to the problem caused by the lack of knowledge of the rotation messure, in that the dispersion measure will not be known at the time of the source's initial identification, and in fact, for many pulsars the DM of the source is not determined until the very observations and analysis used to confirm their identity as pulsars. The relevant question is whether this lack of knowledge of the dispersion measure will affect the visibility of a source's fractional linear polarisation. It is assumed in this analysis of the dispersion measure that the polarisation data has been calibrated with correct rotation measure. Figure 4.9 shows the distributions of both L_{pdv} and $L_{continuum}$ as calculated from the pulsar profiles as calibrated with DM = 0.

Comparing Figure 4.9 to the historgrams of the correctly calibrated linear polarisation in Figure 4.7 it can be seen that the without knowledge of the correct dispersion measure of a pulsar, the visible fractional linear polarisation is significantly reduced. In the case of L_{pdv}, representative of the flux observed in a typical pulsar observation, the distribution is noticeably flatter, indicating a lower number of pulsars with a high amount of visible fractional linear polarisation, and in the case of $L_{continuum}$, there is a marginal shift of the peak towards lower values of polarised flux.

Given the number of impediments to the successful use of linear polarisation as a marker for pulsars in continuum surveys, in addition to the time constraints of the research project, the criterion was not considered a viable enough candidate to complete the same full background source analysis as was conducted for the spectral index parameter. This will be further discussed in Section 4.3.

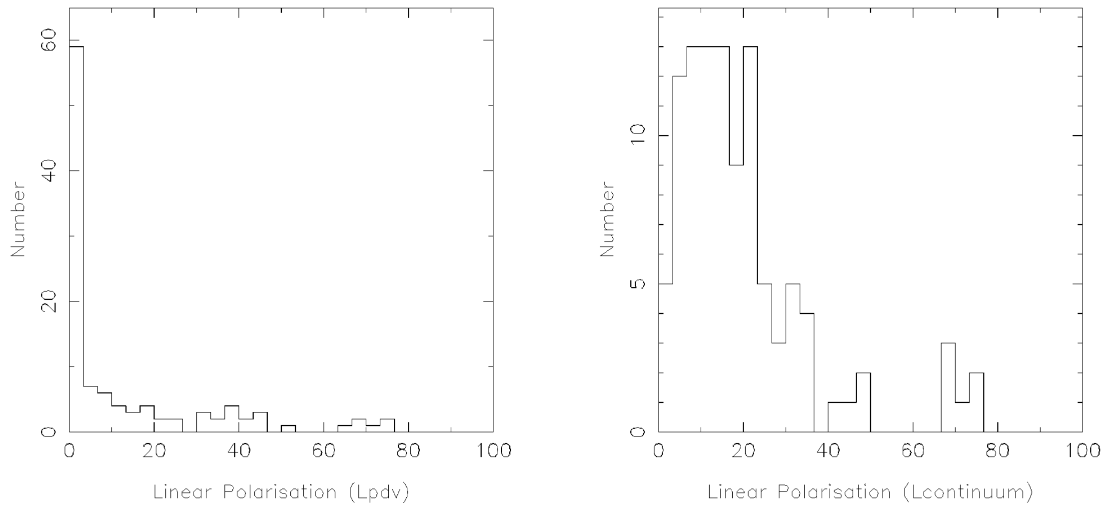

Figure 4.9: Histograms showing the distribution of fractional linear polarisation for pulsars artificially modified so that DM=0. This figure is intended to be viewed in comparison with Figure 4.7, which shows the unaltered distribution of fractional linear polarisation.

4.2.3 Circular Polarisation

As noted in Section 1.2.2, pulsars are known for their high degree of circular polarisation. The same set of pulsar profiles as used in Section 4.2.2 were used to analyse the circular polarisation characteristics of the pulsar population. For the population of background radio sources, a sample of active galaxies was taken from Rayner et al. 2000 ([71]). This sample may not be representative of the true full distribution of background sources, but it does provide a useful comparison against objects classes that EMU and POSSUM are specifically hoping to detect [65]. It should be noted that the polarisation data for these background sources was taken at a frequency of 4.8 GHz compared to the 1.4 GHz used for all other measurements. This change in frequency should have only a marginal effect on the distribution of circular polarisation (Hobbs, 2010, pers. comm. 1 November).

Unlike linear polarisation, there there is no change in the order of operations in the calculation of circularly polarised flux between pulsar observation methods and radio continuum surveys. However certain factors, such as phenomenon of the change in polarisation sense over the period of a single pulse that occurs in several pulsars [6] could lead to the circularly polarised flux negating itself over the course of a full integration in a continuum observation. To investigate any change in visibility, the `getStats` and `overscript.sh` scripts were extended to perform an analysis on circularly polarised flux similar to the analysis on linearly polarised flux detailed in Section 4.2.2. Two values were calculated for each pulse profile:

- V_{pdv}, a measure of the circular polarisation that represents the cirularly polarised flux that would be observed through a standard pulsar observation. This quantity is calculated using the PSRCHIVE application PDV.
- $V_{continuum}$, determined by summing the time series entries for V

Both of these values were then normalised using the total intensity I so that they represented the fractional circularly polarised flux. Distributions of these two parameters can be viewed in Figure

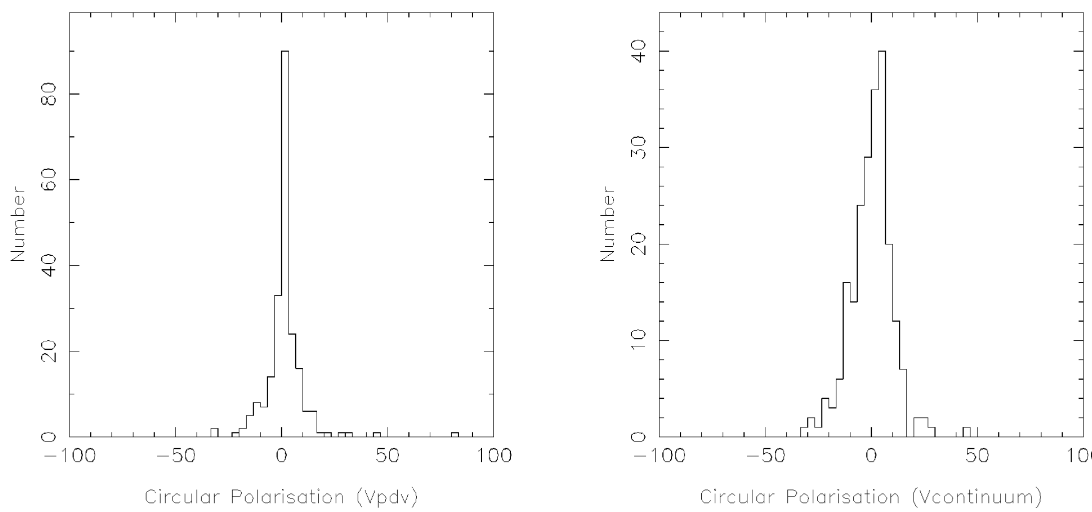

Figure 4.10: Histograms showing the distribution of fractional circular polarisation as determined through pulsars observations (V_{pdv}, on left) and continuum surveys ($V_{continuum}$, on right).

4.10. Ignoring the artificial peak at $V_{pdv} = 0$, both parameters can be seen to approximate the same distribution curve, with the majority of circular polarisations bounded within $|V| < 20\%$, and a maximum range of up to $|V| = 50\%$. The similarity of these plots would seem to indicate that the amount of circularly polarised flux is not significantly reduced in a continuum survey. Further reinforcing this result is Figure 4.11, in which $V_{continuum}$ is plotted against V_{pdv}. The two parameters appear to correlate along the 1:1 relation marked in the graph. Exceptions to this occur at $V_{pdv} = 0$ as part of the same anomaly which generates the artifical spike at $V_{pdv} = 0$ in Figure 4.10. There are also approximately 3 data points in Figure 4.11 for which $|V_{pdv}| \gg |V_{continuum}|$. This anomaly is currently unexplained. The relevant anomlous data points have been removed from the remainder of the analysis, and are outside the scope of this project.

It is also neccessary to analyse the effects that a lack of knowledge of both the rotation and dispersion measures will have on the visibility of circularly polarised flux. As can be seen in Figure 4.8 in Section 4.2.2, the circularly polarised component of the flux in the pulse profile of pulsar PSR J1633-5015 remains unaffected when the profile is modified so that RM = 0. This is to be theoretically expected in accordance with the definition of the rotation measure in Section 1.2.2.2. A more complete analysis of the effects using circular polarisation data not calibrated with the correct rotation measure is shown in Figure 4.12, which presents the distributions of both V_{pdv} and $V_{continuum}$ when RM = 0. Comparing these histograms to those presented in Figure 4.10, it can be seen that there is no significant change in the RM = 0 distributions.

Similarly analysing the effect that a lack of knowledge of the dispersion measure has on the visibility of circularly polarised flux results in the histograms shown in Figure 4.13. Comparing these to the original distributions in Figure 4.10, both histograms apear to be similar in overall shape and range. However in both of the DM = 0 plots in Figure 4.13, the range of the distribution is decreased for the correctly calibrated distribution, and there is a greater concentration of pulsars at lower values of $|V|$. Hence, it can be seen that the removal of dispersion measure has a noticeable effect on the visible circularly polarised flux. However, even despite this reduction in visible circularly polarised flux, a significant fraction still remains. Therefore, it can be concluded that overall, a significant amount of fractional circularly polarised flux will still remain in a radio continuum survey, even if neither the

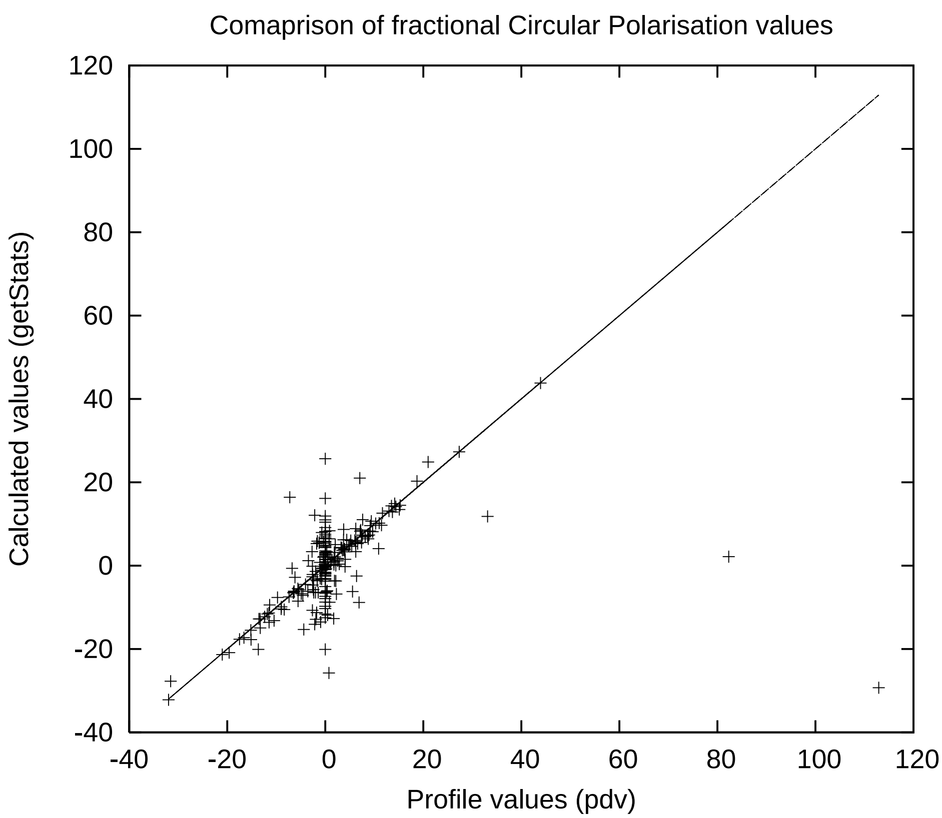

Figure 4.11: Diagram showing the relationship between the two measures of fractional circular polarisation, V_{pdv} and $V_{continuum}$ (listed in this diagram as *getStats* on the vertical axis). The solid line describes a 1:1 path, showing that the two measures clearly correlate. Exceptions include an anomaly at $V_{pdv} = 0$, and three unusual data points for which $|V_{pdv}| \gg |V_{continuum}|$.

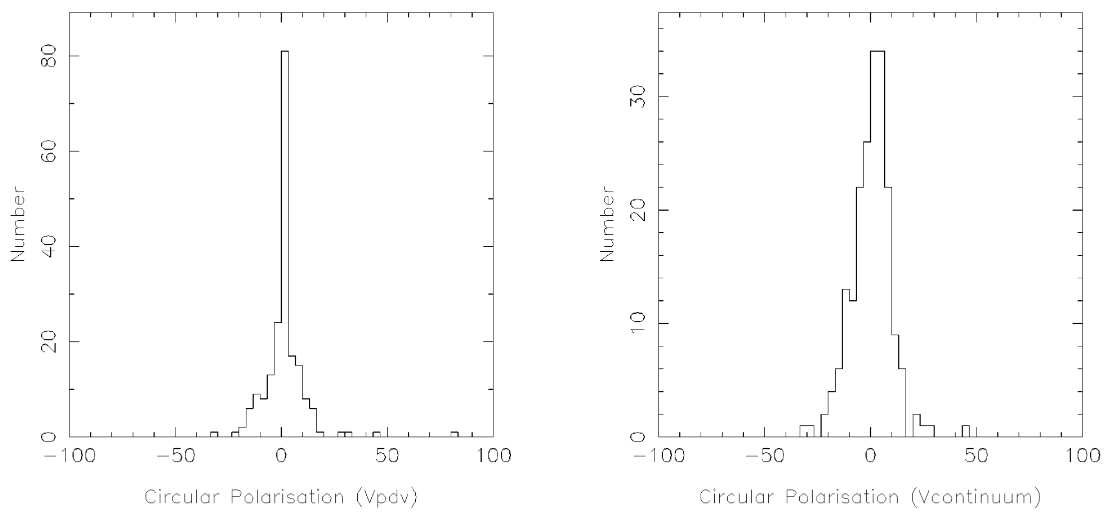

Figure 4.12: Historgrams showing the distribution of fractional circular polarisations for pulsars artificially modified so that RM = 0. The two plots show no change from the histograms in Figure 4.10, in which the circularly polarised flux of pulsars is calculated with their correctly calibrated values of RM.

rotation or dispersion measures of the pulsar are known.

A comparitive cutoff analysis of pulsar and background source populations similar to that carried out for the spectral index parameter in Section 4.2.1 can now be performed. In this analysis, the absolute value of the fractional circularly polarised flux $|V_{continuum}|$ is used, as the left or right sense of the circular polarisation is irrelevant in identifying highly circularly polarised sources, only its magnitude. Given that pulsars are known for high values of $|V|$, a lower cutoff of $|V|$ is used. Figure 4.14 presents the fraction of pulsars missed against miscellaneous background radio objects detected for a given lower cutoff of $|V_{continuum}|$. It is immediately apparent from this plot that the background source data is constrained within a very small region of fractional circular polarisation. Figure 4.15 presents the same data as in Figure 4.14, but with a magnified range over $0\% \leq |V_{continuum}| \leq 5\%$, so that the features of the background source curve can be examined.

From these two Figures, it can be seen that the fractional circular polarisation of the background sources taken from Rayner et al. 2000 ([71]) is remarkably small, with the total percentage of sources selected by a lower cutoff of $|V_{continuum}|$ dropping to virtually zero within the first 1% of circular polarisation. However, although its ascent is much slower than the reduction in fractional amount of background sources, the fractional number of pulsars missed through the use of the circular polarisation cutoff still climbs rapidly to $\sim 80\%$ of pulsars missed with a lower cutoff of $|V_{continuum}| = 10\%$, and to $\sim 95\%$ of pulsars missed with a lower cutoff of $|V_{continuum}| = 20\%$.

4.3 Discussion

Following this analysis, some conclusions can be drawn about the appropriateness of each of the specified criteria in choosing pulsar candidates from the sources produced by the EMU and POSSUM surveys. Due to the various factors inhibiting the visibility of linear polarisation in radio continuum surveys, including the different methods of averaging the Stokes parameters as well as the complications

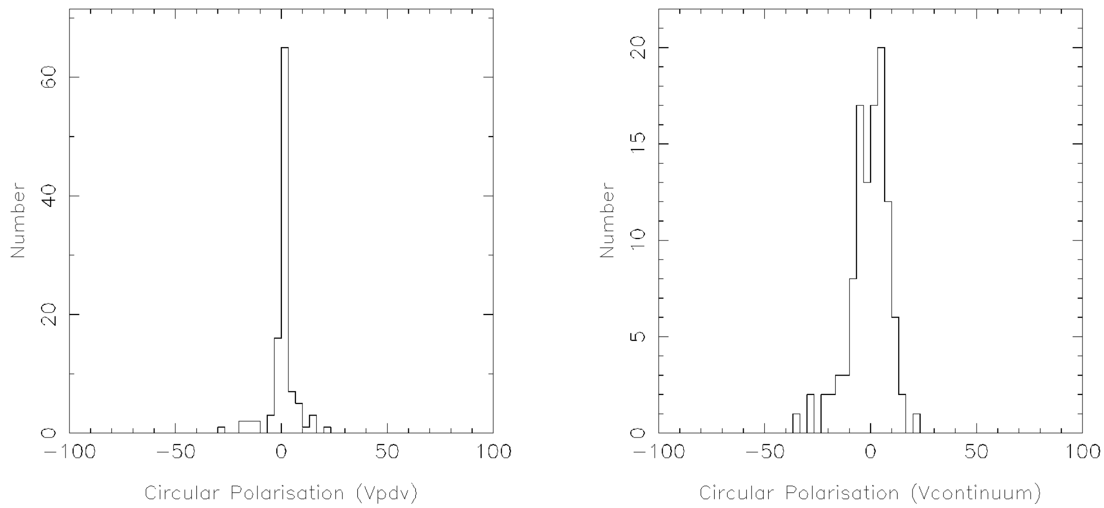

Figure 4.13: Historgrams showing the distribution of fractional circular polarisations for pulsars artificially modified so that DM = 0.

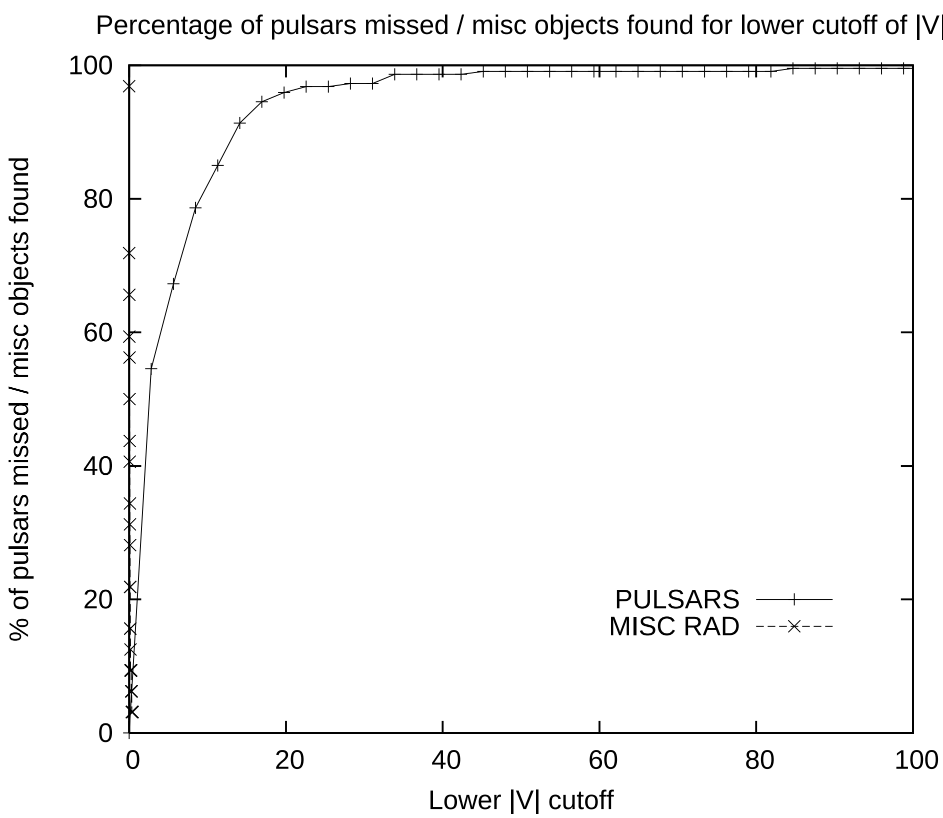

Figure 4.14: A plot showing the fraction of pulsars/background sources that will be missed/included respectively in the sample of sources selected using a lower limit on the value of $|V_{continuum}|$ as indicated on the horizontal axis.

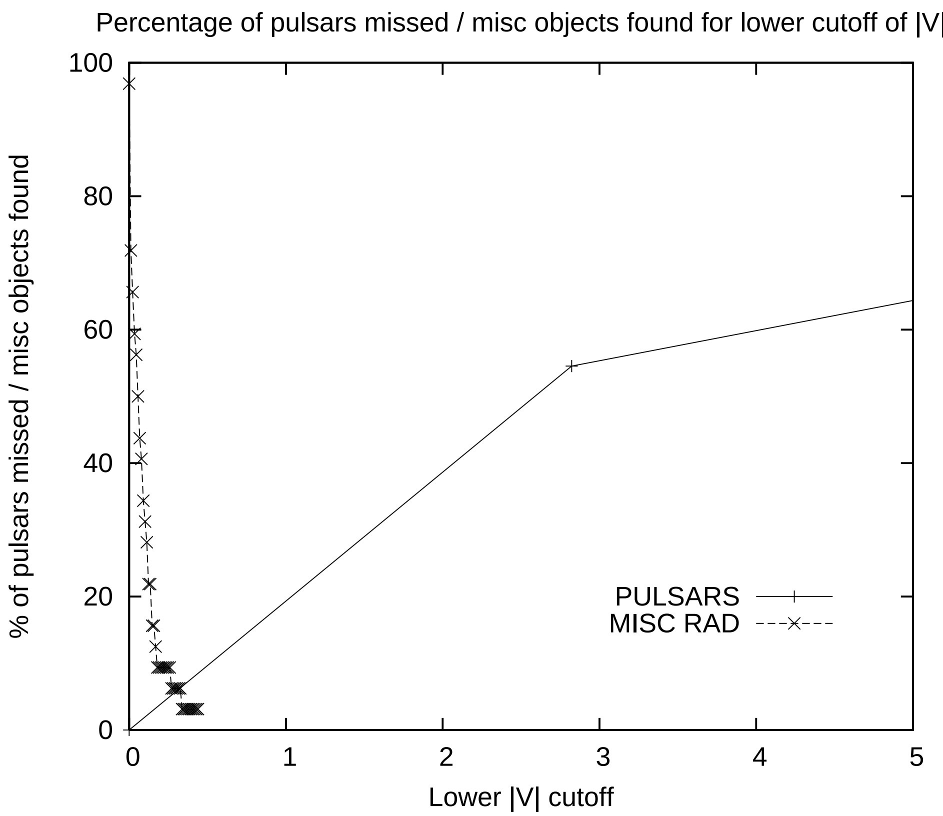

Figure 4.15: A zoomed-in view of the $0\% \leq |V_{continuum}| \leq 5\%$ range of the plot presented in Figure 4.14.

introduced by the lack of knowledge of both the rotation and dispersion measures at the time of source selection, it can be determined that for real-time source selection, the fractional linear polarisation of a detected source is not a practical criterion. It is clear from the analysis in Section 4.2.2 that a lack of knowledge of the rotation measure can in some cases completely destroy the visible linearly polarised flux, and a lack of knowledge of the dispersion measure produces a distribution of fractional linear polarisation of pulsars similar to that of background sources. Examples of this background distribution can be found in Mesa et al. 2002 ([73]) and Grant et al. 2010 ([72]). While it is likely that both the rotation and dispersion measures will eventually be determined for the sources identified by the two surveys, these parameters will likely take considerable time to compute. Unless new methods of instantaneous extraction of the linearly polarised flux components can be developed, fractional linear polarisation is an unsuited criteria for rapid source selection.

A potentially more suitable criteria is found in the pulsar spectral index. As demonstrated in Figure 4.6, it is possible to select an upper cutoff value of spectral index that maximises the fraction of pulsars allowed into the selection of candidate sources while minimising the fraction of false detections of background radio sources. The calculation of such an optimum spectral index cutoff is beyond the scope of this thesis, but one key factor that must be taken into consideration is the relative number of sources in both the pulsar and background radio source populations. As calculated in Section 4.2.1, out of the $\sim 60,000$ sources detected every 12 hours by the EMU and POSSUM surveys, a maximum of 0.4% of these are likely to be pulsars (the real fraction is likely to be much lower). Using this information, over $\sim 59,800$ of the sources detected per pointing in the continuum surveys are likely to be non-pulsar sources. Selecting a spectral index cutoff that allows even 1% of these sources into the selection of pulsar candidates would introduce $\sim$ 600 false candidates. Hence, an optimal spectral index cutoff value would need to lie near the value of $\alpha = -3$ in order to reduce the number of background sources to as small a number as possible, but choosing such a cutoff value would simultaneously remove $\sim$ 99% of pulsars from the candidate pulsar selection. While any sources that satisfied this crtierion would stand a very high chance of being true pulsars, this cutoff would render almost all pulsars detected by EMU and POSSUM undetected. This result explains the non-detection of any pulsars in the IFRS candidates chosen for analysis in Chapter 3. Therefore, it would seem that the spectral index parameter is also not a suitable candidate for a criterion pulsar source selection in continuum surveys.

That being the case, if a source selected through the use of another criterion happens to possess a spectral index appropriate to the pulsar population, this will further increase the attractiveness of that source as a candidate pulsar. However, one other impediment standing in the way of the use of spectral indices is the neccessary requirement of data at multiple frequencies in order to calculate a value of α. With a planned bandwidth for ASKAP of 300 MHz, it is possible that an approximate spectral index could be calculated using radio fluxes at opposite ends of this frequency range over the course of a single observation, but such calculations are likely to have a large margin of error. The need for additional data will be partially resolved through the planned implementation of the source cross-identification pipeline described in Section 4.1, but as with the calculation of rotation and dispersion measure in the case of fractional linear polarisation, this will take large amounts of processing power and time to carry out. In addition, given the expected $\sim$ 70 million sources to be produced by EMU, it is certain that a large portion of the sources identified will not have counterparts in data taken of the same region using different frequencies. In some cases, this non-detection of counterparts may be able to place useful constraints on the possible value of a spectral index, however, in many cases this will mean that a spectral index can not be calculated in real-time, further diminishing its suitability in determining candidate sources.

The final criterion considered in this analysis is that of fractional circular polarisation. This crtierion stands out by far as the most ideal of the three criteria analysed, as the visiblity of circularly polarised flux is not affected by a lack of knowledge of rotation measure, and appears to be only marginally reduced by the integration techniques of continuum surveys and by a lack of knowledge of the dispersion measure. In addition, the cutoff analysis presented in Figures 4.14 and 4.15 indicate that high fractional circular polarisations are almost exclusive to pulsars, with even a lower cutoff limit of $|V| = 1\%$ excluding virtually all of the background radio sources and only missing 20% of pulsars from the selected candidate sources. However, this study was conducted only over a very limited range of background radio sources, which may not be typical of the true distribution of background radio sources that exhibit considerable degrees of circular polarisation. Further investigation of the properties of the background source population are warranted in order to resolve this potential issue. There is also the question of how far the data reduction of POSSUM in producing circular polarisation data will lag behind the primary EMU survey, but given that both of these surveys are still in the design stage, any answer to this question would be speculative at best. At this stage it would seem that a cutoff using the fractional circular polarised flux is the best choice for a suitable selection criterion of candidate pulsars, but more inevestigation and study is warranted to determine its true effectiveness.

One additional factor in favour of the use of circular polarisation as a criterion for source selection is that even if a significant number of background radio sources are collected in the selection of candidate pulsars, those that are not pulsars are likely to be objects of reasonable scientific interest in their own right. A prime example of this is the case of CU Virginis, an unusual object sometimes referred as a 'stellar pulsar' [76], in that it is not a neutron star but instead belongs to a class of stars known as *magnetic chemically peculiar* (MCP) stars. CU Virginis is also seen to emit pulsations previously considered to be unique to pulsars, with a period of approximately half a day [76]. The star is also unusual in that its profile is characterised by two peaks of 100% circularly polarised flux at 1400 MHz [75]. Such a star as this, although not a pulsar, would be included in the candidate pulsar sources selected from the EMU and POSSUM surveys through the use of a circular polarisation criterion, but despite the fact that it is not a pulsar, such a source would be well worth selecting for thorough study.

Chapter 5

Conclusions & Further Work

5.1 The Infrared-Faint Radio Sources

In Chapter 3, a search was conducted for short-term radio pulsations from 17 of the ATLAS infrared-faint radio sources, and after considerable analysis, it was concluded that pulsed emission cannot account for the observed radio fluxes in any of the 17 sources. Since the sensitivity limit of the observations is well below the observed fluxes of the chosen IFRS, it is unlikely that any of these enigmatic sources are simply close by pulsars in our own Galaxy. In short, none of the IFRS studied in this project were determined to be pulsars, despite the rudimentary application of selection criteria in an effort to isolate pulsars from the rest of the continuum detections.

Hence, the nature of the IFRS studied in this project, as well as the identities of the majority of the IFRS detected by ATLAS, remain undetermined. Current research, as detailed in Section 3.1, suggests that the IFRS may be made up of several different types of objects, with radio-loud AGN and quasars as some of the prime candidates. However, despite the non-detection of pulsars in any of our 17 chosen IFRS, there still remains the possibility that pulsars may be responsible for future IFRS detections in the EMU and POSSUM surveys. As noted in Section 3.5, EMU and POSSUM are likely to uncover on the order of one million new IFRS, and applying source selection criteria of the type described in Chapter 4 in order to select suitable pulsar candidates from these new IFRS will not only lead to a better understanding of both the nature of the IFRS and of the usefulness and application of the crtieria, but may yet lead to the discovery of new and unusual sources, many of them hopefully pulsars.

5.2 Pulsar selection criteria, EMU, POSSUM & ASKAP

Based upon the analysis presented in Chapter 4, it is clear that the most promising of the studied selection criteria for use in selection EMU and POSSUM sources as candidates for pulsars is that of fractional circularly polarised flux. The difference in the distributions of fractional circularly polarised flux between pulsars and the background population is great enough such that a lower critical value of the fractional circular polarisation can be chosen such that all of the sources selected as candidate pulsars will be true detections. However, this recommendation is a cautious one, as the inherent assumptions made in choosing the background source population for comparison may have provided a biased result. Investigating this possible bias was to have been the next step of analysis in the project, but due to time constraints this had to be abandoned. Hence, one key piece of future work is to further evaluate the circular polarisation charcteristics of the general population of radio sources so that a better assessment of the applicability of the circularly polarised flux criterion can be made.

Even if the distribution of background sources warrants a higher value of $|V_{continuum}|$than indicated by the figures in Section 4.2.3, it is not likely that this shift in the ideal fractional circular polarisation cutoff should increase by a considerable amount. Even if the cutoff shift does turn out to be significant, and a majority of pulsars are missed by the new cutoff, those allowed through as candidate pulsars will be scientifically interesting candidates, pulsars or not. Therefore, it can be concluded that from the options examined in this thesis, the best candidate for a source selection criterion is the use of a cutoff of fractional circular polarisation.

As for the remaining selection criteria, although linear polarisation is at this stage unusable as a real-time source selection criterion, it may be possible to employ this parameter is choosing pulsar candidates in studies of the EMU and POSSUM catalogues following the determination of the rotation and dispersion measures for a large number of sources. Further analysis comparing the distribution of fractional linear polarised flux in the pulsar population to that of the background source population will first need to be conducted. With regards to the use of spectral index as a criterion, it is clear that this parameter is unsuitable for use the sole criterion upon which sources can be selected as pulsar candidates. A cutoff set low enough to exclude all but a small number of background sources will also exclude almost all pulsars from selection as candidates, and raising the cutoff by any considerable fraction will cause any true pulsars in the selected candidates to be drowned out by an overwhelming number of false detections. This result explains why the IFRS in Chapter 3, chosen for their steep values of spectral index, were not identified as pulsars. The spetral index parameter may be useful in narrowing down pulsar candidates selected by other means, but it cannot on its own serve as a useful selection criterion.

Appendix A

Data processing scripts

This Appendix contains some of the data processing scripts key to the implementation of the analysis techniques performed in this project. Each script contains a description of the required inputs and an explanation of its operation and output

A.1 Cutoff

```
#!/bin/bash

# Andrew Cameron, UNSW, 3219329
# cutoff.sh - Version 1.3
# last updated 28/10/2010

# Program to produce cutoff data files for plotting
# Scans through a dataset of one column, uses max and min in that column to set range
# Then, given the number of increments X as input, sets X values of the cutoff to test,
# with the values equally spaced between the max and min.
# Then calculates the number of sources included/missed above/below each cutoff,
# determines the result as a percentage of the total sources, and
# sends results, cutoff value and source percentage, out to file for later plotting

# $1 is the name of the input file to scan
# $2 is the name of the output file to place entries into
# $3 is the number of increments to use - set to separate variable
# $4 specifies whether we are to use an upper or lower cutoff (set to u for upper, l for lower)
# $5 specifies whether we are to count those items missed or those included (missed (m) or included
(i))
# $6 specified whether to use absolute values (a) or relative values (r) of entries in file

increments=${3}

echo "CUTOFF PLOTTER - VERSION 1.3"
echo "> begin script - scan for max/min"

# read through the file to find max and min values
lines=0 # counts number of lines
max=0   # stores max value
min=0   # stores min value
while read dataline
do
        if [ $lines -eq 0 ]; then
                max=$dataline
                min=$dataline
        else
                if [ $(echo "$max < $dataline" | bc ) -eq 1 ]; then
                        max=$dataline
                fi

                if [ $(echo "$min > $dataline" | bc ) -eq 1 ]; then
                        min=$dataline
                fi
        fi

        lines=$(($lines+1))
done < ${1}

# reconfigure max and min in case the absolute value flag is set
# sets min = 0 and max = whichever is the greatest ab. val of original max and min
if [ ${6} = "a" ]; then
        # square to make both max and min positive
        if [ $(echo "$min*$min > $max*$max" | bc) -eq 1 ]; then
                # swap max for abv. value of min
                max=$(echo "scale=9; sqrt($min*$min)" | bc)
        else
                # swap max for abv. value of max
                max=$(echo "scale=9; sqrt($max*$max)" | bc)
        fi

        min=0
fi

echo "> scan complete"
echo "> max = $max | min = $min"
echo "> number of entries = $lines"

# for this first version, we want to plot how many pulsars are missed by
# setting particular cutoffs of spectral index
# we scan from min to max, working out how many pulsars no longer lie above the min value
# using the number of increments specified

echo ""
```

```
echo "> initialise scanning increment value"
incval=$(echo "scale=9; ($max - $min)/($increments)" | bc ) # this value is positive
echo "> increment initialised"

echo "> initialise scanning parameters"

# set up whether we scan down or up, and whether we count those missed or included
if [ $4 = "u" ]; then
        curval=$max # initialises value of scan
        echo "> ...scanning using upper cutoff"
elif [ $4 = "l" ]; then
        curval=$min # initialises value of scan
        echo "> ...scanning using lower cutoff"
fi

if [ $5 = "m" ]; then
        echo "> ...counting entries missed"
elif [ $5 = "i" ]; then
        echo "> ...counting entries included"
fi

echo "> scanning parameters initialised"

echo "> initialising storage arrays"
# now we make arrays to save on the number of repeitions we require to complete the analysis
i=0 # counter variable

while [ $i -lt $increments ];
do
        # make increment array
        inc_array[$i]=$curval

        # increment stored value
        if [ $4 = "u" ]; then
                curval=$(echo "scale=9; $curval - $incval" | bc )
        elif [ $4 = "l" ]; then
                curval=$(echo "scale=9; $curval + $incval" | bc )
        fi

        # make count array - set to zero as initial vlue
        count_array[$i]=0

        i=$(($i+1))
done

echo "> storage arrays initialised"


i=0 # counter variable
echo "> begin analysis"

while read dataline
do
        echo "***************************"
        echo "> reading file - line $i"
        echo "> begin increment scan"

        # implement the absolute value functionality
        if [ ${6} = "a" ]; then
                if [ $(echo "$dataline < 0" | bc) -eq 1 ]; then
                        # make the value positive
                        dataline=$(echo "scale=9; (-1)*$dataline" | bc)
                fi
        fi


        # now we need to scan across all increment values
        j=0 #second counter

        while [ $j -lt $increments ];
        do

                # select increment for curval
                curval=${inc_array[$j]}
```

```
                if [ $5 = "m" -a $4 = "u" ]; then
                        if [ $(echo "$dataline > $curval" | bc ) -eq 1 ]; then
                                # if the cutoff has missed this object
                                # increase counter
                                count_array[$j]=$((${count_array[$j]}+1))
                        fi
                elif [ $5 = "i" -a $4 = "u" ]; then
                        if [ $(echo "$dataline < $curval" | bc ) -eq 1 ]; then
                                # if the cutoff has included this object
                                # increase counter
                                count_array[$j]=$((${count_array[$j]}+1))
                        fi
                elif [ $5 = "m" -a $4 = "l" ]; then
                        if [ $(echo "$dataline < $curval" | bc ) -eq 1 ]; then
                                # if the cutoff has missed this object
                                # increase counter
                                count_array[$j]=$((${count_array[$j]}+1))
                        fi
                elif [ $5 = "i"  -a $4 = "l" ]; then
                        if [ $(echo "$dataline > $curval" | bc ) -eq 1 ]; then
                                # if the cutoff has included this object
                                # increase counter
                                count_array[$j]=$((${count_array[$j]}+1))
                        fi
                fi

                j=$(($j+1))
        done

        echo "> increment scan complete"


        i=$(($i+1))
done < ${1}

echo "> file read complete"

# normalise the count to a percentage
i=0 # counter variable

while [ $i -lt $increments ];
do

        # calculate percentage
        percent[$i]=$(echo "scale=9; ${count_array[$i]}*100/$lines" | bc )

        echo "> result $i normalised"
        # write value to file
        if [ $i -eq 0 ]; then
                echo "${inc_array[$i]} ${percent[$i]}" > ${2}
        else
                echo "${inc_array[$i]} ${percent[$i]}" >> ${2}
        fi

        echo "> result written to file"

        i=$(($i+1))
done

echo "****************************"
echo "> analysis complete"
echo "> script complete - terminating"
```

A.2 GetStats

```
#!/usr/openwin/bin/tcsh
#

# Andrew Cameron & George Hobbs, UNSW & CSIRO
# 3219329
# getStats - last updated 12/11/2010

# script uses custom statistics package written by George Hobbs
# available on CSIRO serves at
# /u/hob044/software/new_c/stats/stats

# script to perform specified mathematical operations on "file.asc"
# this is to be externally set up from a pulse profile file
# produces several parameters and outputs them with labels to standard out

# new version also takes in additional parameters from the command line
# $1 - name of pulse profile file from which file.asc has been generated
# $2 - fractional linear flux component as calculated by pdv
# $3 - fractional circular flux component as calculated by pdv

set totI = `/u/hob044/software/new_c/stats/stats -f file.asc -col 2 -sum | grep Sum | awk '{print $2}'`
set totQ = `/u/hob044/software/new_c/stats/stats -f file.asc -col 3 -sum | grep Sum | awk '{print $2}'`
set totU = `/u/hob044/software/new_c/stats/stats -f file.asc -col 4 -sum | grep Sum | awk '{print $2}'`
set totV = `/u/hob044/software/new_c/stats/stats -f file.asc -col 5 -sum | grep Sum | awk '{print $2}'`
set totL = `echo $totQ $totU | awk '{print sqrt($1*$1+$2*$2)}'`
# totL is sum of the square of the average sum of the individual polarisation components
# totL = <Q>^2 + <U>^2

# use argument $1 to grab name of object being examined
set name = `vap -c name $1 | grep -v name | awk '{print $2}'`
# use arguments $2 and $3 to display additional parameters calculated by pdv
set li = `echo $2`
set vi = `echo $3`


# Calculate linear polarisation for each time bin
awk '{print sqrt($3*$3+$4*$4)}' file.asc >! linear.asc
set linear = `/u/hob044/software/new_c/stats/stats -f linear.asc -col 1 -sum | grep Sum | awk '{print
$2}'`
# linear is the average of the sum of the squares of the individual polarisation components
# linear = <Q^2 + U^2>

#echo $linear $totI | awk '{print " ",$1,$1/$2}'


echo "(1)name (2)sumI (3)sumQ (4)sumU (5)sumV (6)sqrt(sQ*sQ+sU*sU) (7)sQ/sI (8)sU/SI (9)sV/sI (10)sqrt
(sQ*sQ+sU*sU)/sI (11)linear/sI (12)pdv(L/I) (13)pdv(V/I)"
echo $totI $totQ $totU $totV $totL $linear $name $li $vi | awk '{print $7,$1,$2,$3,$4,$5,$2/$1*100,$3/
$1*100,$4/$1*100,$5/$1*100,$6/$1*100,$8*100,$9*100}'
```

A.3 Overscript

```bash
#!/bin/bash

# Andrew Cameron, UNSW/CSIRO, 3219329
# script to be executed from /DATA/BRAHE_1/hob044/simonCalibratedProfiles/test

# This script is designed to oversee the analysis of
# a large collection of pulse profile data files.
# A list of the files is compiled, then each file is transformed
# into the ASCII 'file.asc' for execution by getStats.
# Only profiles with a S/N over a given value are used.
# Other information on files is also taken.
# Finally, the script compiles the data received from getStats into
# a useful format for later plotting and analysis.

# Input parameters
# $1 - signal to noise cutoff - only profiles with an S/N above this number are used.

# get a list of all the files in the directory of type ".SFTC" and store in temp file
# S/N cutoff must be above a certain threshold

sn_cutoff=${1}
# get S/N data

pdv -FTfp ../*.SFTC | grep -v Freq | awk '{print $1,$10}' > temp_sn

# select only filenames which have S/N greater than cutoff
# use counter to control specific operations
i=0

while read sn_line
do

        filename=$(echo "$sn_line" | awk '{print $1}' )
        sn=$(echo "$sn_line" | awk '{print $2}' )

        if [ $(echo "$sn > $sn_cutoff" | bc) -eq 1 ]; then
                echo "SN = $sn"
                if [ $i -eq 0 ]; then
                        echo $filename > temp_filelist
                else
                        echo $filename >> temp_filelist
                fi
        fi

        # increment counter
        i=$(($i+1))

done < temp_sn

# for every file in the temp list, perform the operation
# use counter to control specific operations
i=0

while read dataline
do

        echo $dataline

        # extract ASCII file
        # get number of channels
        pdv -txFT $dataline > file_temp.asc

        # use new counter to extract relevant information
        j=0
        while read line
        do
                if [ $j -eq 0 ]; then
                        # if we have the first line, extract number of bins
                        bins=$(echo "$line" | awk '{print $12}')
                elif [ $j -eq $(($bins + 2)) ]; then
                        # if we have the line that stores calculated L/I and V/I
                        li=$(echo "$line" | awk '{print $6}')
                        vi=$(echo "$line" | awk '{print $7}')
                fi
```

```
                # increment j
                j=$(($j+1))

        done < file_temp.asc

        # cleanup
        rm file_temp.asc

        # make file for stats app
        pdv -txFT $dataline | grep -v File | grep -v SFTC | awk '{print $3,$4,$5,$6,$7}' > file.asc

        # run stats script and extract to file
        if [ $i -eq 0 ]; then
                ./getStats $dataline $li $vi > result.out
        else
                ./getStats $dataline $li $vi | grep -v sumI >> result.out
        fi


        # increment counter
        i=$(($i+1))

done < temp_filelist

# cleanup

rm temp_filelist
```

Appendix B

Publishable Material

This Appendix contains a copy of the paper "Are the infrared-faint radio sources pulsars?", which was submitted on 9th November, 2010 to the *Monthly Notices of the Royal Astronomical Society* (MNRAS). The paper forms the basis for Chapter 3, and has not yet been accepted for publication at the time of writing. It is currently in a period of revision after having been independently reviewed and critiqued by MNRAS, and current indications are that the paper will be accepted once this revision process is complete. The version of the paper provided here is that which was initially submitted to MNRAS.

Mon. Not. R. Astron. Soc. **000**, 000–000 (0000) Printed 9 November 2010 (MN LaTeX style file v2.2)

Are the infrared-faint radio sources pulsars?

A. D. Cameron,[1,2] M. Keith,[2] G. Hobbs,[2] R. P. Norris,[2] M. Y. Mao[2,3,4] & E. Middelberg[5]

[1] *School of Physics, University of New South Wales, Sydney, NSW 2052, Australia*
[2] *CSIRO Astronomy & Space Science, PO Box 76, Epping NSW 1710, Australia*
[3] *School of Mathematics and Physics, University of Tasmania, Private Bag 37, Hobart, 7001, Australia*
[4] *Anglo-Australian Observatory, PO Box 296, Epping, NSW, 1710, Australia*
[5] *Astronomisches Institut, Ruhr-Universität Bochum, Universitätsstr. 150, 44801 Bochum, Germany*

ABSTRACT

Infrared-Faint Radio Sources (IFRS) are objects which are strong at radio wavelengths but undetected in sensitive Spitzer observations at infrared wavelengths. Their nature is uncertain and most have not yet been associated with any known astrophysical object. One possibility is that they are radio pulsars. To test this hypothesis we undertook observations of 17 of these sources with the Parkes Radio telescope. Our results limit the radio emission to a pulsed flux density of less than 0.21 mJy, well below the flux density of the IFRS. We therefore conclude that these IFRS are not radio pulsars.

Key words: surveys, pulsars: general

1 INTRODUCTION

Infrared-Faint Radio Sources (IFRS) are objects which typically have flux densities of several mJy at 1.4 GHz, but are undetected at 3.6 μm using sensitive *Spitzer Space Telescope* observations with μJy sensitivities (Norris et al. 2006). They were an unexpected discovery in the Australia Telescope Large Area Survey (ATLAS), which, covering seven square degrees at 1400 MHz to ~30 μJy, is the widest deep field radio survey attempted thus far (Norris et al. 2006; Middelberg et al. 2008a). There are ~ 50 IFRS in ATLAS, accounting for 2.5% of the current ATLAS source catalogue. Most of the IFRS are unresolved at 1.4 GHz and have flux densities of up to tens of mJy.

The ATLAS project surveys two regions of sky (Figure 1). The first region includes the Chandra Deep Field South (CDFS) (Giacconi et al. 2001) which encompasses the Great Observatories Origins Deep Survey (GOODS) field (Giavalisco et al. 2004). The second region coincides with the European Large Area ISO Survey-South1 (ELAIS-S1). Both regions have also been covered by the *Spitzer* Wide-Area Infrared Extragalactic (SWIRE) survey program (Lonsdale et al. 2003). The second region is close to (but does not overlap) the region covered by the recent Parkes High Latitude Pulsar Survey (Burgay et al. 2006).

The primary goals of ATLAS are to trace the cosmic evolution of active galactic nuclei (AGN) and star-forming galaxies. The detected sources are expected to follow relatively well-known spectral energy distributions (SED) that predict infrared emission detectable by *Spitzer* from any strong radio source. Since the discovery of IFRS in 2006, several publications have attempted to understand their nature and emission mechanisms. Very long baseline interferometry (VLBI) observations of a total of six IFRS by Norris et al. (2007) and Middelberg et al. (2008b) have resulted in the detection of high-brightness temperature cores in two IFRS. Recently, Huynh et al. (2010) investigated the four IFRS in the GOODS field, for which ultra-deep Spitzer imaging had recently become available, and attempted to fit template SEDs corresponding to known classes of galaxies and quasars. Norris et al. (2010) have extended this work using deep Spitzer imaging data from the Spitzer Extragalactic Representative Volume Survey project (Lacy et al. 2010), and have shown that most IFRS sources have extreme values of S20/S3.6, which can be fitted by a high-redshift radio-loud galaxy or quasar. They also stacked the deep Spitzer data to show that a typical IFRS must have a median 3.6 μm flux density of 0.2 μJy, giving extreme values of the radio-infrared flux density ratio. Middelberg et al. (2010) have found the spectra of IFRS are remarkably steep, with a median spectral index of -1.4 and a prominent lack of spectral indices larger than -0.7.

The nature of IFRS remains unclear, largely because they are invisible to even the most sensitive optical/infrared observations. While at least some are likely to be high-redshift radio galaxies or quasars, it is also likely that the class may encompass several types of object. Other candidates for IFRS include heavily obscured AGN, stray radio lobes, radio relics and radio pulsars (Norris et al. 2006, 2007; Middelberg et al. 008b; Garn & Alexander 2008). Norris et al. (2007) propose that IFRS may even represent a phase of AGN evolution.

For 17 of these sources the measured flux densities and spectral indices are consistent with those measured for pulsars in our own galaxy (Manchester et al. 2005)[1] . As the ATLAS survey regions are well away from the Galactic plane, it is unlikely that all 17 of these sources are pulsars, but it is possible that some are. If so, then it is important to identify them so that (a) they can be removed from the extragalactic source statistics, and (b) so they can be accounted for in models of pulsar populations. If a significant fraction of putative extragalactic radio sources are pulsars, then it is important to identify them so that they do not contaminate radio source count statistics, which are used as a tool to understand the cosmic evolution of star-forming galaxies and AGN.

However, it is difficult to estimate how many pulsars would be expected in any given region of the sky. The most recent pulsar surveys have covered regions close to the Galactic plane (e.g., Manchester et al. 2001). These pulsar surveys have discovered a large number of new pulsars, but relatively few millisecond pulsars. The Galaxy is likely to contain similar number of normal and millisecond pulsars (Lyne et al. 1998), but the millisecond pulsars are likely to have travelled significant distances from the Galactic plane and are difficult to find due to their relatively low luminosities, their fast spin-rates and because they are commonly in binary systems, which disrupts the regular periodicity of their emitted pulses. The only deep 20-cm pulsar survey covering a large area that is far from the Galactic plane is the Parkes High Latitude Pulsar Survey, which covers Galactic longitudes $220° < l < 260°$ and latitudes $|b| < 60°$ (Burgay et al. 2006), with 6456 pointings of 265 seconds each. This survey detected 42 pulsars with a survey sensitivity of pulsed flux ~ 0.5 mJy. Even though this survey made relatively few discoveries, the pulsars detected away from the Galactic plane were of great astrophysical interest. They included the first double pulsar system PSR J0737−3039 (Lyne et al. 2004) and three other millisecond pulsars. Burgay et al. (2006) discussed the Galactic latitude distribution of their detections in detail, and suggested a roughly uniform distribution. However, this survey was relatively insensitive to millisecond pulsars, because of the restricted sampling time and number of frequency channels, and so the total number of millisecond pulsars detected was small. Hence, it is currently impossible to make a reasonable estimate of the number of pulsars likely to be detected per square degree at high Galactic latitude. With a survey sensitive to millisecond pulsars it seems reasonable that at least one detectable pulsar exists in the ATLAS survey region of roughly seven square degrees, but because this number is so poorly known, it adds a further motivation for this study.

It should be noted that detections and discoveries of pulsars in radio continuum data are not without precedent. Examples include PSR B1937+21, the first millisecond pulsar (Backer et al. 1982), PSR B1821−24, found during a VLA imaging search of globular clusters (Hamilton et al. 1985), PSR B1951+32, initially identified as a steep-spectrum polarised point source central to the supernova remnant CTB 80 (Strom 1987), and PSR J0218+4232, originally uncovered by the Westerbork Synthesis Radio Telescope (WSRT) (Navarro et al. 1995).

[1] http://www.atnf.csiro.au/research/pulsar/psrcat/

2 OBSERVATIONS

We selected 17 of the IFRS based on their flux density and spectral index. The sources range from 0.5 mJy to 23 mJy and from very steep to almost flat spectral indices (−2.4 to −0.2). These parameters are certainly similar to those of the known pulsar population, which have flux densities that range from 0.01 to 1100 mJy at an observing frequency close to 1400 MHz and have known spectral indices ranging between −3.5 and +0.9 with a median of −1.7 (Manchester et al. 2005). It should be noted that the lower value of the pulsar flux range is not due to any physical characteristic of pulsars, but is instead due to the physical limitations in the sensitivity of our instrumentation.

In Table 1 we tabulate the source names, positions, flux density and spectral index of the IFRS. For each source we carried out a 35 minute observation using the Parkes 64-m radio telescope equipped with the 20-cm 13-multibeam receiver (although only the central beam was utilised for our analysis), with 340 MHz of bandwidth centred on 1352 MHz. We used the Berkeley Parkes Swinburne Recorder (BPSR), a high resolution digital filterbank, providing 870 frequency channels, 2-bit samples every 64 μs. This observing setup is almost identical to the High Time Resolution Universe Pulsar Survey project (Keith et al. 2010), using a similar bandwidth, observing frequency backend system and sampling rate, with high sensitivity to millisecond pulsars. The data were recorded to magnetic tape for off-line processing. The data were processed using the HITRUN pipeline (see Keith et al. 2010 for details) to search for periodic signals in dedispersed time series with trial dispersion measures (DMs) in the range of 0 to 1000 cm^{-3} pc.

We determine the theoretical sensitivity of our observations using the radiometer equation, which gives the fundamental limiting flux density of the central beam,

$$S_{min} = \frac{\sigma(T_{sys} + T_{sky})}{G\sqrt{2B\tau_{obs}}}\sqrt{\frac{W}{1-W}}. \quad (1)$$

In this equation, σ is the cutoff S/N for a positive detection, T_{sys} is the system noise temperature, T_{sky} is the sky noise temperature, G is the system gain, B is the observing bandwidth, τ_{obs} is the integration time of the observations and W is the fractional pulse width. The typical value of W for pulsars is approximately 10 percent of the pulse period, although it can be as high as 50 percent. At this galactic latitude, T_{sky} is negligible. Scaling our parameters from those of Keith et al. (2010), setting $\sigma = 8$, $T_{sys} = 23$ K, and $G = 0.735$, we arrive at a sensitivity to pulsed emission of $S_{min} = 0.07$ mJy for a 10 percent pulse duty cycle, or $S_{min} = 0.21$ mJy for a 50 percent pulse duty cycle. As all of our chosen IFRS candidates possess continuum fluxes above the higher of the two flux limits, if any of them are indeed pulsars they should be easily detectable by our observations at the $8-\sigma$ confidence level.

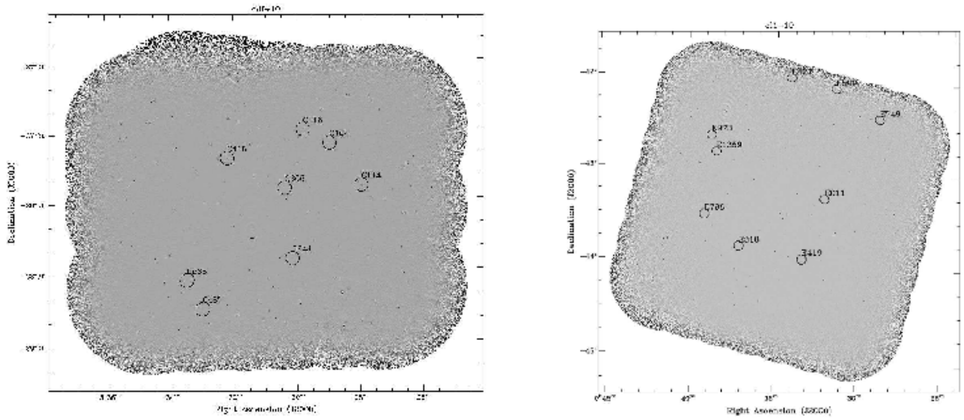

Figure 1. The two ATLAS fields: CDFS (left panel) and ELAIS (right panel). The circles indicate the positions of the chosen IFRS and the beams that have been surveyed for pulsars.

Table 1. Parameters of the infrared-faint radio sources selected for analysis as potential pulsars. All flux and spectral index data is obtained from Middelberg et al. (2010), with the exception of ES1259 (Middelberg et al. 2008a) and CS255 (Norris et al. 2006).

Source	Right ascension (hms)	Declination (dms)	20cm Flux density (mJy)	Spectral index
ES011	00:32:7.444	−44:39:57.8	9.5	−1.44
ES318	00:37:05.54	−44:07:33.7	2.0	−0.78
ES419	00:33:22.80	−43:59:15.4	4.4	−1.35
ES427	00:34:11.59	−43:58:17.0	22.3	−1.08
ES509	00:31:38.63	−43:52:20.8	22.7	−1.02
ES749	00:29:05.23	−43:34:03.9	10.3	−1.08
ES798	00:39:07.93	−43:32:05.8	11.7	−0.81
ES973	00:38:44.14	−43:19:20.4	11.6	−1.15
ES1259	00:38:27.171	−42:51:33.8	4.5	
CS114	03:27:59.89	−27:55:54.7	7.7	−1.34
CS164	03:29:00.20	−27:37:54.8	1.6	−0.92
CS215	03:29:50.02	−27:31:52.6	1.6	−0.76
CS241	03:30:10.22	−28:26:53.0	1.0	−1.96
CS255	03:30:24.08	−27:56:58.7	0.5	
CS415	03:32:13.97	−27:43:51.1	2.6	−2.38
CS487	03:33:01.20	−28:47:20.8	1.5	−0.21
CS538	03:33:30.20	−28:35:11.2	2.0	−0.88

3 RESULTS AND DISCUSSION

The folded pulse profiles (intensity as a function of pulse phase) were viewed by eye for all candidates with a signal-to-noise ratio above 8σ. The observed pulse profiles for each candidate and their pulse periods were clearly caused by radio frequency interference or processing artefacts. For example, one candidate with a signal-to-noise ratio of 13σ was detected with a frequency of 50.01 Hz and a sinusoidal pulse profile, indicating RFI originating with the mains power supply. We note that the mean flux density of the IFRS is approximately 6.9 mJy, and the median flux is approximately 4.4 mJy. If these are due to pulsars, they would be detectable in these observations at a level of 263σ and 168σ respectively. We conclude that none of the IFRS observed in this project was found to be a pulsar with a pulse strength of at least 0.21 mJy.

The absence of pulsar detections in this project emphasises the difficulty of identifying pulsar candidates through continuum surveys. Despite the four detections described in Section 1, the vast majority of continuum (i.e., low time resolution) pulsar surveys have found no positive results, examples including Kaplan et al. (2000) and Crawford et al. (2000). Also, while our analysis attempted to take advantage of the typically steep values of pulsar spectral indices in selecting our targets, the principle means of searching for pulsar candidates in continuum surveys has been to identify sources with significant linear and/or circular polarisation (Han et al. 1998; Han et al. 2009). Further studies using these selection criteria may yield better results.

Finally, the Evolutionary Map of the Universe (EMU) survey[2], to be carried out using the Australian Square Kilometre Array Pathfinder (ASKAP), is likely to detect 70 million radio sources with a sensitivity limit of $\sim 10\mu$Jy. Over a million of these sources are likely to be IFRS. It is possible that searching these radio continuum sources will provide means by which ASKAP will discovery millisecond and binary pulsars.

4 CONCLUSIONS

We have searched for short-term radio pulsations originating from 17 of the ATLAS infrared faint sources and find that pulsed emission cannot account for the observed radio flux. Since the sensitivity limit of our observations is well below the observed fluxes of the chosen IFRS, it is unlikely that any of these enigmatic sources are simply close-by pulsars in our own Galaxy. Hence, the nature of these sources is yet to be determined.

ACKNOWLEDGEMENTS

We thank Chris Hales for the use of his processed images in Figure 1. GH is the recipient of an Australian Research Council QEII Fellowship (project #DP0878388). The Parkes telescope is part of the Australia Telescope which is funded by the Commonwealth of Australia for operation as a National Facility managed by CSIRO.

REFERENCES

Backer D. C., Kulkarni S. R., Heiles C., Davis M. M., Goss W. M., 1982, Nature, 300, 615
Burgay M., Joshi B. C., D'Amico N., Possenti A., Lyne A. G., Manchester R. N., McLaughlin M. A., Kramer M., Camilo F., Freire P. C. C., 2006, MNRAS, 368, 283
Crawford F., Kaspi V. M., Bell J. F., 2000, AJ, 119, 2376
Garn T., Alexander P., 2008, MNRAS, 391, 1000
Giacconi R., Rosati P., Tozzi P., Nonino M., Hasinger G., Norman C., Bergeron J., Borgani S., Gilli R., Gilmozzi R., Zheng W., 2001, ApJ, 551, 624
Giavalisco M., Ferguson H. C., Koekemoer A. M., Dickinson M., Alexander D. M., Bauer F. E., 2004, ApJ, 600, L93
Hamilton T. T., Helfand D. J., Becker R. H., 1985, AJ, 90, 606
Han J. L., Demorest P. B., van Straten W., Lyne A. G., 2009, ApJS, 181, 557
Han J. L., Manchester R. N., Xu R. X., Qiao G. J., 1998, MNRAS, 300, 373
Huynh M. T., Norris R. P., Siana B., Middelberg E., 2010, ApJ, 710, 698
Kaplan D. L., Cordes J. M., Condon J. J., Djorgovski S. G., 2000, ApJ, 529, 859
Keith M. J., Jameson A., van Straten W., Bailes M., Johnston S., Kramer M., Possenti A., Bates S. D., Bhat N. D. R., Burgay M., Burke-Spolaor S., D'Amico N., Levin L., McMahon P. L., Milia S., Stappers B. W., 2010, MNRAS, pp 1356–+
Lacy M., Farrah D., Mauduit J. C., Surace J. A., Zeimann G., Huynh M., 72 co-authors 2010, ApJ, submitted
Lonsdale C. J., Smith H. E., Rowan-Robinson M., Surace J., Shupe D., Xu C., 2003, PASP, 115, 897
Lyne A. G., Burgay M., Kramer M., Possenti A., Manchester R. N., Camilo F., McLaughlin M. A., Lorimer D. R., D'Amico N., Joshi B. C., Reynolds J., Freire P. C. C., 2004, Science, 303, 1153
Lyne A. G., Manchester R. N., Lorimer D. R., Bailes M., D'Amico N., Tauris T. M., Johnston S., Bell J. F., Nicastro L., 1998, MNRAS, 295, 743
Manchester R. N., Hobbs G. B., Teoh A., Hobbs M., 2005, AJ, 129, 1993
Manchester R. N., Lyne A. G., Camilo F., Bell J. F., Kaspi V. M., D'Amico N., McKay N. P. F., Crawford F., Stairs I. H., Possenti A., Morris D. J., Sheppard D. C., 2001, MNRAS, 328, 17
Middelberg E., Norris R. P., Cornwell T. J., Voronkov M. A., Siana B. D., Boyle B. J., Ciliegi P., Jackson C. A., Huynh M. T., Berta S., Rubele S., Lonsdale C. J., Ivison R. J., Smail I., 2008a, AJ, 135, 1276
Middelberg E., Norris R. P., Hales C. A., Seymour N., Johnston-Hollitt M., Huynh M., Lenc E., Mao M. Y., 2010, A&A, in press
Middelberg E., Norris R. P., Tingay S., Mao M. Y., Phillips C. J., Hotan A. W., 2008b, A&A, 491, 435
Navarro J., de Bruyn A. G., Frail D. A., Kulkarni S. R., Lyne A. G., 1995, ApJ, 455, L55+
Norris R. P., Afonso J., Appleton P. N., Boyle B. J., Ciliegi P., Croom S. M., Huynh M. T., Jackson C. A., Koekemoer A. M., Lonsdale C. J., Middelberg E., Mobasher B., Oliver S. J., Polletta M., Siana B. D., Smail I., Voronkov M. A., 2006, AJ, 132, 2409
Norris R. P., Afonso J., Cava A., Farrah D., Huynh M. T., Ivision R. J., Jarvis M., Lacy M., Mao M., Maraston C., Mauduit J. C., Middelberg E., Oliver S., Seymour N., Surace J., 2010, ApJ, submitted
Norris R. P., Tingay S., Phillips C., Middelberg E., Deller A., Appleton P. N., 2007, MNRAS, 378, 1434
Strom R. G., 1987, ApJ, 319, L103

[2] http://www.atnf.csiro.au/people/rnorris/emu/

Bibliography

[1] Han, JL & Tian, WW 1999, 'Pulsars identified from the NRAO VLA Sky Survey,' *Astronomy & Astrophysics Supplement Series,* vol. 136, pp. 571-577

[2] Condon, JJ, Cotton, WD, Greisen, EW, Yin, QF, Perley, RA, Taylor, GB & Broderick, JJ 1998, 'The NRAO VLA Sky Survey,' *The Astronomical Journal,* vol. 115, pp. 1693-1716

[3] Kaplan, DL, Condon, JJ, Arzoumanian, Z & Cordes, JM 1998, 'Pulsars in the NRAO VLA Sky Survey,' *The Astrophysical Journal Supplement Series,* vol. 119, pp. 75-82

[4] Gould, DM & Lyne, AG 1998 'Multifrequency polarimetry of 300 radio pulsars,' *Monthly Notices of the Royal Astronomical Society*, vol. 301, pp. 235-260

[5] Han, JL, Demorest, PB, van Straten, W & Lyne, AG 2009, 'Polarisation Observations of 100 Pulsars at 774 MHz by the Green Bank Telescope,' *The Astrophysical Journal Supplement Series,* vol. 181, pp. 557-571

[6] Han, JL, Manchester, RN, Xu, RX & Qiao, GJ 1998, 'Circular Polarisation in Integrated Pulse Profiles,' *Monthly Notices of the Royal Astronomical Society*, vol. 300, pp. 373-387

[7] Shi, H, Liang, H, Han, JL & Hunstead, RW 2010, 'Radio sources with ultra-high polarisation,' *ArXiv.org > astro-ph*, last viewed 22 July 2010, <http://arxiv.org/abs/1007.2367>

[8] Kouwenhoven, MLA 2000, 'Pulsars in the Westerbork Northern Sky Survey,' *Astronomy & Astrophysics Supplement Series*, vol. 145, pp. 243-254

[9] Crawford, F, Kaspi, VM & Bell, JF 2000, 'A search for submillisecond pulsations in unidentified FIRST and NVSS radio sources,' *The Astronomical Journal,* vol. 119, pp. 2376-2381

[10] Avramenko, AE, Ilyasov, YP & Potapov, VA 2000, 'Identification of pulsars among the sky survey objects,' *Baltic Astronomy*, vol. 9, pp. 631-632

[11] Kaplan, DL, Cordes, JM, Condon, JJ & Djorgovski, SG 2000, 'Compact radio sources with the steepest spectra,' *The Astrophysical Journal*, vol. 529, pp. 859-865

[12] Graham-Smith, F 2003, 'The radio emission from pulsars,' *Reports on Progress in Physics*, vol. 66, pp. 173-238

[13] Rawlings, S 2008, *Phase-I SKA: Summary of Science Case,* viewed 22 July 2010, <www-astro.physics.ox.ac.uk/~sr/astronet.pdf>

[14] Backer, DC 1995, 'Millisecond Pulsar Radiation Properties,' *Journal of Astrophysics and Astronomy*, vol. 16, pp. 165-171

[15] Rengelink, RB, Tang, Y, de Bruyn, AG, Miley, GK, Bremer, MN, Röttgering, HJA & Bremer, MAR 1997, 'The Westerbork Northern Sky Survey (WENSS) I. A 570 square degree Mini-Survey around the North Ecliptic Pole,' *Astronomy & Astrophysics Supplement Series*, vol. 124, pp. 259-280

[16] Tian, WW, Strom, RG, Stappers, B, Zhang, XZ, Wu, XJ & Ramachandran, R 2000, 'Millisecond Pulsars and a WRST Search for Candidates,' *ASP Conference Series,* vol. 202 (eds. Kramer, M, Wex, N & Wielebinski, R), pp. 45-46

[17] Norris, RP, Hunyh, MT, Jackson, CA, Boyle, BJ, Ekers, RD, Mitchell, DA, Sault, RJ, Wieringa, MH, Williams, RE, Hopkins, AM & Higdon, J 2005, 'Radio observations of the Hubble Deep Field-South Region. I. Survey description and initial results,' *The Astronomical Journal*, vol. 130, pp. 1358-1372

[18] Hunyh, MT, Jackson, CA, Norris, RP & Prandoni, I 2005, 'Radio observations of the Hubble Deep Field-South Region. II. The 1.4 GHz catalog and source counts,' *The Astronomical Journal*, vol. 130, pp. 1373-1388

[19] 'Circular polarisation' 2010, *Wikipedia*, viewed 26 July 2010, <http://en.wikipedia.org/wiki/Circular_polarization>

[20] Backer, DC, Kulkarni, SR, Heiles, C, Davis, MM & Goss, WM 1982, 'A millisecond pulsar,' *Nature*, vol. 300, pp. 615-618

[21] Navarro, J, de Bruyn, AG, Frail, DA, Kulkarni, SR & Lyne, AG 1995, 'A very luminous binary millisecond pulsar,' *The Astrophysical Journal,* vol. 455, pp. L55-L58

[22] Hamilton, TT, Helfand, DJ & Becker, RH 1985, 'A search for millisecond pulsars in globular clusters,' *The Astronomical Journal*, vol. 90, pp. 606-608

[23] Strom, RG 1987, 'Pulsar-like emission from the supernova remnant CTB 80,' *The Astrophysical Journal*, vol. 319, pp. L103-107

[24] Lyne, AG, Brinklow, A, Middleditch, J, Kulkarni, SR, Backer, DC & Clifton, TR 1987, 'The discovery of a millisecond pulsar in the globular cluster M28,' *Nature*, vol. 328, pp. 399-401

[25] Lorimer, DR & Kramer, M 2005, *Handbook of Pulsar Astronomy*, Cambridge University Press, Cambridge, UK

[26] Huynh, MT, Norris, RP, Siana, B & Middelberg, E 2010, 'Evidence for Infrared-Faint Radio Sources as $z > 1$ radio-loud Active Galactic Nuclei,' *The Astrophysical Journal*, vol. 710, pp. 698-705

[27] Middelberg, E, Norris, RP, Tingay, S, Mao, MY, Phillips, CJ & Hotan, AW 2008, 'The first VLBI image of an infrared-faint radio source,' *Astronomy & Astrophysics*, vol. 491, pp. 435-439

[28] *NVSS Source Catalog* December 10 1997, The NRAO VLA Sky Survey, viewed 29 July 2010, <ftp://nvss.cv.nrao.edu/pub/nvss/catalog.ps>

[29] *ATLAS: Australia Telescope Large Area Survey*, Australia Telescope National Facility, viewed 29 July 2010, <http://www.atnf.csiro.au/research/deep/index.html>

[30] Manchester, RN & Taylor, JH 1977, *Pulsars*, W.H. Freeman and Company, USA

[31] Lenc, E, Norris, R, Hopkins, A, Sharp, R, Hyunh, M, Mao, M, Middelberg, E & Randall, K 2009, 'The ATLAS Survey of the CDFS and ELAIS-S1 Fields,' *in proceedings of 'Panoramic Radio Astronomy: Wide-field 1-2 GHz research on galaxy evolution,'* Groningen, the Netherlands.

[32] Hunt, M 2001, 'Molecules in Southern Molecular Clouds: A Millimeter-wave Study of Dense Cores,' PhD. thesis, University of Western Sydney.

[33] 'Jansky' 2010, *Wikipedia*, viewed 3 June 2010, <http://en.wikipedia.org/wiki/Jansky>.

[34] Baars, JWM 2007, *The paraboidal reflector antenna in radio astronomy and communication*, Springer, New York.

[35] Shapiro, SL, Teukolsky, SA & Lightman, AP (rev) 1983, 'Black Holes, White Dwarfs and Neutron Stars: The Physics of Compact Objects,' *Physics Today*, vol. 36, iss. 10, p. 89-90

[36] Kellerman, KI, Pauliny-Toth, IIK & Williams, PJS 1969, 'The spectra of radio sources in the revised 3C catalogue,' *The Astrophysical Journal*, vol. 157, pp. 1-34

[37] Kaplan, DL, Cordes, JM & Condon, JJ 2000, 'Radio morphologies and spectra of compact radio sources with the steepest spectra,' *The Astrophysical Journal Supplement Series*, vol. 126, pp. 37-62

[38] Maron, O, Kijak, J, Kramer, M & Wielebinski, R 2000, 'Pulsar spectra of radio emission,' *Astronomy & Astrophysics Supplement Series,* vol. 147, pp. 195-203

[39] Henry GR & Paik, JH 1969, 'Distribution of Pulsar Duty Cycles,' *Nature*, vol. 224, pp. 1188-1189

[40] Manchester, RN, Lyne, AG, Camilo, F, Bell, JF, Kaspi, VM, D'Amico, N, McKay, NPF, Crawford, F, Stairs, IH, Possenti, A, Kramer, M & Sheppard, DC 2001, 'The Parkes multi-beam pulsar survey - I. Observing and data analysis systems, discovery and timing of 100 pulsars,' *Monthly Notices of the Royal Astronomical Society,* vol. 328, pp. 17-35

[41] Keith, MJ, Jameson, A, van Straten W, Bailes, M, Johnston, S, Kramer, M, Possenti, A, Bates, SD, Bhat, NDR, Burgay, M, Burke-Spolaor, S, D'Amico, N, Levin, L, McMahon, PL, Milia, S & Stappers, BW 2010, 'The High Time Resolution Universe Pulsar Survey - I. System configuration and initial discoveries,' *Monthly Notices of the Royal Astronomical Society,* publised online, doi: 10.1111/j.1365-2966.2010.17325.x

[42] Norris, RP, Afonso, J, Appleton, PN, Boyle, BJ, Ciliegi, P, Croom, SM, Huynh, MT, Jackson, CA, Koekemoer, AM, Lonsdale, CJ, Middelberg, E, Mobasher, B, Oliver, SJ, Polletta, M, Siana, BD, Smail, I & Voronkov, MA 2006, 'Deep ATLAS Radio Observations of the Chandra Deep Field-South/Spitzer Wide-Area Infrared Extragalactic Field,' *The Astronomical Journal,* vol. 132, pp. 2409 - 2423

[43] Yun, MS, Reddy, NA & Condon, JJ 2001, 'Radio Properties of Infraered-Selected Galaxies in the IRAS 2 Jy Sample,' The Astrophysical Journal, vol. 554, pp. 803-822

[44] Norris, RP, Tingay, S, Phillips, C, Middelberg, E, Deller, A & Appleton, PN 2007, 'Very long baseline inteferometry detection of an Infrared-Faint Radio Source,' *Monthly Notices of the Royal Astronomical Society,* vol. 378, pp. 1434-1438

[45] Garn, T & Alexander, P 2008, 'Deep 610-MHz Giant Metrewave Radio Telescope observations of the Spitzer extragalactic First Look Survey field - III. The radio properties of the infrared-radio sources,' *Monthly Notices of the Royal Astronomical Society,* vol. 391, pp. 1000-1008

[46] Manchester, RN, Hobbs, GB, Teoh, A & Hobbs, M 2005, 'The Australia Telescope National Facility Pulsae Catalogue,' *The Astronomical Journal*, vol. 129, pp. 1993-2006

[47] *Spitzer,* California Institute of Technology, viewed 3 November 2010, <http://ssc.spitzer.caltech.edu/>

[48] 'Great Observatories program' 2010, *Wikipedia*, viewed 3 November 2010, <http://en.wikipedia.org/wiki/Great_Observatories>

[49] 'Spitzer Space Telescope - Instruments' 2010, *Wikipedia*, viewed 3 November 2010, <http://en.wikipedia.org/wiki/Spitzer_Space_Telescope#Instruments>

[50] Hotan, AW, van Straten, W & Manchester, RN 2004, 'PSRCHIVE and PSRFITS: An Open Approach to Radio Pulsar Data Storage and Analysis,' *Publications of the Astronomical Society of Australia*, vol. 21, pp. 302-309

[51] Middelberg, E, Norris, RP, Hales, CA, Seymour, N, Johnston-Hollitt, M, Huynh, M, Lenc, E & Mao, MY 2010, 'The Radio Properties of Infrared-Faint Radio Sources,' *Astronomy & Astrophysics,* in press

[52] Lacy, M, Farrah, D, Mauduit, J-C, Surace, JA, Zeimann, G, Huynh, M & 72 co-authors 2010, 'The Spitzer Extragalactic Representative Volume Survey (SERVS): survey definition and goals,' *The Astrophysical Journal*, submitted.

[53] Norris, RP, Afonso, J, Cava, A, Farrah, D, Huynh, MT, Ivison, RJ, Jarvis, M, Lacy, M, Mao, M, Maraston, C, Mauduit, J-C, Middelberg, E, Oliver, S, Seymour, N & Surace, J 2010, 'Deep Spitzer observations of infrared-faint radio sources: high-redshift radio-loud AGN?' *The Astrophysical Journal*, submitted.

[54] Lyne, AG, Manchester, RN, Lorimer, DR, Bailes, M, D'Amico, N, Tauris, TM, Johnston, S, Bell, JF &Nicastro, L 1998, 'The Parkes Southern Pulsar Survey - II. Final results and population analysis,' *Monthly Notices of the Royal Astronomical Society,* vol. 295, pp. 743-755

[55] Lyne, AG, Burgay, M, Kramer, M, Possenti, A, Manchester, RN, Camilo, F, McLaughlin, MA, Lorimer, DR, D'Amico, N, Joshi, BC, Reynolds, J & Freire, PCC 2004, 'A Double-Pulsar System: A Rare Laboratory for Relativistic Gravity and Plasma Physics,' *Science*, vol. 303, pp. 1153-1157

[56] Burgay, M, Joshi, BC, D'Amico, N, Possenti, A, Lyne, AG, Manchester, RN, McLaughlin, MA, Kramer, M, Camilo, F & Freire, PCC 2006, 'The Parkes High-Latitude Pulsar Survey,' *Monthly Notices of the Royal Astronomical Society,* vol. 368, pp. 283-292

[57] Middelberg, E, Norris, RP, Cornwell, TJ, Voronkov, MA, Siana, BD, Boyle, BJ, Ciliegi, P, Jackson, CA, Hunyh, MT, Berta, S, Rubele, S, Lonsdale, CJ, Ivison, RJ & Smail, I 2008, 'Deep Australia Telescope Large Area Survey Radio Observations of the European Large Area ISO Survey S1/Spitzer Wide-Area Infrared Extragalactic Field,' *The Astronomical Journal,* vol. 135, pp. 1276-1290

[58] Kimball, AE & Ivezic, Z 2008, 'A unified catalog of radio objects detected by NVSS, FIRST, WENSS, GB6 and SDSS,' *The Astronomical Journal*, vol. 136, pp. 684-712

[59] *ATCA Users Guide: Australia Telescope Compact Array Users Guide,* CSIRO Astronomy and Space Science, viewed 9 November 2010, <http://www.narrabri.atnf.csiro.au/observing/users_guide/html/atug.html>

[60] *CABB,* CSIRO Astronomy and Space Science, viewed 9 November 2010, <http://www.narrabri.atnf.csiro.au/observing/CABB.html>

[61] *Stokes Parameters and Polarisation,* Australia Telescope National Facility, viewed 9 November 2010, <http://www.atnf.csiro.au/computing/software/atca_aips/node11.html>

[62] 'Stokes parameters' 2010, *Wikipedia*, viewed 9 November 2010, <http://en.wikipedia.org/wiki/Stokes_parameters>

[63] 'Faraday effect' 2010, *Wikipedia*, viewed 9 November 2010, <http://en.wikipedia.org/wiki/Faraday_effect>

[64] Carr, NG 2007, 'Biomolecules in Sagittarius B2,' Honours thesis, University of New South Wales

[65] Norris, RP 2009, 'ASKAP-EMU: Overcoming the challenges of wide deep continuum surveys,' in *Proceedings of Science*, presented at *Panoramic Radio Astronomy: Wide-field 1-2 GHz research on galaxy evolution - PRA2009*, Groningen, the Netherlands, June 2-5

[66] Commonwealth Science and Industrial Research Organisation, 2009, *ASKAP Survey Science Projects*, (L Ball, Acting Director), CSIRO Australia Telescope National Facility Sydney.

[67] Stairs, IH & Team Members, 2010, 'COAST: Compact Objects with ASKAP: Surveys and Timing, Internal Review Document,' CSIRO Astronomy and Space Science, viewed 10 November

[68] *ASKAP Home,* CSIRO Astronomy and Space Science, viewed 10 November 2010, <http://www.atnf.csiro.au/projects/askap/index.html>

[69] 'Square kilometre array' 2010, *Scholarpedia*, viewed 10 November 2010, <http://www.scholarpedia.org/article/Square_kilometre_array>

[70] *EMU: Evolutionary Map of the Universe,* CSIRO Astronomy and Space Science, viewed 10 November 2010, <http://www.atnf.csiro.au/people/rnorris/emu/>

[71] Rayner, DP, Norris, RP & Sault, RJ 2000, 'Radio circular polarization of active galaxies,' *Monthly Notices of the Royal Astronomical Society*, vol. 319, pp. 484-496

[72] Grant, JK, Taylor, AR, Stil, JM, Landecker, TL, Kothes, R, Ransom, RR & Scott, D 2010, 'The DRAO Planck Deep Fields: The Polarization Properties of Radio Galaxies at 1.4 GHz,' *The Astrophysical Journal*, vol. 714, pp. 1689-1701

[73] Mesa, D, Baccigalupi, C, De Zotti, G, Gregorini, L, Mack, K-H, Vigotti, M & Klein, U 2002, 'Polarization properties of extragalactic radio sources and their contribution to microwave polarisation fluctuations,' *Astronomy & Astrophysics*, vol. 396, pp. 463-471

[74] *ASKAP POSSUM*, University of Sydney, viewed 12 November 2010, <http://www.physics.usyd.edu.au/sifa/possum/>

[75] Ravi, V, Hobbs, G, Wickramasinghe, D, Champion, DJ, Keith, M, Manchester, RN, Norris, RP, Bray, JD, Ferrario, L & Melrose, D 2010, 'Observations of radio pulses from CU Virginis,' *Monthly Notices of the Royal Astronomical Society*, vol. 408, pp. L99-L103

[76] Kellett, BJ, Graffagnino, V, Bingham, R, Muxlow, TWB & Gunn, AG 2007, 'CU-Virginis - The First Stellar Pulsar,' *ArXiv.org > astro-ph*, last viewed 12 November 2010, <http://arxiv.org/abs/astro-ph/0701214>

[77] *Parkes Users Guide: Parkes RadioTelescope Users Guide,* CSIRO Astronomy and Space Science, viewed 13 November 2010, <http://www.parkes.atnf.csiro.au/observing/documentation/user_guide/pks_ug.html>

[78] *CAS - Swinburne Pulsar Group - BPSR,* Swinburne University of Technology, viewed 13 November 2010, <http://astronomy.swin.edu.au/pulsar/?topic=bpsr>

[79] Karastergiou, A, Johnston, S & Manchester, RN 2005, 'Polarization profiles of southern pulsars at 3.1 GHz,' *Monthly Notices of the Royal Astronomical Society,* vol. 359, pp. 481-492

[80] Keith, MJ, Eatough, RP, Lyne, AG, Kramer, M, Possenti, A, Camilo, F & Manchester, RN 2009, 'Discovery of 28 pulsars using new techniques for sorting pulsar candidates,' *Monthly Notices of the Royal Astronomical Society,* vol. 395, pp. 837-846